Evaluation of Cardiac and Skeletal Muscle Progenitor Cell Dynamics in Growth Restricted Fetuses

by

Neeka Bayat-Barooni

A dissertation accepted and approved in partial fulfillment of the requirements for the degree of

Doctor of Philosophy

in Human Physiology

Dissertation Committee:

Carrie E. McCurdy, PhD, Chair & Advisor

Ashley Walker, PhD, Core Member

Laura D. Brown, MD, Core Member

Hans Dreyer, PhD, Core Member

Nick Willett, PhD, Institutional Representative

University of Oregon

Fall 2024

DISSERTATION ABSTRACT

Neeka Bayat-Barooni

Doctor of Philosophy in Human Physiology

Evaluation of Cardiac and Skeletal Muscle Progenitor Cell Dynamics in Growth Restricted Fetuses

Fetal growth restriction (FGR) increases the risk of cardiometabolic disease due in part to deficits in cardiac and skeletal muscle growth that are not fully compensated for after birth. Deficits in fetal cardiomyocyte number and maturity are thought to mediate lifelong cardiac dysfunction in FGR offspring. Similarly, the total number of skeletal muscle myofibers is set *in utero*. Thus, reductions in fetal myofiber number and hypertrophic enlargement limit skeletal muscle growth and metabolic function throughout the lifespan. Previous studies identify decreased cell cycle activity in cardiac and skeletal muscle of FGR fetuses. Additionally, reductions in myogenic regulator factor (MRF) expression and in the frequency of binucleated cardiomyocytes imply impairments in terminal differentiation and maturation in FGR muscle. Due to limitations in current techniques, whether cardiac and skeletal muscle progenitor cells of FGR fetuses exhibit decreased proliferation and/or myogenic capacity *in vivo* remains a critical gap in knowledge.

Using an ovine model of placental insufficiency and FGR, this dissertation aimed to identify the cellular origins of dysregulated cardiac and skeletal muscle development in FGR fetuses. We hypothesized that intrauterine stress exposure disrupts proliferation and differentiation programs in muscle progenitor cells of FGR fetuses, thereby limiting cardiac and skeletal muscle growth and function both *in utero* and throughout postnatal life. To test this hypothesis, we developed a novel flow cytometry approach to evaluate cardiomyocyte and skeletal myoblast development in late-

gestation FGR and CON fetuses.

We identified impairments in cardiomyocyte development in FGR hearts, with distinct phenotypes specific to the left and right ventricles (LV, RV). Cardiomyocyte endocycling was upregulated in both ventricles of FGR fetuses. However, this increase appeared to compromise LV cardiomyocyte differentiation and maturity, while RV cardiomyocyte proliferation was notably reduced in FGR hearts. In the skeletal muscle of FGR fetuses, we observed decreased rates of myoblast proliferation and fewer myoblasts in the early stages of myogenesis. The proportion of unfused, late-differentiation myoblasts was increased in FGR, but this is likely due to impairments in myoblast fusion, as indicated by decreased Myomaker abundance in FGR skeletal muscle. Both cardiomyocyte and skeletal myoblast dynamics correlated with fetal IGF-1 concentrations. Our findings suggest that exogenous growth factor stimulation may be necessary or sufficient to restore fetal cardiac and skeletal muscle growth, potentially reducing the risk of cardiometabolic disease in offspring with prior FGR.

ACKNOWLEDGMENTS

I am so incredibly thankful to all the people who have mentored me, supported me, and helped make this research possible.

To my dissertation committee, Dr. Ashley Walker, Dr. Hans Dreyer, Dr. Nick Willett, and Dr. Laura Brown, thank you for your guidance and encouragement. I am truly grateful for your support and the opportunity to learn from each of you. To my Ph.D. advisor, Dr. Carrie McCurdy, thank you for believing in me and pushing me to strive for much more than I ever thought I was capable of. Thank you for entertaining all of my ideas and challenging me to pursue complex topics. I sincerely appreciate your patience and expertise.

To my lab mates (the McCurd Herd), thank you for sharing your knowledge, friendship, and enthusiasm with me. Special thanks to Dr. Byron Hetrick for introducing me to flow cytometry and teaching me how to do good science; to Matt for somehow making hundreds of hours of umbilical cord dissections and immunophenotyping a positive experience; and to Keenan for all of your love, compassion, and encouragement. Thank you to the veterinarians and staff at the Perinatal Research Center for caring for the animals and making it possible for me to pursue this research.

To Jenna, Kaitlyn, Kelsey, Jess, Ellen, and Kenzie, thank you for bringing balance, joy, and laughter to my life outside of the lab. I feel so lucky to have met all of you. To the friends who are really family, Shannon, Su, Clemence, and Lily – thank you for the facetimes, the girls' trips, and your endless love and support. I am so grateful to have you in my life. To Mike'l, thank you for being my support system, my diary, my comedic relief, and my number one fan. Thank you for

feeding me, inspiring me, and biking alongside me when I have to run in the dark; for listening to me, hyping me up, and giving me the biggest, best squeezes when I need them most.

Finally, to my family – thank you for literally everything. To my sister and favorite person in the whole wide world, thank you for singlehandedly keeping my sparkle alive and always reminding me that "it's not that serious". To my mommy, thank you for answering my 6+ phone calls per day and making sure we never go more than a few months without seeing each other. Thank you for teaching me that I can do anything I set my mind to, and for being my favorite #girlboss and greatest inspiration. To my dad, thank you for your unwavering support and belief in my abilities, for always making me laugh, and for teaching me the value of education. I love you guys sooooo much. This dissertation is as much a reflection of you and your support as it is of my work.

This research was supported by funding from the National Institutes of Health, the University of Oregon Office of the Vice President for Research and Innovation, the University of Oregon Center for the Study of Women in Society, and the Eugene & Clarissa Evonuk Memorial Graduate Fellowship. I am incredibly grateful to these organizations and their selection committees for believing in my research and investing in my scientific career.

TABLE OF CONTENTS

LIST OF FIGURES

Chapter Page

I. INTRODUCTION

Current reports estimate that one in five children in the United States are insulin resistant, a primary risk factor in the development of type 2 diabetes and cardiovascular disease. Rising rates of obesity, insulin resistance, and uncontrolled hypertension among adults reflect a gradual decline in the healthspan of the U.S. population. While diet and lifestyle have considerable influence on metabolic health, and genetic factors may predispose some individuals to obesity and cardiovascular disease, experimental and epidemiological data reveal significant associations between cardiometabolic dysfunction and exposure to suboptimal conditions *in utero*.

Intrauterine stress exposure can cause deficits in fetal tissue and organ development that are not completely compensated for after birth. The gestational environment is especially critical for lifelong cardiac and skeletal muscle growth, as adult cardiomyocyte and skeletal myofiber numbers are established *in utero*. Inadequate cardiomyocyte endowment places greater strain on fewer cells to maintain contractile forces throughout the lifespan; thus, increasing vulnerability to heart failure, especially as the cardiomyocyte population begins to decline with age. Similarly, lifelong skeletal muscle growth is limited by the total number of myofibers. As the primary site for insulin-stimulated glucose uptake, deficits in skeletal muscle mass often precede impairments in substrate handling and insulin sensitivity that lead to metabolic disease. Muscle progenitor cell programs, including proliferation, differentiation, and hypertrophy, are highly sensitive to the surrounding microenvironment, especially during periods of rapid growth. Therefore, reductions in intrauterine nutrient, oxygen, and growth factor availability can significantly alter the fate and function of fetal cardiac and skeletal myocytes. Further understanding of how early-life

environmental stress disrupts cardiac and skeletal muscle development is needed to effectively address the multigenerational transmission of cardiometabolic disease.

REVIEW of the LITERATURE

The Developmental Origins of Health and Disease

After identifying that the rising death rates from ischemic heart disease could not be explained by adult lifestyle risk factors such as smoking, diet, or elevated blood pressure (1), Dr. David Barker investigated birth records in England and Wales to determine whether cardiovascular disease had earlier origins. He compared the maps of deaths from heart disease and infant mortality 70 years prior and identified that the highest rates of infant and adult cardiovascular mortality existed in the same geographical regions (2–5). In subsequent studies, Barker and colleagues determined that low birthweight was the strongest predictor of heart disease and stroke in adulthood (1, 6). Thus, Barker postulated that adverse early-life exposures disrupt fetal development and increase the likelihood of infant mortality and/or vulnerability to chronic disease in later life (7–9).

Since Barker's initial hypothesis, hundreds of epidemiological and experimental studies have demonstrated that poor fetal growth increases the risk for developing cardiovascular disease (10–22), obesity (23–26), insulin resistance (27–29), and type 2 diabetes mellitus in adulthood (30, 31). Yet, these findings do not imply that birthweight has a causal role in determining lifelong health and the risk of chronic disease. Instead, birthweight serves as an accessible indicator of alterations in fetal growth trajectories, which likely result from adaptations to an unfavorable intrauterine environment. Developmental plasticity during early life allows the fetus to modify

growth patterns, hormone production, and metabolic processes in response to signals from the surrounding environment (32). This adaptability increases the chances of survival under adverse intrauterine conditions. However, since prenatal development is critical for establishing lifelong organ structure, function, and metabolism, alterations in fetal growth trajectories may lead to persistent phenotypes that are often maladaptive for postnatal health (33, 34). Therefore, the current Developmental Origins of Health and Disease (DOHaD) framework posits that adverse early-life exposures impede organ growth and development, resulting in an increased risk for cardiometabolic disease later in life (35).

Maternal Health & Nutrition

The nutritional, hormonal, and metabolic environment of the developing fetus is predominantly shaped by maternal health and diet both during and prior to pregnancy (36–39). As such, maternal conditions including diabetes (40–43), obesity (36, 44–49), nutrient restriction (50, 51), "Western style" diet (52–58), substance use (59, 60), and environmental toxin exposure (61, 62) can impact fetal developmental trajectories and long-term health. Recent findings also suggest that paternal exposures may impact the intrauterine milieu (63–66), though to a lesser extent, and thus will not be the focus of this research.

Intrauterine stress can result from direct exposure to maternal insults or from indirect exposure to placental modifications and secondary messengers that mediate the effects of environmental disturbances (37, 67–72). As glucose is readily transported across the placenta, uncontrolled maternal diabetes significantly increases the concentration of glucose that is transferred to the fetus. This can cause fetal overgrowth (*i.e.,* macrosomia) and metabolic adaptations that contribute to health complications later in life. Maternal obesity and "Western-

style" diet (high-fat, high-sugar), in the absence of insulin resistance or GDM, have similar implications for intrauterine development and offspring health. Both conditions are characterized by elevated levels of substrates and free fatty acids, chronic inflammation, and alterations in circulating adipokines (73–80). Studies in human and animal models demonstrate that these alterations to the maternal environment can lead to excess nutrients, metabolic hormones (*e.g.,* insulin and leptin), and proinflammatory cytokines in fetal circulation (44, 69, 81–83). As the placenta is particularly sensitive to metabolic and pro-inflammatory signaling (84), maternal adiposity and malnutrition can also disrupt placental substrate transport and stimulate cellular stress programs in both the placenta and the developing fetus (76, 85–88).

Many small and lipophilic particles are able to passively cross the placenta to directly interact with the developing fetus (89). Therefore, maternal substance use during pregnancy can expose the developing fetus to substances like alcohol and nicotine, potentially leading to fetal alcohol spectrum disorder, neonatal withdrawal syndrome, or preterm birth (90–92). Similarly, maternal exposure to environmental toxins, such as bisphenols or environmental pollutants, can adversely affect fetal development, potentially leading to birth defects or neurocognitive delays (61, 93, 94).

Numerous epidemiological studies link maternal famine exposure during pregnancy to reductions in fetal birthweight and an increased risk for cardiovascular disease (11, 17, 68). Deficits in maternal calorie intake and/or the consumption of specific nutrients can cause asymmetrical fetal growth restriction (FGR) due to reductions in intrauterine substrate availability (95). Additionally, maternal nutrient restriction impairs placental development, causing reductions

in placental size, vascularity, and endocrine function, that further limit nutrient transport and fetal growth (67, 68, 96).

The Placenta

The transfer of substances between maternal and fetal circulation is influenced by uteroplacental and umbilical blood flow, nutrient and oxygen gradients, and the size and physiology of the placenta (97, 98). Therefore, the placenta plays a critical role in determining fetal growth trajectories and lifelong health (99). The placenta is a dynamic tissue that evolves from a small, simple structure into a highly vascularized organ with complex signaling and transport systems that adapt to meet the needs of the developing fetus (67). It acts as the interface between maternal and fetal circulation, facilitating the exchange of nutrients, gasses, and waste products throughout pregnancy (96). Additionally, the placenta produces hormones, growth factors, and cytokines that are released into fetal and maternal circulation (100). Thus, the placenta regulates both the maternal and fetal microenvironments and plays an active role in regulating the maternal-fetal developmental ecosystem.

The placenta grows throughout pregnancy to enhance the surface area for maternal-fetal exchange and meet the needs of the developing fetus. Structural and functional adjustments also allow the placenta to respond to alterations in maternal circulation and buffer the fetus from acute environmental insults (101). However, chronic stress exposure, particularly during critical periods of placental development, can impede placental growth and restrict blood flow to the developing fetus (99). Impairments in placental structure, morphology, and function that limit fetal nutrient and oxygen delivery are collectively referred to as placental insufficiency, which affects 10% of all pregnancies and is the leading cause of FGR (97, 102, 103). Placental insufficiency and FGR

can result from several maternal conditions, including undernutrition, hypertension, vascular dysfunction, and preeclampsia (97, 104). Moreover, intrauterine exposure to placental insufficiency and FGR increases the risk of preterm birth, perinatal mortality, and cardiometabolic dysfunction in later life (68, 105, 106).

Mechanisms of Fetal Programming

Fetal Growth Restriction

Fetal growth restriction (FGR) is most commonly caused by placental insufficiency, though several other maternal, placental, and fetal conditions can lead to FGR (97, 107). Reductions in placental size and/or transport capacity limit fetal oxygen content, nutrient delivery, and growth factor signaling, creating a hypoxic, hypoglycemic, hyperadrenergic intrauterine environment (98, 107). In response to the decrease in substrate availability, fetal blood flow is maintained to the vital organs at the expense of the peripheral tissues, which are less metabolically active *in utero* (98). As a result, fetuses are likely to experience asymmetrical growth restriction, with 25-40% reductions in skeletal muscle mass compared to healthy fetuses of the same gestational age (104, 108). While these adaptive mechanisms promote survival *in utero*, disruptions in fetal growth trajectories often produce unfavorable phenotypes that persist after birth (109–112). Due to the finite window of developmental plasticity, reductions in lean mass and cardiac development cannot be completely compensated for in postnatal life (113, 114). Therefore, FGR offspring are more susceptible to cardiovascular disease, insulin resistance, and type 2 diabetes in adulthood.

The Heart

FGR fetuses have decreased cardiac muscle mass, contractility, diastolic function, and ventricular wall thickness (115, 116). Previous studies also identify alterations in cardiomyocyte morphology, cell cycle activity, maturity, and gene expression in FGR hearts. In children and adults with prior FGR, aberrant signaling pathways, compromised cardiac growth, and impairments in systolic and diastolic function suggest that fetal cardiac phenotypes worsen throughout postnatal life. Moreover, clinical and experimental data link these changes in cardiac structure and function to the development of cardiovascular disease in adulthood.

Fetal cardiac growth consists of cardiomyocyte proliferation, differentiation, and enlargement. During early-mid gestation, cellular proliferation is the primary mediator of cardiac growth. In the third trimester, nuclear division (karyokinesis) becomes uncoupled from cytokinesis to produce binucleated cardiomyocytes (117, 118). The binucleated cells then undergo changes in size, shape, sarcomere organization, mitochondrial volume, and myofibril arrangement as they complete differentiation and become mature cardiomyocytes (119). While the remaining mononucleated cardiomyocytes will continue to proliferate throughout the final third of gestation, terminal differentiation is responsible for the rapid increase in cardiac muscle mass during this period. In most large mammals, including humans and sheep, cardiomyocyte proliferation stops shortly after birth, and subsequent growth is limited to cardiac hypertrophy (120). Given that total number of cardiomyocytes and the degree of cardiac maturity are established shortly after birth, lifelong cardiac function is highly dependent on cardiomyocyte growth during fetal development.

Previous studies identify reductions in cell cycle activity in FGR hearts, suggesting potential impairments in fetal cardiomyocyte proliferation that may explain deficits in

cardiomyocyte endowment. However, cardiomyocyte differentiation also involves cell cycle entry and DNA synthesis for binucleation. Further, multinucleated cardiomyocytes are known to continue cycling to increase DNA content through endoreplication. Therefore, decreased cell cycle activity in FGR cardiomyocytes may reflect alterations in cellular ploidy or maturation *in utero*, and additional research is necessary to distinguish which processes are impaired in FGR fetuses.

Skeletal Muscle

Skeletal muscle is comprised of thousands of myofibers that are formed by muscle progenitor cells that differentiate and fuse together to make larger, multinucleated myotubes. Primary myogenesis occurs during the first and second trimesters of pregnancy, creating a myofiber scaffold to support subsequent skeletal muscle growth. In the second and early third trimesters, a final wave of myotubes is formed to fill in any unoccupied space within the myofiber scaffold. The total number of myofibers is set once secondary myogenesis is complete (121), and further skeletal muscle growth is restricted to myofiber hypertrophy, rather than the addition of new myofibers. Still, hypertrophic enlargement requires myoblast fusion and myonuclear accretion to increase myofiber DNA and protein content to levels that can sustain an increase in cytoplasmic volume. Thus, the lifelong capacity for skeletal muscle growth is dependent on myogenesis and myofiber formation during fetal development.

Models of placental insufficiency and FGR have persistent reductions in myofiber number and cross-sectional area that are linked to long-term deficits in lean mass and muscle insulin sensitivity (122–127). Abnormal fetal growth trajectories often precede the development of metabolically unfavorable phenotypes, which can manifest through early postnatal “catch-up” periods of rapid adipose tissue expansion. However, given that skeletal muscle is responsible for

80-90% of insulin-stimulated glucose uptake, deficits in lean mass alone can be detrimental to lifelong metabolic health (128–130). Impairments in skeletal muscle metabolism often lead to increased adiposity, systemic insulin resistance, and ectopic fat storage. If left unmanaged, this can predispose FGR offspring to type 2 diabetes and cardiovascular disease in adult life.

Previously reported deficits in myonuclear accretion indicate that myofibers of FGR offspring lack the cellular machinery to support hypertrophic growth *in utero* (131). This also implies that the muscle progenitor cells residing outside and around the mature skeletal myofibers are compromised in FGR fetuses. Because myofiber hypertrophy is dependent on the incorporation of new myonuclei, especially during critical windows of development, we postulated that skeletal muscle growth in FGR fetuses is limited by impairments in myoblast proliferation and differentiation *in utero* (122–127). However, current studies have yet to establish a comprehensive understanding of the alterations in fetal myogenesis prior to myoblast fusion that are restricting skeletal muscle growth in FGR fetuses.

Current Gaps in Knowledge

Associations between fetal growth restriction and adult cardiometabolic disease are well established, yet the molecular mechanisms that mediate alterations in prenatal cardiac and skeletal muscle development remain a critical gap in knowledge. Previous studies have identified that fetuses affected by placental insufficiency have deficits in cardiac and skeletal muscle growth that persist into adulthood. This is attributed to reductions in both the size and the total number of cardiomyocytes and skeletal muscle myofibers in FGR offspring. Yet, the mechanisms underlying impairments in fetal myogenesis that program lifelong deficits in cardiac and skeletal muscle remain unknown.

Overarching Hypothesis

I hypothesized that reductions in muscle progenitor cell proliferation and differentiation restrict cardiac and skeletal muscle growth in FGR fetuses exposed to placental insufficiency. Additionally, I proposed that the rates of fetal cardiomyocyte and skeletal myoblast proliferation and differentiation are directly related to the concentrations of growth factors in fetal circulation.

Research Purpose

This dissertation aimed to identify the specific mechanisms of fetal cardiomyocyte and skeletal myoblast development that are impaired in FGR. By distinguishing the precise stages of cardiac and skeletal myogenesis that are disrupted *in utero* and measuring the relationships between growth factor availability and fetal myocyte dynamics, this research addressed critical knowledge gaps regarding the molecular mechanisms that limit fetal growth and compromise cardiac and skeletal muscle function into adulthood.

Specific Aims

Aim 1. Identify the mechanisms of impaired cardiac development in FGR (Chapter III). *Hypothesis: Cardiac muscle growth in FGR fetuses is limited by reductions in the rates of cardiomyocyte proliferation and terminal differentiation in utero.* Left and right ventricle cardiomyocytes were isolated from late-gestation fetal sheep with and without exposure to placental insufficiency and FGR. Cellular DNA content and EdU incorporation were measured by flow cytometry to determine the rates of cardiomyocyte division and maturation *in utero.* The relationships between circulating growth factors and fetal cardiomyocyte dynamics were assessed by Pearson correlation.

Aim 2. Identify the alterations in fetal myogenesis that restrict skeletal muscle growth following exposure to placental insufficiency (Chapter IV). *Hypothesis: Disruptions in myoblast proliferation and/or differentiation restrict skeletal muscle growth in FGR offspring.* Cell cycle progression, myogenic lineage commitment, and terminal differentiation were assessed in skeletal myoblasts isolated from the biceps femoris of late-gestation fetal sheep exposed to either placental insufficiency and FGR or healthy control conditions *in utero*. Additionally, the abundance of myomaker—a key mediator of myoblast fusion—was measured in whole skeletal muscle tissue from growth restricted and normally grown fetuses. The associations between fetal growth factor concentrations and skeletal myoblast dynamics were analyzed using Pearson correlation coefficients.

II. EXPERIMENTAL APPROACH

Models of Fetal Growth Restriction

Animal Models

Due to practical limitations and ethical concerns, many questions about the processes underlying the relationship between fetal development and adult health and disease cannot be tested in human pregnancies. Instead, animal models are often utilized to study disruptions in early development within a controlled environment. While no model organism is able to perfectly reproduce human pregnancy, the ovine model of FGR is widely used due to its ability to mimic human physiology, developmental timing, and fetal organ size and function.

Small rodent models are significantly less expensive and easier to manage than sheep and other large mammals, but their sizable litters differ from the primarily singleton human pregnancies and it is often difficult to obtain fetal measures from a large number of small animals (132). Although the shorter gestation period and lifespan reduce the time needed to study entire pregnancies and adult health outcomes, rats and mice are born before their organs fully mature and continue to develop postnatally (132, 133). Thus, most small mammals are not able to accurately reproduce the critical window of intrauterine development that occurs in humans. Sheep, however, have predominantly singleton pregnancies with developmental timelines that are consistent with humans (107, 134, 135). Most organs are formed during the first and second trimesters, and like humans, fetal sheep have skeletal muscle and cardiovascular systems that are functionally mature near the end of the third trimester (104, 107, 113, 135, 136). Additionally, sheep exhibit similar responses to intrauterine stress, including fetal endocrine and cardiovascular adaptations that

mimic the conditions observed in human pregnancies, as well as comparable alterations in pre- and postnatal growth trajectories associated with FGR (99, 107, 132, 135–139).

Sheep have been used extensively to model both the immature and adult human heart due to similarities in cardiac function and the patterns of cardiomyocyte development (140–142). In humans (143–147) and sheep (117, 118, 140, 148, 149), the fetal heart is comprised of primarily immature, mononucleated (2C) cardiomyocytes that proliferate to amplify the cell population until cell cycle activity starts to decline in late gestation. Cardiomyocyte proliferation ceases around the time of birth in both species (118, 145, 149–153), allowing fetal sheep to model the critical window of cardiomyocyte endowment observed in humans. Additionally, binucleation is associated with terminal differentiation in human and sheep hearts, and cardiomyocyte polyploidy is observed in both species (154–159).

Sheep and humans also exhibit similar patterns of skeletal muscle development (45, 114, 160–162), with comparable reductions in lean mass as a result of FGR (104, 109, 111, 113, 163–167). In both humans and sheep, primary and secondary myogenesis during the first and second trimesters establish the total number of myofibers (168–170). This is followed by myofiber enlargement in the final third of gestation and postnatally, as subsequent muscle growth depends exclusively on myofiber hypertrophy (171–174). Therefore, fetal sheep effectively model the biological impact of FGR on human skeletal muscle.

While sheep require a large animal facility and are more costly to maintain than smaller animal models, they are generally less expensive than non-human primates and offer specific advantages due to their tolerance for *in utero* manipulation (132). The capacity to handle fetal surgeries throughout pregnancy allows for serial blood sampling from both sides of the placenta

in unanesthetized and unstressed sheep (134, 135, 175). These measures provide important information about fetal blood flow and plasma substrate concentrations across gestation (99, 176–178). Additionally, researchers are able to manipulate specific aspects of the intrauterine environment, such as hormone levels or hemodynamics, to investigate their roles in regulating outcomes associated with FGR (140). Tools like EdU (used in this study) can be administered directly to fetal sheep to capture dynamic processes occurring *in utero*, making it easier to identify the molecular mechanisms underlying adaptations to intrauterine stress. However, some experimental techniques may be more challenging due to limitations in the availability of antibodies and reagents that have been validated in sheep.

While there are many similarities between human and sheep pregnancies, it is important to note that placentation differs significantly between species (132). Specifically, humans have a discoidal placenta that is round and relatively flat, while sheep have a cotyledonary placenta composed of circular structures distributed across the chorionic membrane (132). In healthy human pregnancies, there is extensive trophoblast invasion, which allows maternal blood to come into direct contact with fetal tissues. In contrast, sheep have syndesmochorial placentation with minimal trophoblast invasion (179). Maternal and fetal blood are separated by additional layers of tissue, and perfusion experiments indicate that the permeability of the placenta is reduced in sheep compared to humans (180). Despite these differences, there are several well-established methods to induce FGR in sheep (99, 132, 134, 135). This flexibility allows scientists to select the intervention that is best suited for their research and employ different models to investigate specific aspects of FGR.

Methods to Induce FGR in Sheep

Several experimental approaches are used to induce growth restriction in fetal sheep. Since FGR in human pregnancies can result from a variety of maternal, placental, or fetal conditions, ovine models have been developed to replicate a range of factors associated with intrauterine stress and FGR. Each approach causes chronic alterations in placental function that inhibit the transfer of oxygen and nutrients to the fetus and cause reductions in fetal growth (107, 134). However, some models of FGR are produced by maternal interventions while others involve direct manipulation of the placenta or fetus (132). Differences in the timing and duration of placental insufficiency associated with each model allow for studies of FGR in both early and late gestation, as observed in human pregnancies (176). Additionally, the fetal neuroendocrine and cardiovascular responses vary depending on the method used to induce FGR, so each model offers unique insight into the mechanisms and consequences of intrauterine stress exposure.

The degree and duration of fetal hypoxia and hypoglycemia increase with the severity of FGR, which is highly variable across ovine and human pregnancies (99, 134, 181). Maternal undernutrition through global deficits in calorie intake during mid- or late gestation causes reductions in placental development and FGR (11, 134). Fetal glycemia, uterine blood flow, and capillary density are reduced by maternal nutrient restriction, but deficits in fetal growth are less severe than those observed in other experimental models (107, 182). Interestingly, maternal nutrient restriction in early gestation does not produce placental insufficiency or FGR in fetal sheep (183). However, overfeeding adolescent sheep throughout gestation causes placental insufficiency and growth restriction, with hypoxic and hypoglycemic conditions that mimic human FGR (99, 134, 184, 185).

Maternal and fetal hypoxia can also be induced by exposing ewes to high altitudes or hypoxic chambers during pregnancy (107, 132, 186). Reductions in intrauterine oxygen availability obstruct placental and fetal growth and alter fetal blood flow throughout gestation (136, 137, 139, 187). Surgical removal of most endometrial caruncles from the uterus prior to conception limits placentome formation from the beginning of pregnancy and restricts fetal growth throughout gestation (187–189). This method reduces oxygen and nutrient transfer to the fetus and decreases plasma concentrations of IGF-1 without directly exposing the fetus to the initial insult (107, 190, 191). Fetal placental embolization through daily microsphere injections decreases the surface area available for substrate transport, causing reductions in fetal arterial oxygen content, hypoglycemia, and growth restriction (192, 193). In this model, fetal sheep become hypertensive, with alterations in umbilical blood flow that are consistent with the conditions observed in human FGR (194, 195). Single umbilical artery ligation causes FGR by reducing placental blood flow and substrate delivery to the fetus (107). Fetal brain and medullary function are often spared in this model; however, preterm delivery is common and may limit the capacity to test some hypotheses using this intervention (196).

Study Design

The hypotheses in this dissertation are tested using an ovine model of hyperthermia-induced placental insufficiency and FGR. Between early- to mid-gestation, pregnant ewes are housed in environmental chambers that cycle between 30-35°C every 12 hours (***Fig. 2.1***). The chronic heat treatment impairs placental development (***Table 2.1***), causing reductions in placentome size and transport capacity that lead to fetal hypoxia, hypoglycemia, and reduced amino acid concentrations *in utero* (102, 135, 175). Prior studies also report decreased umbilical

blood flow and increased placental vascular resistance following chronic heat exposure, which is consistent with the conditions observed in human FGR (99, 107). This method of placental insufficiency slows fetal growth in mid- to late gestation and produces many of the metabolic and organ-specific adaptations that are observed in humans with placental insufficiency and FGR (197).

Since heat exposure from early to mid-gestation is sufficient to induce placental insufficiency and subsequent FGR, the pregnant ewe is removed from the environmental stressor at least two weeks prior to fetal evaluation (197, 198). This approach allows us to study the fetus without the confounding effects of the extrauterine environment. Additionally, as sheep are able to tolerate intrauterine manipulation, we are able to measure fetal substrate levels throughout pregnancy and characterize the changes associated with FGR. In this model of hyperthermia-induced placental insufficiency, placental weight begins to decrease toward the end of the first trimester, and hypoxia is detected near 90 dGa (99, 102, 114, 175). This is followed by an increase in norepinephrine and reductions in fetal plasma glucose, insulin, and IGF-1 concentrations that are sustained into late gestation (99, 102, 107, 114, 137, 177). The hormonal trajectories observed in this model reflect the intrauterine environments observed in human pregnancies affected by FGR (177), and several studies indicate that the alterations in circulating growth factors play a critical role in mediating the progression of FGR phenotypes observed throughout pregnancy (69, 113, 114, 140, 170, 190, 191, 199).

Figures

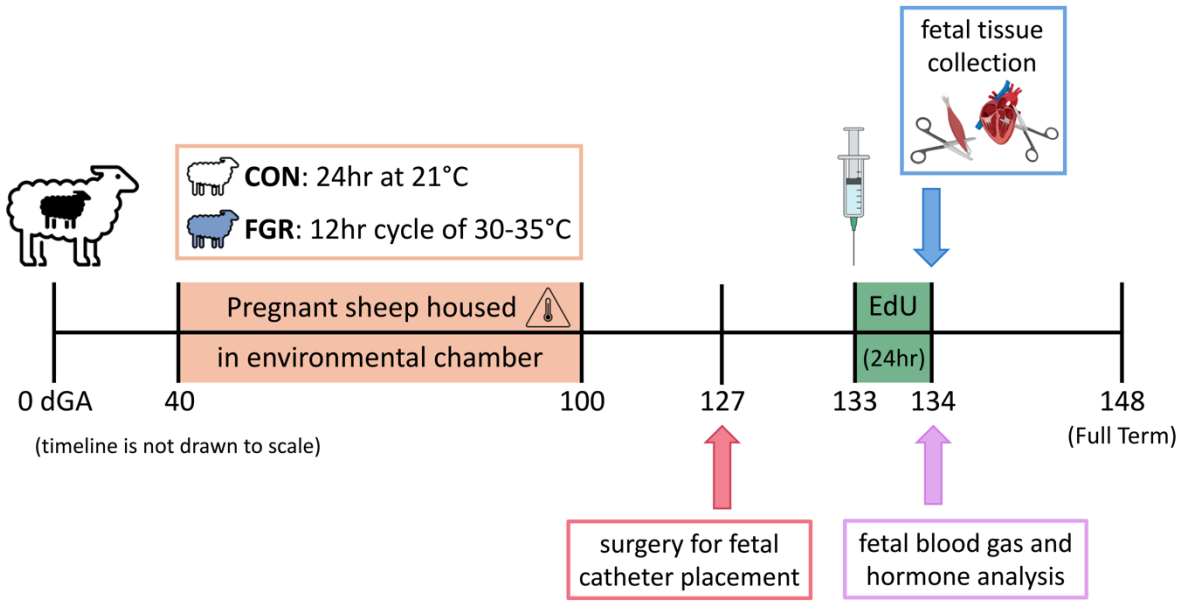

Figure 2.1. **Ovine model of placental insufficiency and fetal growth restriction**. Pregnant ewes randomly assigned to FGR (n=12) or CON (n=13) groups and housed in an environmental chamber from 40 to 100 days gestation (dGA). Ewes were exposed to elevated ambient temperatures (20°C for 12 hrs, 35°C for 12 hrs; 35-40% humidity) to induce placental insufficiency and FGR or normal ambient temperatures (21°C for 24 hrs; 35-40% humidity) to produce CON pregnancies. Surgery was performed in late gestation pregnant ewes (126 ± 2 dGA) to place maternal and fetal catheters, and an intravenous bolus of EdU was administered directly to the fetus 24 hours prior to tissue collection (133 ± 1 dGA). Fetal cardiac and skeletal muscle biopsies were collected at 133 ± 1 dGA for analysis by flow cytometry.

Table 2.1. Fetal physiological parameters.

	CON (n=12)	FGR (n=13)	*P*-value
Fetal sex (male/female)	1/11	6/7	
Gestational age (days)	133 ± 0.4	134 ± 0.4	**0.03**
Crown-rump length (cm)	50.5 ± 0.5	42.2 ± 1.1	**<0.0001**
Lower extremity limb length (cm)	34.4 ± 0.4	29.0 ± 0.7	**<0.0001**
Fetal body mass (g)	3384 ± 85	2070 ± 145	**<0.0001**
Brain (g)	51.7 ± 1.4	49.1 ± 1.2	0.16
Brain/Fetal body mass (g/Kg)	15.4 ± 0.6	24.2 ± 1.4	**<0.0001**
Heart (g)	25.0 ± 0.8	13.9 ± 1.2	**<0.0001**
Heart/Fetal body mass (g/Kg)	7.4 ± 0.1	6.8 ± 0.2	**0.01**
Left Ventricle (g)	8.0 ± 0.4	4.9 ± 0.5	**<0.001**
LV/Heart mass (g/g)	0.32 ± 0.02	0.35 ± 0.02	0.23
Right Ventricle (g)	5.0 ± 0.4	3.3 ± 0.3	**0.002**
RV/Heart mass (g/g)	0.21 ± 0.02	0.24 ± 0.01	0.17
Septum (g)	2.7 ± 0.2	1.7 ± 0.2	**0.0001**
Septum/Heart mass (g/g)	0.11 ± 0.01	0.12 ± 0.01	0.30
Atria + Great Vessels (g)	7.2 ± 1.0	3.9 ± 0.7	**0.01**
Atria + Great Vessels/Heart mass (g/g)	0.28 ± 0.03	0.28 ± 0.03	0.92
Soleus (g)	0.28 ± 0.05	0.11 ± 0.01	**0.004**
Gastrocnemius (g)	9.2 ± 0.4	5.2 ± 0.5	**<0.0001**
Flexor digitorum superficialis (g)	2.8 ± 0.1	1.5 ± 0.2	**<0.0001**
Tibialis anterior (g)	3.6 ± 0.2	2.0 ± 0.7	**<0.0001**
Summed hindlimb muscle* (g)	15.9 ± 0.5	8.75 ± 0.9	**<0.0001**
Summed hindlimb muscle/Fetal weight (g/Kg)	4.7 ± 0.1	4.2 ± 0.1	**0.007**
Total Placentome Weight (g)	348 ± 20	153 ± 16	**<0.0001**
Uteroplacental Weight (g)	1433 ± 58	793 ± 58	**<0.0001**
Fetal Blood Gas Measurements			
Hemoglobin (mmol/L)	7.6 ± 0.3	9.3 ± 0.4	**0.003**
pH	7.4 ± 0.01	7.3 ± 0.01	0.49
$PaCO_2$ (mmHg)	48.7 ± 0.8	49.3 ± 0.8	0.63
PaO_2 (mmHg)	22.6 ± 0.6	18.4 ± 1.2	**0.006**
Plasma Substrates and Hormone Concentrations			
Glucose (mg/dL)	14.8 ± 0.8	9.4 ± 0.8	**<0.0001**
Lactate (mmol/L)	1.3 ± 0.1	1.9 ± 0.5	0.27
IGF-1 (ng/mL)	147 ± 14	74 ± 12	**<0.001**
Insulin (ng/mL)	0.25 ± 0.07	0.14 ± 0.03	0.12
Cortisol (ng/mL)	35.2 ± 6.1	45.2 ± 10.2	0.44

*Gastrocnemius, Tibialis Anterior, Flexor Digitorum Superficialis, Soleus.
Values are means ± SEM. Differences between FGR and CON were evaluated by Student's *t* test.

III. SPECIFIC AIM 1

CARDIOMYOCYTES of GROWTH RESTRICTED FETUSES HAVE REDUCED PROLIFERATION RATES and INCREASED POLYPLOIDY

Manuscript in Review:

Neeka Barooni, Byron Hetrick, Laura D. Brown, Carrie E. McCurdy, Eileen I. Chang. Cardiomyocytes of growth restricted fetuses have reduced proliferation rates and increased polyploidy.

Introduction

Fetal growth restriction (FGR) increases the risk of cardiometabolic disease and heart failure in adulthood (2, 6, 200). FGR is primarily caused by placental insufficiency, which limits oxygen and nutrient delivery to the developing fetus, disrupting normal fetal growth programs (104). In FGR, blood flow is maintained to prioritize vital organs at the expense of other tissues (201–203), resulting in significant reductions in lean mass that persist postnatally (104, 111). Despite receiving preferential blood flow *in utero*, FGR hearts exhibit maladaptive growth patterns that increase vulnerability to cardiac dysfunction in later life (188, 204–207). However, the mechanisms underlying inadequate fetal cardiac muscle development remain unclear.

The fetal heart grows by cardiomyocyte proliferation, differentiation, and enlargement (117, 146, 149). In humans and sheep, cardiomyocyte number is fixed shortly after birth, and subsequent cardiac growth can only be achieved by hypertrophic enlargement (118, 208, 120, 209, 210). During fetal development, cells undergo DNA replication and cell division to expand the cardiomyocyte population. In late gestation, DNA synthesis becomes uncoupled from cytokinesis as mononucleated cardiomyocytes begin to differentiate into mature, binucleated cells (117, 149,

211). At 90% gestation, about 40% of left and right ventricular (LV, RV) myocytes have permanently exited the cell cycle and become binucleated while 60% remain mononucleated and diploid (118). Additionally, fetal cardiomyocytes have been observed to replicate DNA in the absence of cytokinesis through endoreplication or endocycling, but current understanding of the mechanisms and implications of cardiomyocyte polyploidy is limited (212–214).

Deficits in cardiac muscle growth in FGR fetuses are attributed to decreased cardiomyocyte number, volume, and maturation, all of which have strong associations with poor cardiovascular outcomes in adulthood (115, 188, 200, 215, 216). Sheep models of FGR induced by placental insufficiency identify fewer $Ki67^{+}$ cardiomyocytes and decreased expression of cell cycle regulatory genes in FGR hearts compared normally-growing control (CON) fetuses of the same gestational age (115, 188, 215). Previous studies also observe reductions in the percent of mature, binucleated cardiomyocytes in the LV and RV of late gestation FGR sheep (115, 188, 215, 216), indicating that cardiac deficits in FGR offspring may result from decreased cell cycle induction or dysregulated cardiomyocyte differentiation during a critical window of development. However, as current methods of cardiomyocyte analysis rely on snapshots of cell cycle activity, the capacity to distinguish between DNA synthesis for cell division, terminal differentiation, and polyploidy remains limited (217).

Leveraging novel, high throughput analyses of cardiomyocyte ploidy and DNA replication *in utero*, we tested whether reductions in fetal LV and RV proliferation or differentiation could explain deficits in FGR cardiac muscle growth. We hypothesized that the frequency of proliferating cardiomyocytes, indicated by the number of diploid cells produced from DNA replication and cell division *in utero*, would be decreased in FGR fetuses. Additionally, FGR hearts

would have reductions in the fraction of non-replicating, binucleated LV and RV myocytes compared to CON. Using a well-established sheep model of placental insufficiency and FGR (198, 178, 131), we assessed cell cycle progression and *in vivo* DNA synthesis in fetal LV and RV cardiomyocytes. At 90% gestation, EdU (5-ethynyl-2'-deoxyuridine) was administered to all FGR and CON fetuses for 24 hours prior to tissue collection (131, 178). Flow cytometry was used to measure DNA content and detect EdU incorporation in the fraction of cycling cardiomyocytes.

Materials & Methods

Animal Model

Ewes carrying singleton pregnancies were randomly assigned to FGR (n=14) or CON (n=12) groups as previously described (218, 219) and illustrated in ***Figure 2.1***. To induce placental insufficiency and subsequent FGR, ewes were housed in an environmental chamber with elevated ambient temperatures (40°C for 12 hrs, 35°C for 12 hrs; 35-40% humidity) from 40 ± 1 to 81 ± 3 days gestation (dGA; term = 149 dGA). Pregnant ewes in the CON group were housed in an environmental chamber with normal ambient temperatures (21°C for 24 hrs; 35-40% humidity) from 40 ± 1 to 87 ± 9 dGA. Following environmental chamber exposure, ewes from both groups were housed at normal ambient temperatures for the remainder of the study. Maternal feed intake was similar between FGR and CON groups, and all ewes were given *ad libitum* access to water.

All animal studies were performed at the University of Colorado Perinatal Research Center (Aurora, CO) on Columbia–Rambouillet mixed-breed ewes that were bred and housed in environmental chambers at the University of Arizona (Tucson, AZ) and transported to the University of Colorado prior to any surgical procedures. Animal care and experimental protocols were approved by the University of Colorado Institutional Animal Care and Use Committee

(IACUC protocol #00334). All animal procedures were in compliance with the standards of the US Department of Agriculture, the National Institutes of Health, and the Association for Assessment and Accreditation of Laboratory Animal Care International. The manuscript adheres to the ARRIVE guidelines 2.0 for reporting animal research (220).

Surgical Procedures

Surgery was performed in late gestation pregnant ewes (126 ± 2 dGA) to place maternal and fetal catheters as previously described (131, 221–223). The maternal femoral vein was catheterized for the purpose of euthanasia. A fetal arterial catheter was placed into the pedal artery with the tip in the distal aorta and a fetal venous catheter was placed with the tip in the external iliac vein via the saphenous vein. Sheep were monitored after surgery and recovered for at least six days before experimentation.

Twenty-four hours prior to tissue collection (133 ± 1 dGA), EdU (5-ethynyl-2'-deoxyuridine; Thermo Fisher Scientific Inc., Waltham, MA, USA; Cat. #A10034) diluted in 0.9% NaCl was administered by intravenous bolus directly to the fetus at a dose of 10 mg/kg estimated fetal weight. Considering the frequency and estimated 20-hour duration of cell cycle activity in late gestation fetal sheep (14), all cycling cardiomyocytes are likely to be detected by the 24-hour EdU pulse administered prior to necropsy. Fetal weight was estimated based on measures of lower extremity length at the time of surgery. On the morning of fetal tissue collection (134 ± 1 dGA), fetal arterial blood was collected to measure O_2 content, pH, partial pressure of CO_2 (P_aCO_2), and partial pressure of O_2 (PaO_2) as previously described (124). Fetal plasma glucose and lactate concentrations were measured by YSI 2900 Biochemistry Analyzer (YSI Inc., Yellow Springs, OH, USA) and concentrations of fetal plasma insulin, insulin-like growth factor 1 (IGF-1), and

cortisol were measured by ELISA (124). Ewes were administered intravenous anesthesia (0.2 $mg \cdot kg^{-1}$ diazepam and 20 $mg \cdot kg^{-1}$ ketamine), and fetuses were delivered by maternal laparotomy and hysterotomy. All animals were then euthanized with a lethal dose of pentobarbital sodium (Fatal Plus, Vortech Pharmaceuticals, Dearborn, MI, USA). Fetal sheep were weighed immediately prior to tissue collection and processing of the heart and other organs.

Isolation of Fetal Cardiomyocytes

Fetal hearts were weighed and dissected into LV and RV free walls, septum, and atria with great vessels (trimmed at the bifurcation, approximately 1 cm of ascending aorta and the pulmonary artery). The LV, RV, septum, and atria were weighed and recorded. Then biopsies of approximately 1.5 to 2 cm^2 were excised from the center of the LV and RV for the isolation of primary cardiomyocytes and the remaining tissue was flash frozen in liquid nitrogen and stored at -80°C. The LV and RV biopsies were quickly submerged in ice cold Gibco™ Ham's F-12 Nutrient Mix (ThermoFisher Scientific, Waltham, MA, USA) and washed twice with Hanks' Balanced Salt Solution (HBSS, MilliporeSigma, St. Louis, MO, USA). The epicardial fat and coronary vessels were carefully removed from each ventricular biopsy, and the cardiac muscle was minced and digested in 1% collagenase (Gibco™ Collagenase Type II; ThermoFisher Scientific, Waltham, MA, USA; Cat. #17101015) suspended in HBSS for 30 minutes at 37°C. To stop enzymatic dissociation, 0.5% bovine serum albumin in HBSS was added to the digested tissue in a 1:1 volume ratio. The cell suspension was filtered through 100 µm, 70 µm, and 40 µm cell strainers and centrifuged at 300 x g for 10 minutes at 25°C. The cell pellet was washed in 1X phosphate-buffered saline (PBS) and centrifuged at 450 x g for 5 minutes at 25°C. Cardiomyocytes were fixed in 2%

paraformaldehyde for 15 minutes, then washed and resuspended in 1X PBS. All cells were stored in 1X PBS at 4°C prior to flow cytometry.

Cardiomyocyte Staining

Fixed LV and RV cardiomyocytes were washed with 1X PBS and resuspended in 1X incubation buffer (0.2% Triton X-100 and 1% BSA in 1X PBS) for 15 minutes at 25°C. The permeabilized cells were centrifuged for 5 minutes at 500 x g and Click-iT Plus EdU-AF647 detection assay (EdU-AF647; Thermo Fisher Scientific Inc., Waltham, MA, USA; Cat. #C10635, Lot 2549284) was prepared according to manufacturer instructions. Cardiomyocytes were incubated in 0.5 µL Click-iT EdU detection mixture for 30 minutes at 25°C, then cells were pelleted and washed in 1X incubation buffer. LV and RV cardiomyocytes were identified by staining with 1 µg CD56 primary antibody conjugated to PerCP/Cyanine5.5 (CD56-PC5.5; BioLegend, San Diego, CA, USA; Cat. #304626, Lot B354365) in 0.1 mL incubation buffer for 30 minutes at 25°C. The cell suspension was washed and centrifuged, and samples were stained with 3 µM of DAPI (Cayman Chemical, Ann Arbor, Michigan, USA; Cat. #14285, Lot 0514078-29) in 0.3 mL incubation buffer for 15 minutes at 25°C directly prior to data acquisition. For all wash steps, cells were resuspended in 2 mL of 1X PBS or 1X incubation buffer (as specified) and centrifuged at 500 x g for 5 minutes at 25°C before decanting the supernatant.

Flow Cytometry Analysis

Cardiomyocytes were identified in flow cytometry scatter plots by cell size, internal complexity, and staining for anti-CD56 and DAPI. The relative quantity of DNA in each cell was estimated by DAPI fluorescence intensity, and a gate was drawn to select only the DAPI-positive

cells. Any debris or cell fragments containing less than one copy of DNA were excluded from further analysis (***Fig. 3.1A***). Next, forward scatter height (FS-H) was plotted against forward scatter area (FS-A) to remove clumped or stuck together cells that were measured as one event. Single cells (singlets) were identified by a diagonal gate that included only the events for which FS-H and FS-A were directly proportional (***Fig. 3.1B***). DAPI-positive singlets were carried forward for assessment of CD56-PC-Cy5.5 staining. LV and RV cardiomyocytes were selected by CD56-positive gating (***Fig. 3.1C***), and all subsequent analyses of DNA content and EdU incorporation were restricted to CD56-positive, DAPI-positive singlets.

Within the selected LV and RV cardiomyocyte populations, DAPI staining was used to measure cellular DNA content and determine the frequency distribution of cardiomyocyte ploidy. Cardiomyocytes clustered into three distinct DAPI peaks with increasing fluorescence intensity that identified cells with one, two, and three or more complete copies of the genome (***Fig. 3.1D***). Gates were created to quantify each DAPI peak, and all cardiomyocytes were classified by ploidy values representing the DNA content in each cell. Diploid cells with one complete copy of DNA, condensed into two sets of chromosomes, are described as 2C cardiomyocytes. Cardiomyocytes containing twice as much DNA are labeled as 4C or tetraploid cardiomyocytes. Polyploid cardiomyocytes containing three or more copies of DNA are denoted by 6C+. The number of cardiomyocytes within each gate (2C, 4C, 6C+) was divided by the total LV or RV myocytes (CD56+, DAPI+, singlets) to determine the frequency distribution of cellular DNA content in each ventricle.

Cardiomyocyte ploidy can inform estimations of cell cycle progression and proliferation. However, reliable determination of proliferation versus terminal differentiation is challenging, as

cardiomyocytes engaged in active proliferation and those undergoing multinucleation are indistinguishable by flow cytometry analysis of DAPI alone (213, 224). Therefore, we combined measurements of cellular DNA content (DAPI) and *in vivo* DNA synthesis (EdU incorporation) to identify subpopulations of proliferating, differentiating, and endocycling cardiomyocytes. DAPI signal was plotted against EdU-AF647 to create six distinct populations that clustered by ploidy class and the rate of DNA synthesis *in utero* (***Fig. 3.1E-F***). All EdU-positive cardiomyocytes are located in the upper sections of this plot and were quantified using the green rectangular gate. Subsequent gates were set based on DAPI signal intensity to label proliferating, endocycling, and terminally differentiated cardiomyocytes. We defined cardiomyocyte proliferation as the fraction of cells that replicated DNA and completed cytokinesis in utero (2C EdU+). Terminally differentiated cardiomyocytes were identified by non-replicating, binucleated cells (4C EdU-), and polyploid cells engaged in DNA synthesis (6C+ EdU+) indicated the fraction of endocycling cardiomyocytes *in utero*.

Flow cytometry was performed on a Beckman Coulter CytoFLEX flow cytometer (Beckman Coulter, Indianapolis, IN, USA) and data were analyzed with Kaluza Analysis Software 2.2 (Beckman Coulter, Indianapolis, IN, USA). Gate placement was determined by comparing positive and negative fluorescence peaks from cardiomyocytes that were unstained, stained with a single antibody, or stained with all but one antibody (i.e. fluorescence minus one controls). Fetuses from twin pregnancies were removed from the analysis, and two animals were excluded due to low cell counts (fewer than 7,000 cardiomyocytes) and poor DAPI and/or EdU-AF647 resolution. The n value for each condition is reported in the associated figure legend.

Statistical Analysis

A student's unpaired t-test was used for direct comparison of FGR versus CON groups. Due to random and unequal distribution of fetal sex across treatment groups (FGR: 7M/6F, CON: 1M/10F), we were not able to assess sex differences in this study, though male and female fetuses are noted by triangles and circles, respectively. Correlations between cardiomyocyte parameters and fetal weight, heart or ventricle weight, and circulating hormones were measured in all fetuses (FGR and CON combined) by Pearson correlation coefficient. Statistical analyses were performed in GraphPad Prism (GraphPad Software, La Jolla, CA, USA, Version 10.2.2) and significance was determined at $P \leq 0.05$. Data are presented as mean ± standard error of the mean (SEM) and exact *P*-values are specified.

Results

Fetal Physiology

Physiological characteristics of FGR and CON fetuses are provided in ***Table 2.1***. Body mass was reduced by 40% in FGR fetuses compared to CON. Heart mass was lower in FGR fetuses, even when normalized to total body mass. LV and RV mass decreased by 39% and 34%, respectively, in FGR hearts compared to CON. Plasma insulin and cortisol levels were similar between groups. However, FGR fetuses had lower circulating glucose, PaO_2, and IGF-1 compared to CON.

LV cardiomyocyte ploidy

Flow cytometry analysis of LV myocytes revealed differences in the distribution of cardiomyocyte ploidy in FGR and CON hearts (***Fig. 3.2A***). In the LV, FGR fetuses had an

increased proportion of 2C cardiomyocytes, fewer 4C cardiomyocytes, and a similar percentage of 6C+ cardiomyocytes compared to CON fetuses (***Fig. 3.2B***). Correlations between LV mass and the percentage of cells in each ploidy class were tested across all fetuses to assess whether cardiomyocyte ploidy distribution was linked to LV growth. There was no association ($p = 0.09$) between 2C cardiomyocytes and LV mass (***Fig. 3.2C***). However, the percent of 4C cardiomyocytes correlated positively with LV mass (***Fig. 3.2D***), indicating a link between cardiomyocyte proliferation (i.e. G2) or differentiation (i.e. binucleated cells) and increased cardiac muscle growth. Although the proportion of polyploid cells was similar between FGR and CON groups, correlation analysis revealed a negative linear relationship between 6C+ cardiomyocytes and LV mass across all fetuses (***Fig. 3.2E***).

RV cardiomyocyte ploidy

As in the LV, RV myocytes were classified by DNA copy number to determine the distribution of cardiomyocyte ploidy (***Fig. 3.3A***). FGR and CON fetuses had similar proportions of 2C cardiomyocytes in the RV, but the percentage of 4C cardiomyocytes was reduced in FGR fetuses compared to CON (***Fig. 3.3B***). The percentage of 6C+ cardiomyocytes was similar between groups but trended higher in FGR hearts ($p = 0.06$). There was no relationship between RV mass and the proportion of 2C cardiomyocytes (***Fig. 3.3C***). However, RV mass correlated positively with 4C cardiomyocytes (***Fig. 3.3D***) and negatively with 6C+ cardiomyocytes (***Fig. 3.3E***).

LV cardiomyocyte proliferation, differentiation, and polyploidy

Robust differences in the growth patterns of FGR and CON hearts were detected by calculating the percentage of cardiomyocytes in each subpopulation relative to the total number of LV or RV cardiomyocytes in each animal. FGR fetuses had fewer EdU-positive cardiomyocytes in the LV compared to CON (***Fig. 3.4A***). The percentage of cardiomyocytes that completed cytokinesis after DNA replication, indicated by the 2C EdU-positive population, was similar (p = 0.08) between FGR and CON fetuses (***Fig. 3.4B***). The proportion of 4C EdU-positive LV myocytes was also comparable across groups (***Fig. 3.4C***). However, FGR hearts had nearly twice the percentage of endocycling, 6C+ EdU-positive cardiomyocytes compared to CON (***Fig. 3.4D***). LV mass was not associated with total cell cycle activity (***Fig. 3.4E***) or with 2C and 4C EdU-positive cells normalized to all LV cardiomyocytes (***Fig. 3.4F-G***). There was, however, a negative linear relationship between LV mass and the percentage of 6C+ EdU-positive cardiomyocytes across all groups (***Fig. 3.4H***).

To determine whether FGR fetuses differentially prioritized their cycling capacity in favor of cardiomyocyte proliferation, differentiation, or endoreplication, the ploidy distribution of all EdU-positive cardiomyocytes was evaluated in reference to the total number of EdU-positive cells in each ventricle (***Fig. 3.4I-K***). In the LV, FGR fetuses had fewer EdU-positive cardiomyocytes in 2C and an increased percentage of EdU-positive cardiomyocytes in 6C+ compared to CON (***Fig. 3.4I***). LV mass correlated positively with the percentage of 2C EdU-positive cardiomyocytes (***Fig. 3.4J***) and negatively with 6C+ EdU-positive cardiomyocytes normalized to all EdU-positive cells (***Fig. 3.4K***). Additionally, the proportion of non-replicating, binucleated (4C EdU-negative) cardiomyocytes was reduced in FGR fetuses compared to CON (***Fig. 3.4L***), and LV mass

correlated positively with the percentage of 4C EdU-negative cardiomyocytes in the LV (***Fig. 3.4M***).

RV cardiomyocyte proliferation, differentiation, and polyploidy

In the RV, FGR fetuses had decreased total cell cycle activity compared to CON (***Fig. 3.5A***). When normalized to all RV cardiomyocytes, the percentages of 2C and 4C EdU-positive cells were decreased in FGR hearts (***Fig. 3.5B-C***), while the proportion of 6C+ EdU-positive cardiomyocytes was increased in FGR compared to CON (***Fig. 3.5D***). RV mass correlated positively with the total percentage of EdU-positive cardiomyocytes (***Fig. 3.5E***), as well as the proportions of 2C and 4C EdU-positive cardiomyocytes in the RV (***Fig. 3.5F-G***). Additionally, RV mass was negatively associated with the proportion of 6C+ EdU-positive cardiomyocytes across all FGR and CON fetuses (***Fig. 3.5H***).

When expressed relative to the total number of EdU-positive cardiomyocytes, the percentage of 2C EdU-positive cells was decreased in FGR hearts (***Fig. 3.5I***). FGR and CON fetuses had similar percentages of 4C EdU-positive cells, but the proportion of 6C+ EdU-positive cardiomyocytes was significantly higher in FGR compared to CON (***Fig. 3.5I***). Consistent with the findings noted above, correlation analyses revealed a positive relationship between RV mass and 2C EdU-positive cardiomyocytes (***Fig. 3.5J***) and a negative relationship between RV mass and 6C+ EdU-positive RV myocytes (***Fig. 3.5K)***. The proportion of differentiated (4C EdU-negative) RV cardiomyocytes was similar between FGR and CON groups (***Fig. 3.5L***) but tended to increase ($p = 0.06$) with RV mass (***Fig. 3.5M***).

Associations between circulating factors and ventricular mass

FGR fetuses had lower levels of IGF-1, glucose, and PaO_2 compared to CON (***Table 1***). To assess potential relationships between ventricular growth and fetal substrate and hormone availability *in utero*, LV and RV mass were correlated against concentrations of circulating factors in all FGR and CON sheep. Fetal LV and RV mass correlated positively with circulating levels of IGF-1, glucose, and PaO_2 (***LV: Fig. 3.6A-C, RV: Fig. 3.6F-H***), while fetal insulin and cortisol concentrations were not associated with ventricular growth in late gestation (***LV: Fig. 3.6D-E, RV: Fig. 3.6I-J***).

Associations between IGF-1 and cardiomyocyte growth programs

Given that IGF-1 was associated with increased LV and RV mass, correlation analyses were performed to assess the relationships between circulating levels of IGF-1 and fetal cardiomyocyte proliferation, differentiation, and endoreplication *in utero*. IGF-1 correlated negatively with the percentage of 2C cardiomyocytes (***Fig. 3.7A***) and positively with the percentage of 4C cardiomyocytes in the LV (***Fig. 3.7B***). Fetal IGF-1 levels were not associated with total cell cycle activity in LV cardiomyocytes (***Fig. 3.7C***). There was an inverse relationship between circulating IGF-1 and the percent of 6C+ EdU-positive cells, normalized to all LV cardiomyocytes (***Fig. 3.7D***). Additionally, IGF-1 correlated positively with the proportion of binucleated, terminally differentiated cardiomyocytes in the LV (***Fig. 3.7E***). Similar relationships were observed between LV cardiomyocytes and levels of glucose and PaO_2 in fetal circulation (***Supplemental Fig. 3.1***).

In the RV, IGF-1 levels correlated positively with the proportion of 4C cardiomyocytes (***Fig. 3.7F***) and negatively with the proportion of 6C+ cardiomyocytes (***Fig. 3.7G***). Similar to the LV, there was no significant (p = 0.07) relationship observed between IGF-1 and total RV cell cycle activity (***Fig. 3.7H***). However, fetal IGF-1 was linked to RV proliferation, indicated by positive correlations with 2C and 4C EdU-positive cardiomyocytes (***Fig. 3.7I-J***). Glucose concentrations were linked to increased 4C and decreased 6C+ cardiomyocytes, but there were no additional relationships observed between RV cardiomyocytes and circulating glucose or PaO_2 (***Supplemental Fig. 3.2***).

Discussion

We developed a flow cytometry-based strategy to determine how cardiomyocyte growth patterns are impacted by placental insufficiency and FGR. Our findings are summarized in ***Figure 3.8***. Briefly, we found that FGR fetuses had lower rates of cardiomyocyte proliferation (2C EdU+), despite the availability of an equivalent or larger pool of mononucleated (2C) cells. The percentage of terminally differentiated (4C EdU-) cardiomyocytes was reduced in the LV of FGR fetuses, though endoreplication (6C EdU+) was upregulated in both ventricles of FGR hearts compared to CON. Correlation analysis revealed that LV mass was positively associated with the proportion of mature, binucleated cardiomyocytes, while RV mass correlated with increased cardiomyocyte proliferation across all animals. Fetal IGF-1 concentrations were linked to increased ventricular mass and predicted rates of cardiomyocyte proliferation, differentiation, and polyploidy in late-gestation fetal sheep.

Studies have traditionally relied on labor- and time-intensive cell counting techniques and single markers of cell cycle activity to investigate whether cardiomyocyte growth programs are

compromised in FGR fetuses (115, 116, 188, 204, 209, 215, 225–229). However, given that DNA synthesis is integral to cardiomyocyte proliferation, differentiation, and endoreplication (230–232), current methods do not account for the possibility of binucleation or polyploidy following cell cycle entry (217, 224, 233), though both outcomes are observed during fetal development (117, 118, 234, 235). To address this critical gap in knowledge, we developed an innovative approach that combines *in vivo* DNA labeling with measures of cell cycle progression to reliably differentiate between cardiomyocyte division and the formation of multinucleated or polyploid cells (235–242). Our technique leverages high-throughput flow cytometry to analyze over 40,000 LV and RV cardiomyocytes per animal, a substantial increase from previous assessments that were limited to fewer than 600 cells. Due to the unequal distribution of male and female fetuses, we were not powered to test for sex differences, and further studies are needed to evaluate potential interactions between FGR and fetal sex. However, our analysis of FGR versus CON hearts should not be skewed by the predominantly female control group as females are reported to have smaller hearts than age-matched males (116, 292). To our knowledge, this study is the first to employ dynamic measures of *in vivo* cell cycle activity to differentiate between cardiomyocyte proliferation, binucleation, and endoreplication in FGR fetuses.

Consistent with previous reports (115, 188, 215, 225, 226), we found that cell cycle activity was reduced in FGR hearts. However, by evaluating cardiomyocyte trajectories over a 24-hour period and measuring cytokinesis following DNA synthesis, we were able to differentiate changes in cell cycle activity associated with cardiomyocyte division from those accompanying terminal differentiation or polyploidy. Our analysis revealed decreased rates of cardiomyocyte proliferation in FGR fetuses compared to CON. While the RV showed more pronounced deficits in the overall

percentage of dividing cardiomyocytes, the proportion of 2C EdU+ cells relative to all actively cycling cardiomyocytes was reduced in the LV and RV of FGR fetuses. Correlations across all animals indicate that cardiomyocyte proliferation plays a critical role in RV growth during late gestation but has minimal impact on LV mass at this stage of development. This difference is attributed to the distinct timing of LV versus RV maturation, as LV cardiomyocytes begin terminal differentiation earlier in gestation and RV cardiomyocytes continue to proliferate until shortly after birth (118). Interestingly, we identified a shift towards greater rates of endoreplication in both ventricles FGR hearts, indicating a departure from proliferation and cardiomyocyte expansion in favor of increasing cellular ploidy. While differences in the proportion of polyploid cardiomyocytes have not been reported in models of FGR, likely due to limitations in current techniques, increased polyploidy has been observed in preterm fetal hearts (155) and other models of stress exposure during perinatal development (214, 235, 243–248) and adulthood (156, 159, 249–255). This finding aligns with prior evidence that several key cell cycle regulatory factors are suppressed in FGR hearts (115), including genes involved in G2/M progression, spindle assembly, and cytokinesis. Collectively, these data suggest that impairments in cardiomyocyte proliferation and endoreplication may be driven by dysregulated signaling for cell cycle progression and disrupted mitosis.

We observed decreased binucleation and significant reductions in the percentage of mature, terminally differentiated cardiomyocytes in the LV of FGR fetuses compared to CON. The strong positive correlations between LV mass and the percentages of binucleated (4C) and terminally differentiated (4C EdU-) cardiomyocytes suggest that the degree of cardiomyocyte maturation is a primary determinant of LV growth during late gestation. These findings confirm previously

reported deficits in cardiomyocyte binucleation following placental insufficiency (115, 188, 204, 215) or pre-term birth (155, 256) and support observations of more severe reductions in cardiomyocyte maturity in the LV compared to the RV of FGR hearts. Cardiomyocyte differentiation includes a final round of DNA replication, followed by nuclear division (karyokinesis) in the absence of cytokinesis (117, 118, 149, 215, 257). Therefore, deficits in the proportion of mature, binucleated cardiomyocytes result from altered cell cycle regulation or disrupted differentiation programs. Given that the percentages of 2C EdU+ and 4C EdU+ cardiomyocytes were similar in the LV of FGR and CON fetuses, we theorize that the decreased proportion of binucleated LV cardiomyocytes in FGR hearts results from impaired signaling for terminal differentiation and maturation rather than insufficient DNA replication. Since differentiation is an energetically costly process involving substantial changes to cardiomyocyte size, morphology, metabolism, and sarcomere structure (118, 149, 204, 208, 257–259), reductions in cardiomyocyte maturation could be mediated by limited oxygen, nutrient, and/or growth factor availability in FGR fetuses. Moreover, previous studies have demonstrated that fetal cardiomyocytes are sensitive to systemic pressures and can alter the degree of binucleation and cellular hypertrophy in response to changes in cardiac loading. Additionally, our analysis showed that in FGR fetuses, a greater proportion of binucleated LV cardiomyocytes continued endocycling, increasing DNA content in one or both nuclei instead of withdrawing from the cell cycle to complete terminal differentiation. This may represent an adaptive response in which FGR cardiomyocytes increase cellular ploidy to help manage cardiac workload and compensate for reductions in the total number of cardiomyocytes.

An unexpected but notable finding was the elevated rates of endoreplication in LV and RV cardiomyocytes of FGR fetuses. The preference for increasing ploidy in FGR hearts appeared to occur at the expense of terminal differentiation in the LV and cardiomyocyte proliferation in the RV. This is likely due to differences in the timing of LV and RV cardiomyocyte growth programs. As demonstrated in other models of environmental stress, cardiomyocytes may increase DNA replication in the absence of cell division to mitigate the consequences of anticipated DNA damage, or to improve mitochondria quality control in the presence of elevated reactive oxygen species (116, 212, 219, 237, 247, 253, 260). Additionally, cardiomyocyte polyploidy might represent an energetically favorable strategy to preserve cardiac muscle mass and contractile function following intrauterine exposure placental insufficiency and FGR. By amplifying cellular DNA content, endoreplication is likely to enhance the capacity for transcription and hypertrophic growth without requiring cytoskeleton reorganization or the disruption of cell junctions (119, 211, 212, 216, 254, 261). Thus, FGR fetuses may prolong cell cycle activity to counteract reductions in cardiomyocyte number and cardiac muscle mass. Evidence of FGR cardiomyocyte hypertrophy at the fetal time point is inconsistent, as some studies report hypertrophic cardiomyocyte remodeling (155, 262), while others show that cardiomyocyte size is reduced in late-gestation fetuses (115, 188) or similar between FGR and CON hearts (204, 215). We found strong negative correlations between LV and RV mass and the proportion of 6C EdU+ cardiomyocytes, suggesting that endoreplication impedes ventricular growth in late gestation. However, further research is needed to confirm cardiomyocyte size in FGR fetuses. Still, we postulate that increased endocycling in fetal cardiomyocytes may contribute to the pathological cardiac hypertrophy observed in children and adults with prior FGR, linking fetal adaptations to the development of cardiovascular disease.

To identify potential mediators of cardiomyocyte programming *in utero*, we evaluated the relationships between LV and RV growth and several nutrient and growth factors in fetal circulation. Our analysis revealed positive correlations between fetal LV and RV mass and concentrations of glucose, PaO_2, and IGF-1. We observed that circulating levels of IGF-1 were linked to increased cardiomyocyte proliferation in the RV and a greater proportion of binucleated, terminally differentiated cardiomyocytes in the LV. These findings suggest that the reduced rates of cardiomyocyte proliferation and differentiation in FGR fetuses may be partially attributed to deficits in IGF-1, though it is important to note that similar relationships were detected with fetal glucose and PaO_2. Our data also demonstrated negative correlations between fetal IGF-1 levels and cardiomyocyte polyploidy but showed no associations with total cell cycle activity in either ventricle. Based on these observations, we postulate that IGF-1 signaling may specifically interact with the pathways governing cardiomyocyte division, rather than broadly promoting cell cycle activity across all cardiomyocytes. Our results align with previous research that links fetal IGF-1 concentrations to increased cardiomyocyte numbers in FGR and CON sheep. Likewise, exogenous IGF-1 has been implicated in stimulating cardiomyocyte proliferation, maturation, and enlargement *in utero*, and recent work establishes a dual role for IGF-1 in regulating both proliferation and differentiation of skeletal muscle myoblasts. It is therefore possible that IGF-1 signaling may elicit distinct responses depending on the stage of development or whether cardiomyocytes are mononucleated versus binucleated. Though further research is needed to understand the mechanisms through which IGF-1 activates these divergent programs, our findings suggest that deficits in circulating IGF-1 may play a critical role in moderating the reductions in cardiomyocyte proliferation and maturation observed in FGR fetuses.

By offering insight into cardiomyocyte growth programs in FGR fetuses, our results link lifelong cardiac dysfunction to the regulation of cardiomyocyte maturation *in utero* and provide new information to guide the development of effective intervention strategies. Our findings indicate that previously reported deficits in cardiomyocyte endowment likely result from decreased proliferation rates in FGR fetuses, potentially due to a preference for endoreplication and cardiomyocyte polyploidy. Likewise, deficits in cardiac maturity and contractile function may be attributed to reductions in the percentage of cardiomyocytes that have completed terminal differentiation by late gestation in FGR fetuses. While increased cellular ploidy could partially compensate for poor ventricular growth during fetal development, the concurrent deficits in cardiomyocyte expansion and maturation are of greater concern for long-term cardiac health. Given that mitotic activity is suppressed shortly after birth, inadequate cardiomyocyte expansion during fetal development limits the number of cells available to sustain cardiac function throughout the lifespan (120, 234, 263). Postnatal growth is restricted to cardiomyocyte hypertrophy, which cannot fully compensate for deficits in fetal cardiac development, and is directly linked to heart failure and cardiovascular disease in adulthood (200, 256, 264, 265). Moreover, reductions in the percentage of mature, binucleated LV cardiomyocytes may compromise FGR hearts by permanently decreasing the proportion of terminally differentiated cells with enhanced contractility. This could prematurely expose a larger population of immature cardiomyocytes to elevated systemic pressures before they develop the necessary structural, functional, and metabolic adaptations to tolerate the increased demand. As a result, FGR hearts are vulnerable to hemodynamic changes and highly susceptible to rapid, maladaptive remodeling during birth and early postnatal life. These modifications to cardiac growth and structure are associated with

compromised contractility and impaired relaxation, and due to programming during a critical window of development, perinatal adaptations are likely to persist into adulthood (149, 214, 219, 237, 259, 266). As cardiomyocyte numbers decline with age, and cardiac stress and dysfunction worsen, individuals with former FGR are increasingly likely to develop cardiovascular complications later in life (200, 205, 207).

Using a novel approach to evaluate cardiomyocyte growth patterns *in utero,* we determined that all stages of cardiomyocyte maturation—proliferation, differentiation and endoreplication—are impaired in FGR fetuses with exposure to placental insufficiency. Our data indicate that intrauterine stress stimulates cardiomyocyte endocycling and polyploidy at the expense of proliferation and terminal differentiation. This novel finding represents significant shifts in fetal cardiomyocyte programming, and future research is needed to determine the long-term implications of exaggerated cardiomyocyte polyploidy, especially in FGR. The differences observed between LV and RV growth patterns underscore the importance of considering the timing of therapeutic interventions aimed at restoring cardiomyocyte number and maturation in FGR fetuses. Additionally, our findings challenge the belief that stimulating cell cycle activity is sufficient to improve cardiomyocyte proliferation in FGR fetuses. Instead, we demonstrate that targeting cytokinesis is necessary to ensure cardiomyocyte division following successful DNA replication. Furthermore, effective treatments must regulate cell cycle withdrawal after binucleation to prevent endocycling and restore terminal differentiation in FGR hearts. Finally, our results suggest a critical role for IGF-1 in regulating cardiomyocyte proliferation and differentiation, highlighting it as a potential therapeutic target for restoring cardiac growth during fetal development.

Figures

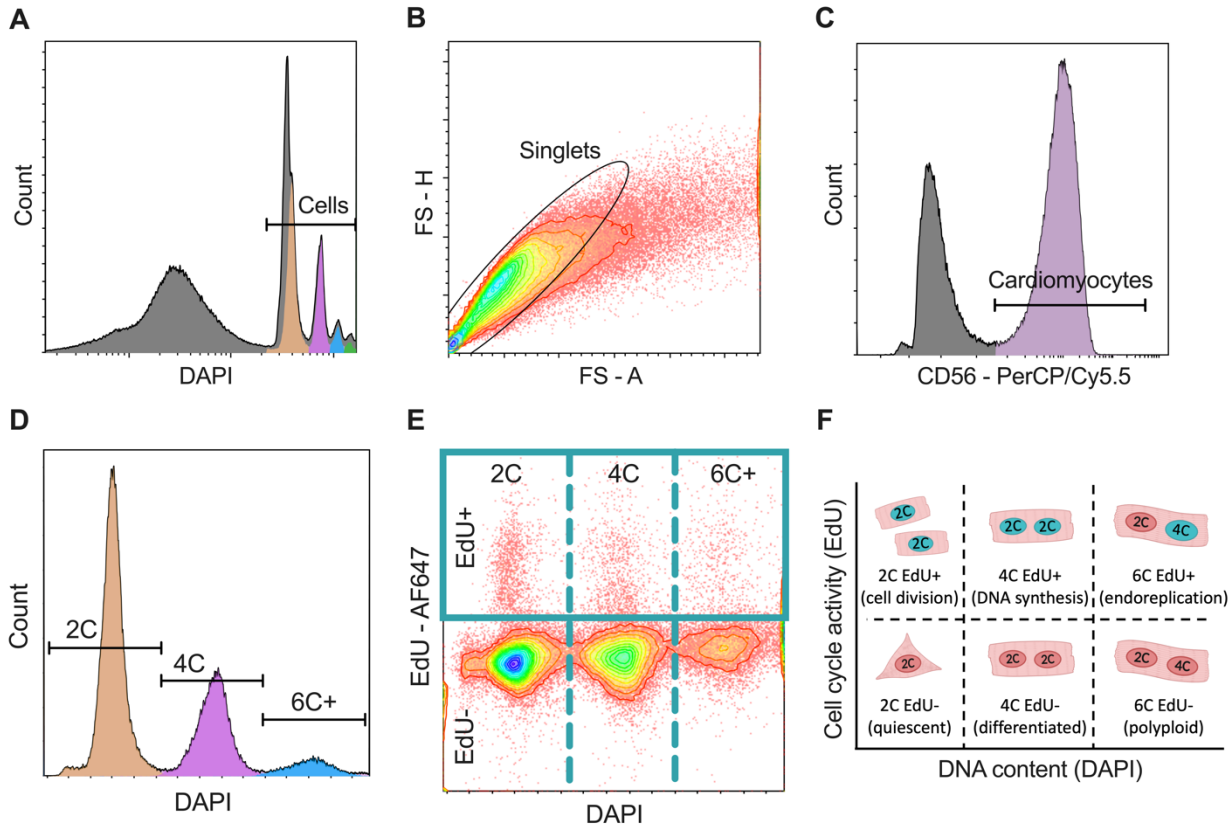

Figure III.1. Gating strategy for analysis of cardiomyocyte DNA content and EdU incorporation by flow cytometry. Representative plots of cardiomyocyte identification by (A) DAPI, (B) forward scatter height versus area, and (C) CD56-PC5.5 antibody. (D) Gating of 2C, 4C, and 6C+ cardiomyocytes based on DAPI fluorescence intensity. (E) Representative plot of DAPI versus EdU-AF647 staining and rectangular gate used to quantify all EdU-positive cardiomyocytes. Dashed, vertical lines separate EdU-positive and negative cardiomyocytes into subpopulations based on DNA content. (F) Graphic illustrating the cardiomyocyte subpopulations defined by each gate on the DAPI vs. EdU plot shown in ***Fig. 3.1E***.

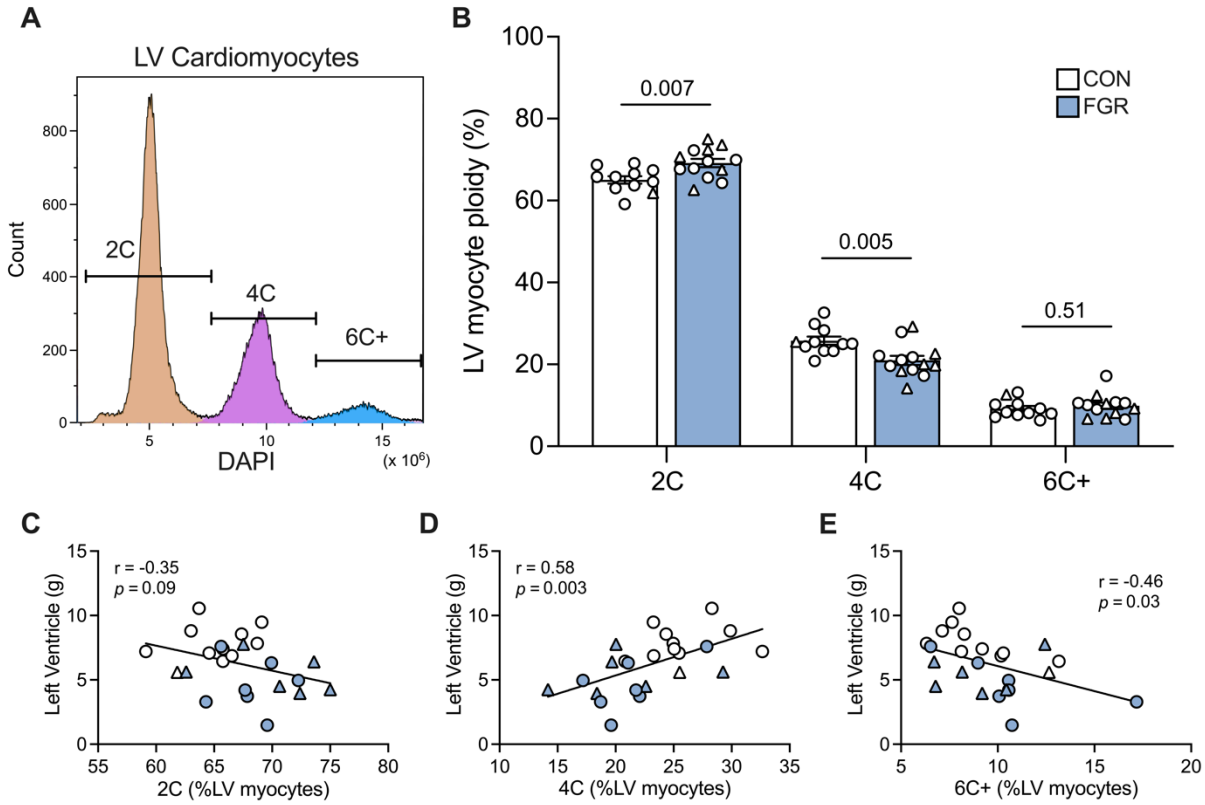

Figure III.2. The distribution of LV cardiomyocyte ploidy differs between FGR and CON fetuses. (A) Flow cytometry plot of DAPI signal and gating to quantify LV cardiomyocyte ploidy. (B) FGR fetuses had increased 2C cardiomyocytes, decreased 4C cardiomyocytes, and a similar percentage of 6C+ cardiomyocytes compared to CON. Data are shown as mean ± SEM and Student's t-test was used to determine differences between FGR (n=13) and CON (n=11) groups. (C) LV mass was not associated with the percentage of 2C cardiomyocytes but (D) correlated positively with 4C cardiomyocytes and (E) negatively with 6C+ cardiomyocytes across all FGR (blue/closed symbols) and CON (white/open symbols) fetuses (n=24). Pearson's correlation coefficients (r) and p-values are listed. Simple linear regressions were fit between LV mass and ploidy level, and best fit lines are plotted with raw data. Males and females are represented by triangles and circles, respectively.

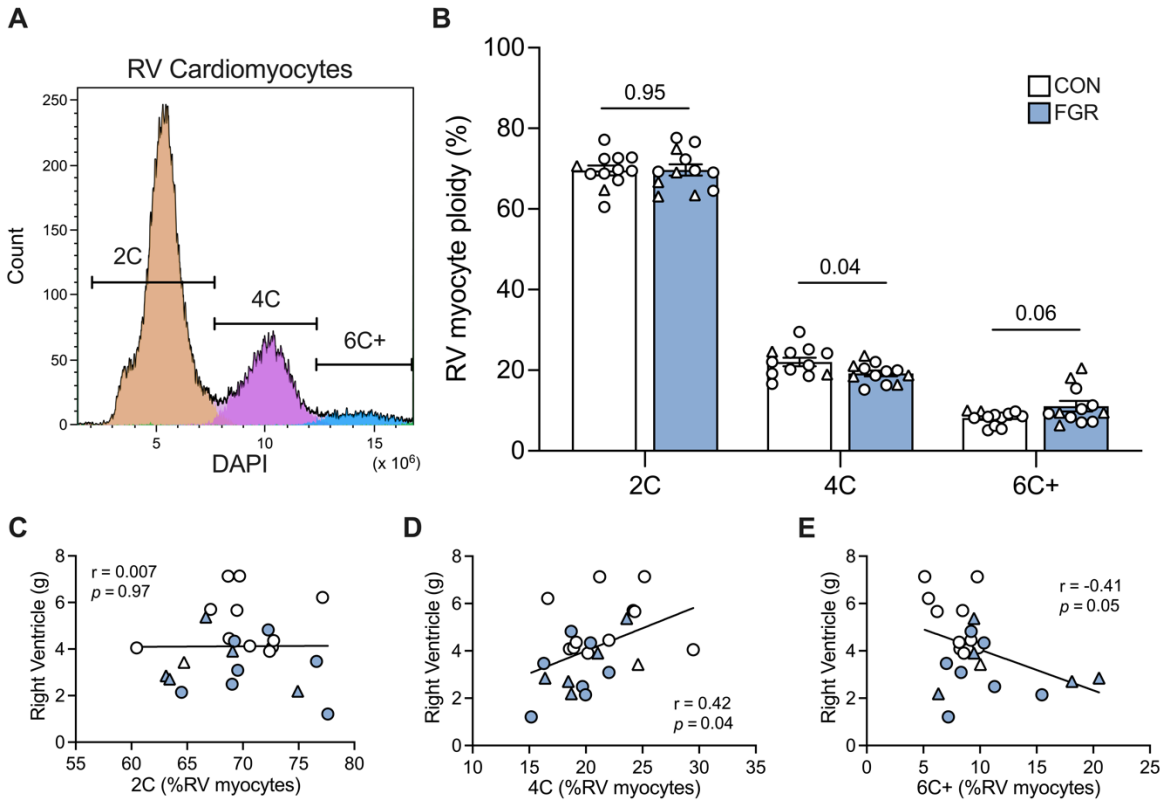

Figure 3.3. RV cardiomyocyte ploidy differs between FGR and CON fetuses. (A) Representative plot of gating to quantify cellular DNA content and determine RV cardiomyocyte ploidy. (B) FGR and CON fetuses had similar proportions of 2C cardiomyocytes in the RV. The percentage of 4C cardiomyocytes was lower in FGR and the percentage of 6C+ cardiomyocytes trended higher in the FGR group compared to CON. Differences between FGR (n=12) and CON (n=12) groups were determined by Student's t-test. Data are mean ± SEM, and exact *p*-values are listed for each condition. (C) No relationship was observed between RV mass and the percentage of 2C cardiomyocytes. However, RV mass was associated with (D) increased 4C cardiomyocytes and (E) decreased 6C+ cardiomyocytes across all FGR (blue/closed symbols) and CON (white/open symbols) fetuses (n=24). Simple linear regressions were fit between RV mass and cardiomyocyte population. Best fit lines and Pearson's correlation coefficients (r) are shown.

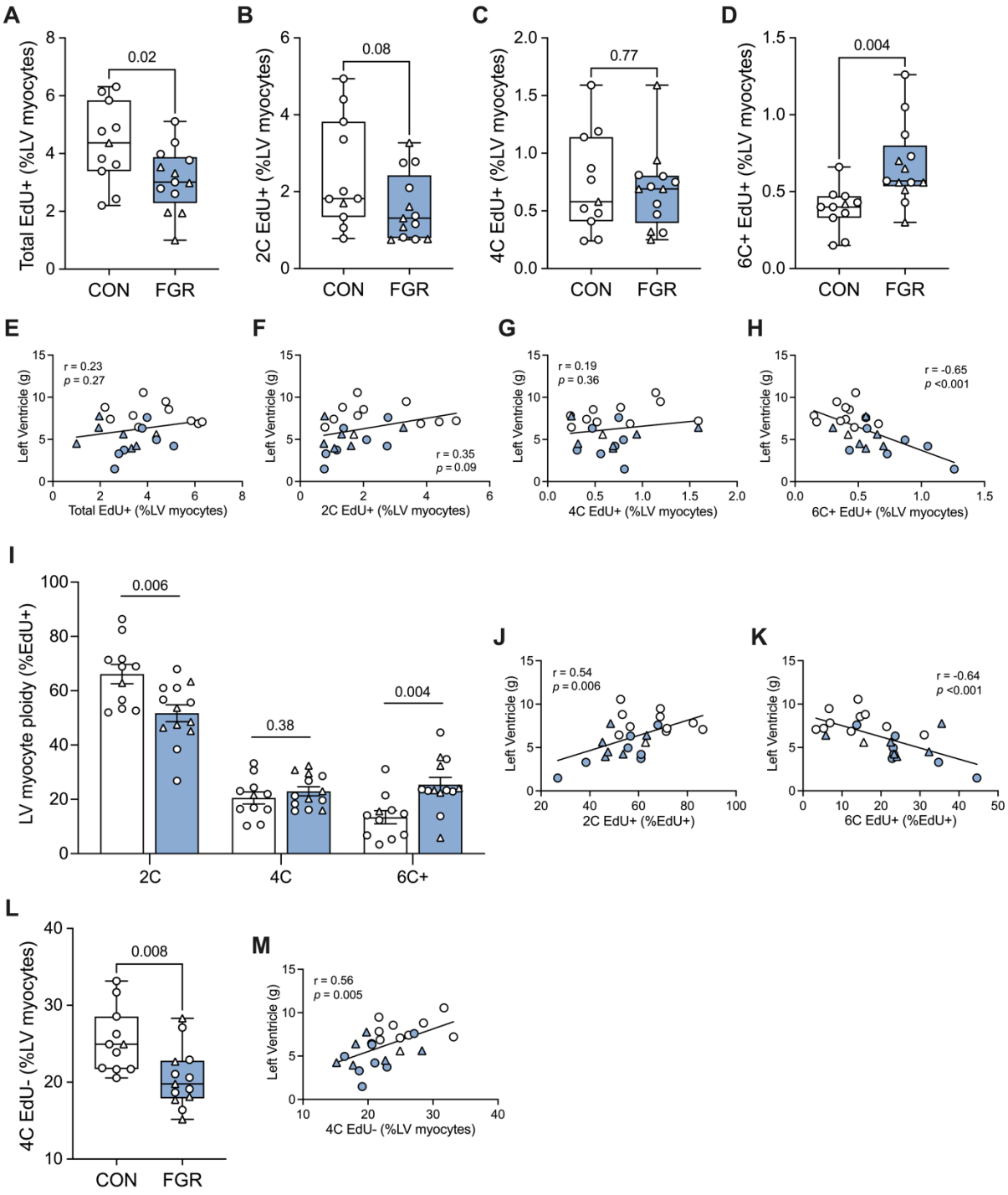

Figure 3.4. LV cardiomyocyte growth programs are altered in FGR fetuses. (A) Total cell cycle activity was lower in the LV of FGR fetuses compared to CON. When normalized to the

total number of LV cardiomyocytes, the percentages of (B) 2C EdU-positive and (C) 4C EdU-positive cells were not different between groups, but (D) the percentage of 6C+ EdU-positive cardiomyocytes was higher in FGR fetuses compared to CON. Pearson's correlation showed no associations between LV mass and (E) total cell cycle activity, (F) 2C EdU-positive cardiomyocytes, or (G) 4C EdU-positive cells expressed relative to all LV cardiomyocytes. However, (H) LV mass correlated negatively with the total percentage of 6C+ EdU-positive LV cardiomyocytes across all fetuses (n=24). (I) The percent distribution of EdU-positive cardiomyocyte ploidy, relative to the total number of EdU-positive LV cardiomyocytes, differed between FGR and CON fetuses. LV mass (J) correlated positively with 2C EdU-positive cardiomyocytes and (K) negatively with 6C+ EdU-positive cardiomyocytes normalized to all EdU-positive cells. (L) The percentage of non-replicating, binucleated cardiomyocytes was lower in the LV of FGR fetuses compared to CON and (M) correlated positively with LV mass across all groups (n=24). Data are shown as mean ± SEM. Student's t-test was used to determine differences between FGR (n=13) and CON (n=11). Exact p-values and Pearson's correlation coefficients (r) are shown. Simple linear regressions were fit between LV mass and LV myocyte subpopulations, and best fit lines are plotted with raw data. Males and females are represented by triangles and circles, respectively.

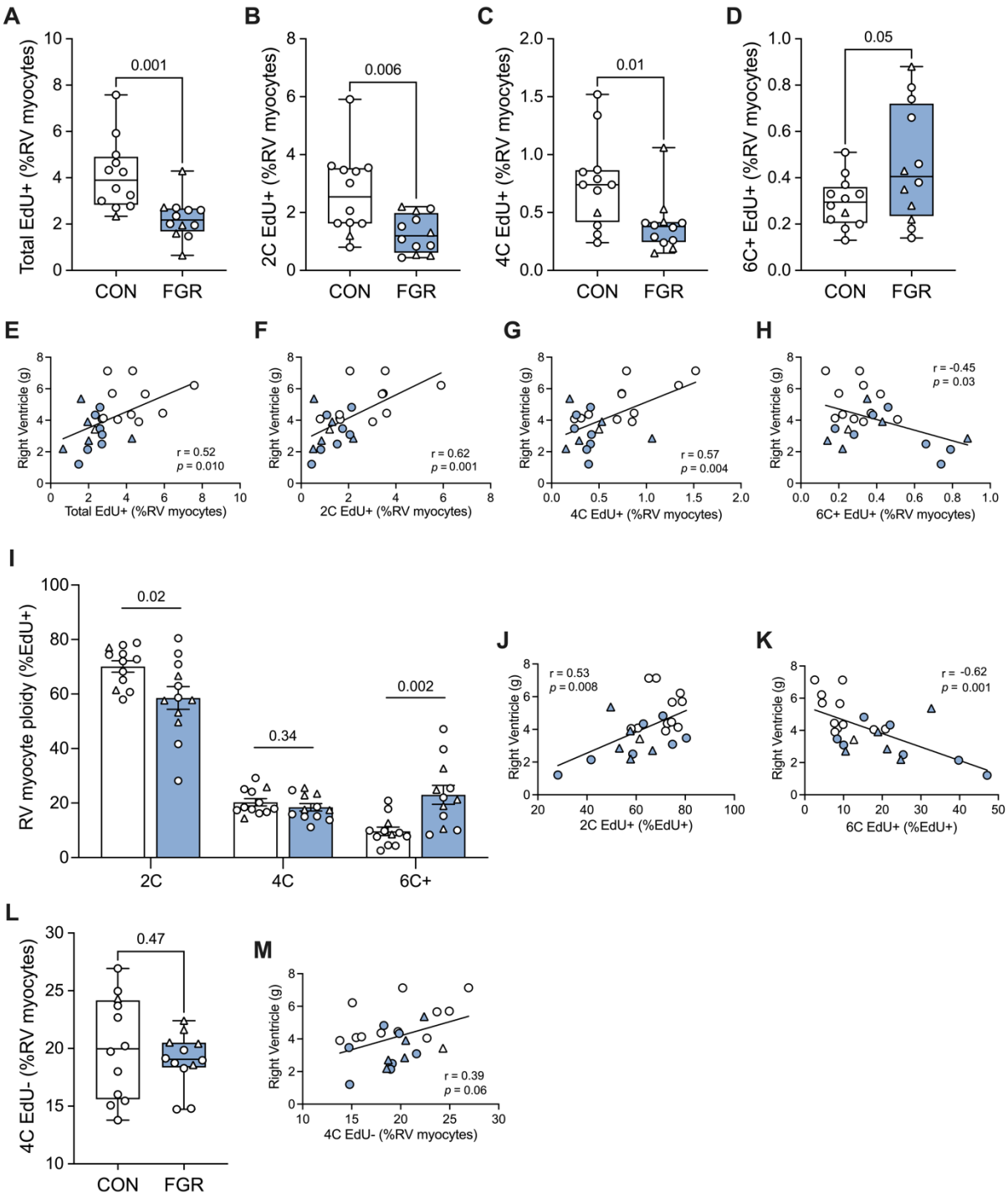

Figure 3.5. RV cardiomyocyte development is impacted by FGR. (A) Total cell cycle activity was lower in the RV of FGR (n=12) fetuses compared to CON (n=12). When expressed relative

to the total number of RV cardiomyocytes, the percentages of (B) 2C EdU-positive and (C) 4C EdU-positive cardiomyocytes were decreased in FGR. (D) The total percentage of 6C+ EdU-positive cardiomyocytes was higher in FGR fetuses compared to CON. RV mass correlated positively with (E) total cell cycle activity and the percentages of (F) 2C EdU-positive and (G) 4C EdU-positive cells normalized to all RV cardiomyocytes. (H) The proportion of 6C+ EdU-positive cardiomyocytes was negatively associated with RV mass across all fetuses (n=24). (I) The percent distribution of EdU-positive cardiomyocyte ploidy, relative to the total number of EdU-positive RV cardiomyocytes, was different between FGR and CON groups. RV mass (J) correlated positively with 2C EdU-positive cardiomyocytes and (K) negatively with 6C+ EdU-positive cardiomyocytes normalized to all EdU-positive cells. (L) The proportion of non-replicating, binucleated cardiomyocytes in the RV was similar between FGR (n=12) and CON (n=12) groups and (M) was not a significant determinant of RV mass across all fetuses (n=24). Data are shown as mean ± SEM. Student's t-test was used to determine differences between FGR and CON. Exact *p*-values and Pearson's correlation coefficients (r) are shown. Simple linear regressions were fit between LV mass and LV myocyte subpopulations, and best fit lines are plotted with raw data. Males and females are represented by triangles and circles, respectively.

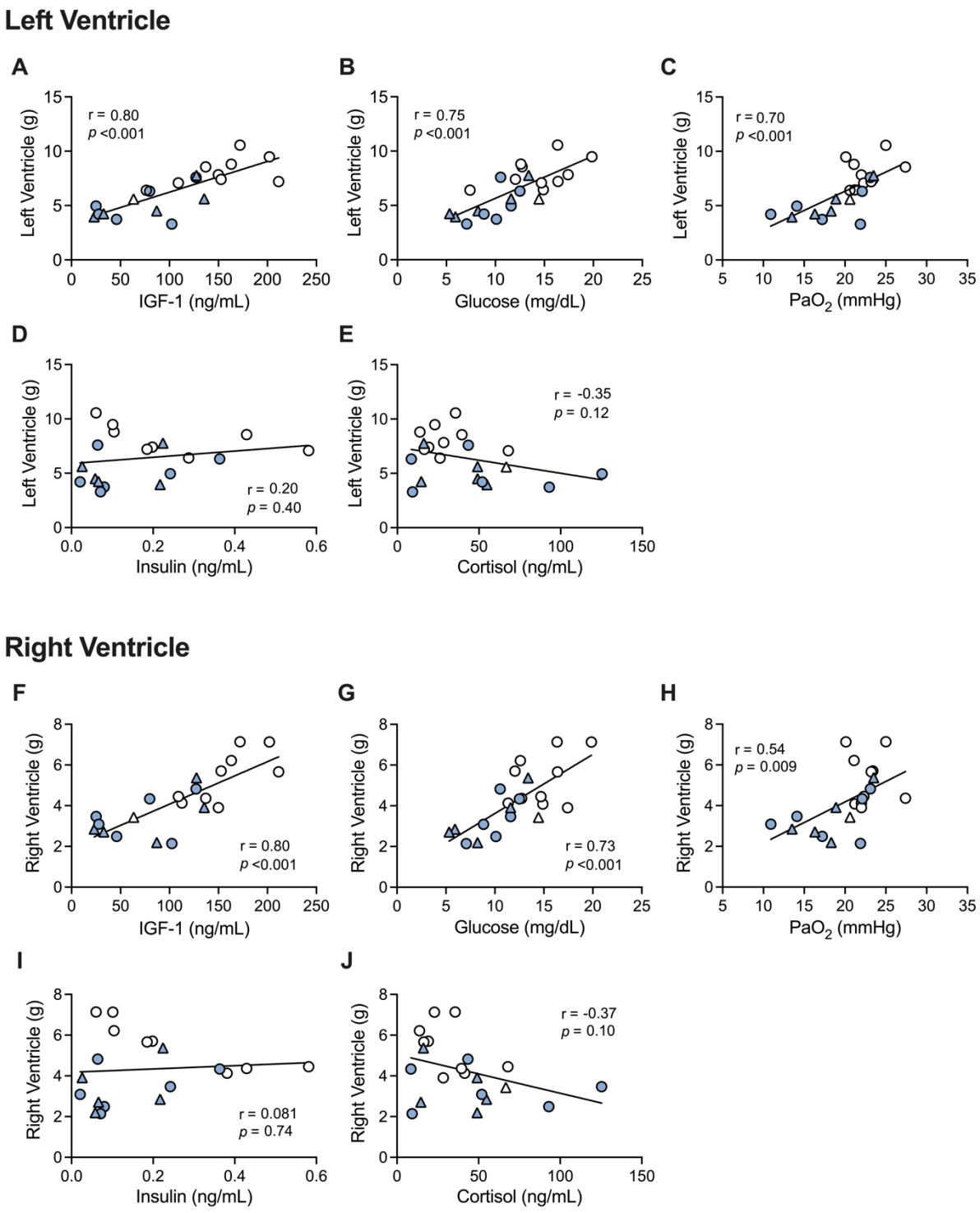

Figure 3.6. LV and RV mass are associated with circulating levels of IGF-1, glucose, and PaO_2. (A) LV mass correlated positively with fetal IGF-1 but was not associated with circulating

concentrations of (B) insulin or (C) cortisol. (D) Glucose and (E) PaO_2 were associated with increased LV mass across all FGR and CON fetuses (n=24). (F) RV mass was positively associated with IGF-1 and did not correlate with fetal (G) insulin or (H) cortisol concentrations. Both (I) glucose and (J) PaO_2 correlated positively with RV mass across all animals (n=24). Pearson's correlations and simple linear regressions were performed for each measure. Best fit lines are plotted with raw data, and Pearson's correlation coefficients (r) and *p*-values are shown for each plot. CON and FGR fetuses are represented by open and closed symbols, respectively.

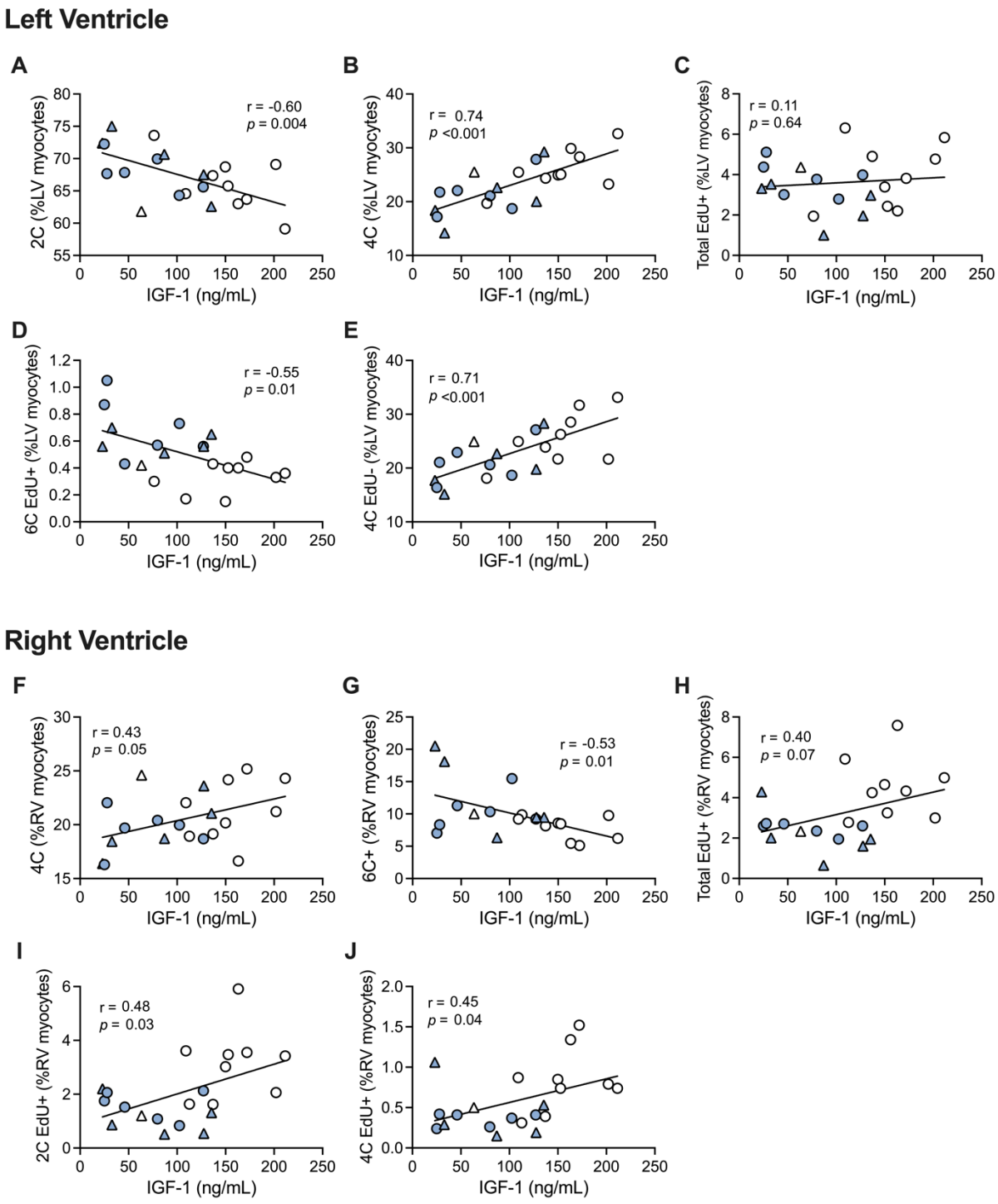

Figure 3.7. Fetal IGF-1 predicts cardiomyocyte proliferation and polyploidy in all fetuses.

(A) Fetal IGF-1 levels correlated negatively with 2C cardiomyocytes and (B) positively with 4C

cardiomyocytes in the LV. (C) Total cell cycle activity in the LV was not associated with IGF-1. (D) Circulating IGF-1 concentration was negatively associated with endoreplication in LV cardiomyocytes and (E) positively associated with the proportion of terminally differentiated LV cardiomyocytes. (F) In the RV, fetal IGF-1 was associated with an increased proportion of 4C cardiomyocytes and (G) a decreased proportion of 6C+ cardiomyocytes. (H) There was no relationship between IGF-1 and the total percentage of EdU-positive cells in the RV. The percentages of (G) 2C EdU-positive and (H) 4C EdU-positive RV cardiomyocytes correlated positively with fetal IGF-1 concentrations across all animals. Simple linear regressions were fit between IGF-1 and each subpopulation of LV or RV cardiomyocytes (n=24). Best fit lines are plotted with raw data. Pearson's correlation coefficients (r) and *p*-values are shown on each graph. CON and FGR fetuses are represented by open and closed symbols, respectively.

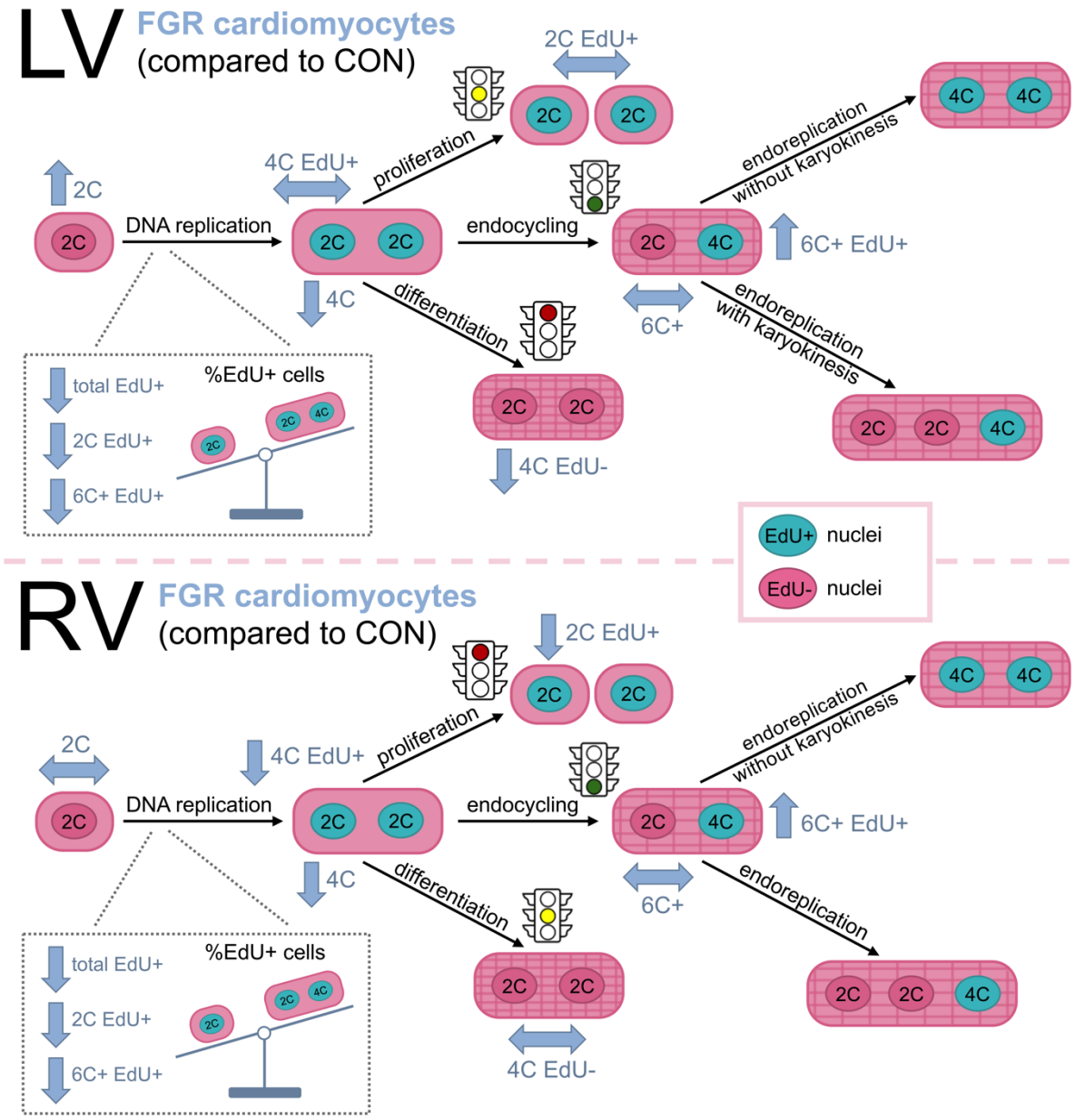

Figure 3.8. Schematic representation of LV and RV cardiomyocyte growth programs in FGR fetuses compared to CON. (A) In the LV, reductions in 4C and 4C EdU-negative cardiomyocytes imply impairments in terminal differentiation. The increased percentage of 6C+ EdU-positive cells suggests that LV cardiomyocytes continue endocycling rather than differentiating or dividing once

DNA synthesis is complete. (B) In the RV, reductions in 2C EdU-positive and 4C EdU-positive cardiomyocytes signify deficits in cardiomyocyte proliferation. Upregulated endocycling, indicated by the expansion of 6C+ EdU-positive cardiomyocytes, suggests that cytokinesis is disrupted in the RV of late-gestation FGR fetuses.

IV. SPECIFIC AIM 2

SKELETAL MYOBLAST PROLIFERATION AND DIFFERENTIATION ARE REDUCED IN GROWTH RESTRICTED FETUSES

Manuscript in Preparation:

Neeka Barooni, Eileen I. Chang, Byron Hetrick, Laura D. Brown, Carrie E. McCurdy. Skeletal myoblast proliferation and differentiation are reduced in growth restricted fetuses.

Introduction

Fetal growth restriction (FGR) and low birthweight increase the risk of developing obesity, type 2 diabetes mellitus, and cardiovascular disease in adulthood (2, 6, 27, 30, 8, 23, 29). Placental insufficiency, which limits nutrient and oxygen delivery to the developing fetus, is the leading cause of fetal growth restriction (104). Skeletal muscle is especially vulnerable to placental insufficiency as fetal blood flow is maintained to prioritize the vital organs at the expense of the peripheral musculature (267, 268). As a result, growth restricted fetuses have greater reductions in skeletal muscle mass relative to body weight that persist postnatally. Given its critical role in systemic insulin sensitivity and glucose disposal, the suppression of fetal skeletal muscle growth is thought to be a primary contributor to the prevalence of cardiometabolic disease among adults with FGR.

Primary myofiber formation occurs during early to mid-gestation, and the total number of myofibers is established *in utero.* Subsequent cycles of myoblast proliferation, differentiation, and fusion throughout mid to late gestation increase fetal myofiber hypertrophy, nuclear accretion and expand the population of resident muscle satellite cells. While progression through myogenesis is

tightly regulated by the sequential expression of myogenic regulatory factors (MRFs), circulating nutrients, growth factors, and signals from the gestational environment are also known to influence myoblast dynamics. In addition to reductions in total lean mass, deficits in myofiber number, size, and myonuclear content suggest that myogenesis is impaired in growth restricted fetuses (269–271, 124, 223, 131). Previous studies observe decreased proliferation and differentiation in skeletal muscle of FGR fetuses, though the rates of *in vitro* myogenesis are similar between satellite cells isolated from FGR and CON muscle when cultured in enriched growth media supplemented with insulin (124). These findings indicate that reduced muscle growth is likely a result of the intrauterine environment and not intrinsic to the muscle progenitor cells of FGR fetuses; thus, the mechanisms that limit myogenesis *in vivo* remain unknown.

Using a novel, high throughput approach to quantify stages of myogenesis *in vivo*, we aimed to identify the mechanisms of dysregulated skeletal muscle development in a well-established model of placental insufficiency and fetal growth restriction. We hypothesized that myoblasts from growth restricted fetuses have impaired myogenesis, with lower rates of proliferation and differentiation compared to CON fetuses of the same gestational age. To test this hypothesis, EdU was administered to late-gestation FGR and CON fetuses for 24 hours prior to necropsy. Myoblasts were then isolated from fetal skeletal muscle biopsies, and flow cytometry was used to measure cell cycle progression and the expression of MRFs responsible for initiating myogenesis and terminal differentiation.

Materials & Methods

Animal Model

Columbia–Rambouillet mixed-breed ewes (University of Arizona, Tucson, AZ) carrying singleton pregnancies were randomly assigned to fetal growth restriction (FGR, n=11) or control (CON, n=10) groups. Pregnant sheep were housed in an environmental chamber with elevated ambient temperatures (40°C for 12 hr and 35°C for 12 hr, 35-40% humidity) from 40 ± 0 to 83 ± 2 days gestation (dGA) to induce placental insufficiency and FGR as previously described (218, 219, 272) and illustrated in ***Figure 2.1***.. Ewes assigned to the control group were housed at normal ambient temperatures (21°C for 24 hr, 35-40% humidity) for the same period of gestation (40 ± 0 to 86 ± 3 dGA). All sheep were maintained in normal ambient temperatures and humidity for the remainder of the study. Ewes were given *ad libitum* access to water, and maternal feed intake was matched between FGR and CON groups.

All studies conducted at the University of Colorado Perinatal Research Center (Aurora, CO) adhered to protocols approved by the University of Colorado Institutional Animal Care and Use Committee. Animal procedures followed the guidelines of the US Department of Agriculture, the National Institutes of Health, and the Association for Assessment and Accreditation of Laboratory Animal Care International. The information presented in this manuscript is in compliance with the ARRIVE guidelines 2.0 for reporting animal research (220).

Surgical Procedures

At 126 dGa, surgery was performed in pregnant ewes to place maternal and fetal catheters as previously described (131, 221–223). The maternal femoral vein was catheterized for the

administration of euthanasia. A fetal arterial catheter was placed into the pedal artery with the tip in the distal aorta and a fetal venous catheter was placed with the tip in the external iliac vein via the saphenous vein. Sheep were monitored following the surgery and allowed to recover for at least six days before further experimentation. Twenty-four hours before tissue collection, EdU (Sigma-Aldrich, St. Louis, MO) diluted in 0.9% NaCl was administered directly to the fetus at a dosage of 20 mg/kg fetal weight, estimated from measurements of lower extremity length. On the day of muscle collection (134 dGA), hemoglobin, pH, and the partial pressures of CO_2 (P_aCO_2) and O_2 (PaO_2) were measured in fetal arterial blood. Fetal insulin, insulin-like growth factor 1 (IGF-1), and cortisol were measured using an enzyme-linked immunosorbent assay as described previously (124). Plasma glucose and lactate concentrations were determined by YSI 2900 Biochemistry Analyzer (YSI Inc., Yellow Springs, OH, USA). Ewes received intravenous anesthesia (0.2 $mg \cdot kg^{-1}$ diazepam and 20 $mg \cdot kg^{-1}$ ketamine; I.V.) and fetuses were delivered via maternal laparotomy and hysterotomy. The fetal biceps femoris was exposed for biopsy, and muscle samples were immediately frozen in liquid nitrogen and stored at −80°C for protein analysis. All animals were euthanized by a lethal dose of pentobarbital sodium (Fatal Plus; Vortech Pharmaceuticals, Dearborn, MI). Fetal sheep were weighed before subsequent tissue collection and processing.

Isolation of Fetal Myoblasts

After weighing fetal sheep. the biceps femoris muscle was submerged in cold Gibco™ Ham's F-12 Nutrient Mix (ThermoFisher Scientific, Waltham, MA) and washed twice with Hanks' Balanced Salt Solution (HBSS, MilliporeSigma, St. Louis, MO). Any remaining connective tissue was removed before the muscle was minced and digested in 1% collagenase (dissolved in HBSS)

for 30 minutes at 37°C. Bovine serum albumin (0.5% BSA in HBSS) was added to the tissue suspension in a 1:1 ratio to stop enzymatic digestion. Then the solution was filtered through 100 µm, 70 µm, and 40 µm cell strainers and centrifuged at 300 x g for 10 minutes at 25°C. The cell pellet was washed twice in 1X phosphate-buffered saline (PBS), and an aliquot was stained with Live/Dead Fixable Near-IR (Thermo Fisher Scientific Inc., Waltham, MA, USA, Cat. #L34992) according to manufacturer's instructions. All myoblasts were fixed in 2% paraformaldehyde for 15 minutes, then washed with 1X PBS and stored in 1X PBS at 4°C until flow cytometry analysis.

Myoblast Staining for Cell Cycle Analysis

For cell cycle analysis, fixed myoblasts were washed with 1X PBS and resuspended in 1X incubation buffer (0.2% Triton X-100 and 1% BSA in 1X PBS) for 15 minutes at 25°C. Click-iT Plus EdU-AF647 detection assay (Thermo Fisher Scientific Inc., Waltham, MA, USA, Cat. #C10635) was prepared according to manufacturer instructions. After centrifugation, myoblasts were incubated in 0.5 µL Click-iT EdU detection mixture for 30 minutes at 25°C. Cells were washed and pelleted, then stained with 1 µg CD56 primary antibody conjugated to PerCP/Cyanine5.5 (CD56-PC5.5, BioLegend, San Diego, CA, USA, Cat. #304626) in 0.1 mL incubation buffer for 30 minutes at 25°C. Myoblasts were washed twice, then resuspended in incubation buffer with 3 µM of DAPI (Cayman Chemical, Ann Arbor, Michigan, USA, Cat. #14285, Lot 0514078-29). Cell suspensions were kept at 25°C, protected from light, for 15 minutes before beginning data acquisition.

Myoblast Staining for Assessment of MRFs

Fixed myoblasts that had previously been stained with viability dye were washed and permeabilized for MRF analysis. After 15 minutes in 1X incubation buffer, cells were centrifuged and resuspended in 0.1 mL of antibody staining solution containing 1 µg CD56-PC5.5 (BioLegend, San Diego, CA, USA, Cat. #304626), 1 µg MyoD conjugated to phycoerythrin (MyoD-PE, Novus, Centennial, CO, USA; Cat. #NBP2-34772PE), 1 µg Myogenin-AF488 (R&D Systems, Minneapolis, MN, USA; Cat. #IC6686G), and 1 µg Pax7-APC (US Biologicals, Salem, MA, USA; Cat. #168852-AF-AP) for 30 minutes at 25°C. Cells were washed twice in 1X incubation buffer and centrifuged at 500 x g for 5 minutes. Myoblasts were stained with DAPI prior to analysis. For all wash steps, cells were resuspended in 2 mL of 1X incubation buffer and centrifuged at 500 x g for 5 minutes at 25°C before decanting the supernatant.

Flow Cytometry Analysis

Flow cytometry plots evaluating cell size, internal complexity, and staining for viability dye, DAPI, and anti-CD56 were used to distinguish myoblasts from tissue debris and other cells in suspension (***Fig. 4.1A-D***). Forward scatter height (FS-H) was plotted against forward scatter area (FS-A) to remove aggregated or adherent cells that were counted as a single event. Single cells (singlets) were defined by a diagonal gate that selectively encompassed events for which FS-H and FS-A were directly proportional (***Fig. 4.1A***). Live cells were then gated based on negative staining for Live/Dead Viability dye (***Fig. 4.1B***). The relative DNA content of each live, singlet was estimated based on DAPI fluorescence intensity, and only the DAPI-positive cells containing at least one complete copy of DNA were carried forward (***Fig. 4.1C***). CD56-PC5.5 positive staining identified myoblasts from the population of live, DAPI-positive singlets (***Fig. 1D***). All

subsequent analyses of myoblast proliferation and differentiation were limited to live, CD56-positive, DAPI-positive singlets.

Cellular DNA content and EdU incorporation were evaluated by flow cytometry to quantify myoblast cell cycle activity and proliferation rates in FGR and CON fetuses. DAPI signal was plotted to visualize the abundance of nuclear DNA in each cell, and gates were set to determine the percentage of resting (G0/1) versus replicating (S/G2) myoblasts (***Fig. 4.1E***). Actively cycling myoblasts that completed DNA synthesis in the 24 hours prior to necropsy were identified by an EdU-AF647 positive signal (***Fig. 4.1F***). Myogenic regulatory factors, anti-MyoD and anti-Myogenin (MyoG) were used to identify non-committed myoblasts (MyoD-/MyoG-) and three distinct phases of myogenic induction (MyoD+/MyoG-), early-differentiation (MyoD+/MyoG+), and late-differentiation (MyoD-/MyoG+) prior to myoblast fusion (***Fig. 4.1G***).

Data were acquired using a Beckman Coulter CytoFLEX flow cytometer (Beckman Coulter, Indianapolis, IN, USA) and FCS Express 7 (DeNovo Software, Pasadena, CA, USA). Gating was determined by comparing unstained, single stained, and fluorescence minus one (FMO) samples. Fetuses from twin pregnancies were excluded, and flow cytometry samples with low cell counts (fewer than 7,000 myoblasts) or poor DAPI/MRF resolution were removed from the analysis. Exact n values for each condition are reported in the figure legends.

Protein Analysis

Frozen biceps femoris muscles were powdered using mortar and pestle. Lysis buffer was prepared as previously described (52), and 0.5 mL was added to pulverized tissue (50-70 mg). Samples were homogenized with six 2.8-mm ceramic beads (VWR International, Radnor, PA,

USA) in a Bead Ruptor (OMNI International, Kennesaw, GA, USA) for two, 30 second pulses at 4°C. The homogenate was rotated on an orbital shaker for 1 hour at 4°C. Samples were then centrifuged at 13,000 x g for 15 minutes at 4°C, and the supernatant was collected and stored at -80°C. Protein concentration was determined using a BCA assay (Thermo Fisher Scientific Inc., Waltham, MA, USA).

For Western blot analysis, samples were prepared by resuspending 20 µg of protein in Laemmli buffer. Samples were then loaded into 12% Criterion TGX Stain-Free gels (Bio-Rad Laboratories, Hercules, CA, USA), and a 130V current was applied for 60-70 minutes. Protein was transferred to Trans-blot Turbo Midi 0.2 µm PVDF membranes (Bio-Rad Laboratories), and stain-free images confirmed successful transfer. Membranes were blocked in EveryBlot Buffer (Bio-Rad Laboratories, Hercules, CA, USA) for 1 hour at room temperature prior to overnight incubation with TMEM8C (Mymk) primary antibody (1:250 dilution, Novus, Centennial, CO, USA; Cat. #NBP2-34175) at 4°C. The following day, membranes were washed in 1X Tris-buffered saline with Tween 20 (TBST) and incubated with horseradish peroxidase (HRP)-conjugated secondary antibodies against rabbit IgG (1:20,000 dilution, Bio-Rad Laboratories) for 1 hour at room temperature. Additional washes with 1X TBST were performed before measuring total protein with Stain-Free technology (Bio-Rad Laboratories). The target was then visualized by chemiluminescence using Clarity Max ECL substrate (Bio-Rad Laboratories) per manufacturer's instructions. All data were collected on a ChemiDoc MP Imaging System and analysis was performed in Image Lab 5.2 (Bio-Rad Laboratories). Target signals were normalized to total protein content.

Statistical Analysis

Statistical analyses were performed in GraphPad Prism (GraphPad Software, La Jolla, CA, USA, Version 10.2.2). All comparisons between FGR and CON groups were evaluated by unpaired student's *t*-test. Pearson's correlation was used to assess the relationships between myoblast dynamics and fetal body weight, skeletal muscle mass and hormone concentrations across all FGR and CON fetuses. Data are reported as mean ± standard error of the mean (SEM). Significance was determined at $P \leq 0.05$, and exact *P*-values are shown for all comparisons. We were not able to assess sex differences due to random and unequal distribution of fetal sex across treatment groups, though male and female fetuses are noted by triangles and circles, respectively.

Results

Fetal Physiology

Physiological characteristics of FGR and CON fetuses are reported in ***Table 2.1***. Fetal body mass was 37% lower in FGR compared to CON. This is partially attributed to deficits in FGR skeletal muscle growth, as seen by reductions in soleus, gastrocnemius, flexor digitorum superficialis, and tibialis anterior mass, as well as the summed mass of hindlimb muscles from FGR versus CON fetuses. Reductions in hindlimb muscle mass persisted when normalized to fetal body weight. Levels of circulating glucose, IGF-1, and PaO_2 were lower in FGR compared to CON fetuses, while lactate, insulin, and cortisol concentrations were not different between groups.

Myoblast Proliferation in vivo

Cellular DNA content was measured by flow cytometry to assess the distribution of resting (G0/1) versus replicating (S/G2) myoblasts in FGR and CON fetuses. FGR fetuses had a larger percentage of muscle progenitor cells in G0/1 compared to CON (***Fig. 4.2A***). Across all FGR and

CON animals, the proportion of myoblasts in G0/1 correlated negatively with fetal body mass (***Fig. 4.2B***) and tended to decrease with hindlimb muscle mass ($p = 0.10$; ***Fig. 4.2C***). FGR fetuses had fewer proliferating myoblasts in S/G2 compared to CON (***Fig. 4.2D***). The percentage of myoblasts in S/G2 correlated positively with fetal weight (***Fig. 4.2E***) but was not associated with hindlimb muscle mass ($p = 0.10$; ***Fig. 4.2F***).

Fetal skeletal muscle proliferation rates were confirmed by quantifying the proportion of actively cycling myoblasts that incorporated EdU *in utero.* The percentage of proliferating myoblasts in FGR fetuses was 43% lower than CON (***Fig. 4.3A***). Correlation analysis identified positive associations between skeletal myoblast proliferation and fetal body mass (***Fig. 4.3A***) as well as hindlimb muscle mass across all fetuses (***Fig. 4.3C***).

Myogenic Lineage Commitment and Terminal Differentiation

To determine if differentiation programs were also impaired in FGR skeletal muscle, MRF expression was evaluated by flow cytometry. The proportion of unfused myoblasts in each stage of myogenesis was determined based on staining for MyoD and MyoG. FGR and CON fetuses had similar proportions of non-committed (MyoD-/MyoG-) muscle progenitor cells (***Fig. 4.4A***), but FGR skeletal muscle had lower percentages of myoblasts that were initiating myogenic lineage commitment (MyoD+/MyoG-) and beginning terminal differentiation (MyoD+/MyoG+) *in utero* (***Fig. 4.4B-C***). Despite having fewer myoblasts in the initial stages of terminal differentiation, FGR fetuses had a 56% increase in the proportion of unfused myocytes in the late stages of differentiation (MyoD-/MyoG+) compared to CON (***Fig. 4.4D***).

Correlation analysis across all FGR and CON fetuses showed that the percentage of non-committed myoblasts did not correlate with fetal weight (***Fig. 4.5A***) or hindlimb muscle mass (***Fig. 4.5E***). Likewise, the proportion of myoblasts undergoing myogenic lineage commitment did not correlate with total body mass ($p = 0.12$; ***Fig. 4.5B***) or muscle mass across groups ($p = 0.19$; ***Fig. 4.5F***). The percentage of myoblasts in early differentiation was positively associated with fetal weight (***Fig. 4.5C***) and muscle mass (***Fig. 4.5G***). Additionally, there was a negative linear relationship between the percentage of late-differentiation myocytes and total body mass (***Fig. 4.5D***) as well as hindlimb muscle mass (***Fig. 4.5H***) across all fetuses.

Myoblast Fusion

Given the increased percentage of unfused late-differentiation myocytes in FGR, we measured the relative abundance of Myomaker (*Mymk*) protein in fetal skeletal muscle to investigate whether these cells were accumulating outside of myofibers due to impairments in myoblast fusion. FGR skeletal muscle had a 30% reduction in *Mymk* compared to CON (***Fig. 4.6A-B***), and *Mymk* abundance correlated positively with both fetal weight (***Fig. 4.6C***) and skeletal muscle mass (***Fig. 4.6D***). Additionally, the percentage of late-differentiation myoblasts correlated negatively with *Mymk* protein content across all FGR and CON fetuses (***Fig. 4.6E***).

Associations Between Circulating Factors and Fetal Growth

We previously observed reductions in circulating glucose, IGF-1, and PaO_2 in FGR fetuses compared to CON (***Table 2.1***). Therefore, to assess the impact of circulating factors on fetal growth, we tested correlations between fetal plasma hormones and hindlimb muscle mass, as well as total body mass, across all FGR and CON fetuses. Fetal glucose, IGF-1, and PaO_2 correlated

positively with total body mass (***Fig. 4.7A-C***) and hindlimb muscle mass (***Fig. 4.7F-H***). Circulating insulin concentrations tended to increase with fetal weight (***Fig. 4.7D***) and correlated positively with hindlimb muscle mass (***Fig. 4.7I***) across all fetuses. Fetal cortisol levels were not associated with total body mass (***Fig. 4.7E***) or hindlimb muscle mass (***Fig. 4.7J***) among FGR and CON fetuses.

Associations Between Fetal IGF-1 and Skeletal Muscle Myogenesis

Fetal IGF-1 concentrations were associated with increased rates of myoblast proliferation, as indicated by negative correlations with G0/1 myoblasts (***Fig. 4.8A***) and positive correlations with myoblasts in S/G2 (***Fig. 4.8B***) as well as the percentage of EdU+ myoblasts (***Fig. 4.8C***). Associations between fetal IGF-1 and myogenesis stages were not statistically significant, though circulating IGF-1 levels tended to increase with the percentage of myoblasts in early differentiation ($p = 0.06$; ***Fig. 4.8D***) and decrease with the proportion of late differentiation myoblasts ($p = 0.12$; ***Fig. 4.8E***). There was, however, a positive correlation between fetal IGF-1 and the relative abundance of *Mymk* across all fetuses (***Fig. 4.8F***).

Discussion

We developed a novel, flow cytometry-based strategy to evaluate fetal skeletal myoblast proliferation and differentiation following exposure to placental insufficiency. To our knowledge, this study is the first to assess myogenesis rates *in vivo* using muscle progenitor cells isolated from FGR and CON fetuses. Our findings are summarized in ***Figure 4.9***. We identified deficits in FGR skeletal muscle proliferation, as evidenced by reductions in the proportion of S/G2 myoblasts and the percentage of EdU+ cells compared to CON. While the proportion of non-committed

myoblasts was similar between FGR and CON groups, the percentage of activated myoblasts that had recently committed to myogenesis was decreased in FGR. Reductions in myogenesis persisted through early differentiation; however, FGR fetuses had a greater proportion of myoblasts in late differentiation compared to CON. Deficits in *Mymk* abundance suggest that the accumulation of late-differentiation myoblasts in FGR skeletal muscle may be due to impairments in myoblast fusion. Additionally, correlations with circulating growth factors imply that fetal IGF-1 could play a critical role in mediating myoblast proliferation and fusion during late gestation.

We observed lower rates of myoblast proliferation in FGR fetuses compared to CON. This is consistent with previous studies that identified reductions in the fraction of actively cycling myonuclei in FGR skeletal muscle (124, 131, 226, 270). However, rather than assessing the number of Ki67/PCNA+ myonuclei within a muscle fiber, we measured myoblast proliferation rates in the single cells residing beneath the basil lamina of mature myofibers. Therefore, our findings differentiate impairments in myoblast proliferation from deficits in myogenesis and/or myoblast fusion that may contribute to reductions in myonuclear accretion. Additionally, we found that skeletal myoblast proliferation correlates positively with fetal body mass and hindlimb muscle mass across all animals. These findings indicate that adequate proliferation rates are critical for increasing lean mass during fetal development, regardless of interactions with differentiation or fusion programs. Reductions in proliferation rates are likely mediated by the suppression of several key cell cycle regulators in FGR skeletal muscle (124, 131). These alterations likely reflect intrauterine adaptations that aim to reduce the energy demands of fetal skeletal muscle during a period of limited nutrient and oxygen availability. However, there is some evidence that the reduced proliferative capacity may be programmed into FGR skeletal myoblasts (270) and persist

into postnatal life (273), restricting skeletal muscle growth and repair through adulthood. Other reports suggest that reductions in myoblast proliferation result from the FGR environment and may be reversed by supplementing growth factor availability during the critical window of fetal development (124, 218).

Our findings identify impairments in FGR skeletal muscle myogenesis that correlate with measures of lean mass across all fetuses. We observed reductions in the proportions of activated and early-differentiation myoblasts in FGR skeletal muscle, suggesting a decrease in myogenic lineage commitment. Due to limitations in current techniques, earlier measures of MRF expression in FGR fetuses were restricted to whole skeletal muscle tissue or myoblasts completing differentiation *in vitro,* which may explain the conflicting results (124, 126, 131). Some studies describe reductions in MyoD and MyoG expression in FGR skeletal muscle that are consistent with our findings (131, 270), while others suggest that global MRF expression remains unchanged between FGR and CON fetuses (124). Furthermore, the deficits we identified in early myogenesis likely contribute to previously reported reductions in activated (MyoD+) and cycling (BrdU+, Ki67+, PCNA+) myonuclei within the sarcolemma of FGR myofibers (124, 131, 270, 274). Whether deficits in myogenesis are intrinsic to FGR skeletal muscle remains unclear. Some studies demonstrate similar rates of myogenesis in myoblasts isolated from FGR and CON fetuses (124, 270), but others observe reductions in MyoG and Desmin expression in FGR myoblasts after differentiation *in vitro* (273).

Surprisingly, we identified an increase in the percentage of late-differentiation myoblasts in FGR fetuses, despite deficits in myogenic lineage commitment and early differentiation. Similar results were reported in a rodent model of FGR induced by maternal inflammation, where the

fraction of MyoG+ nuclei normalized to cross-sectional area was increased in FGR (274). However, this conflicts with evidence suggesting that the percentage of MyoG+ myonuclei is decreased in FGR skeletal muscle (270). Taken together, these findings may reflect an accumulation of unfused MyoG+ myoblasts beneath the basal lamina of developing myofibers due to impairments in myoblast fusion. This would cause the fraction of intramuscular MyoG+ myonuclei to be decreased in FGR. Moreover, reductions in *Mymk* protein abundance support the likelihood of dysregulated myoblast fusion in FGR skeletal muscle.

In the present study, we observed positive associations between fetal IGF-1 concentrations and measures of myoblast proliferation and fusion *in utero.* The proportion of myoblasts in early differentiation tended to increase with fetal IGF-1 ($p = 0.06$); however, neither IGF-1 nor insulin appeared to be a potent stimulator of fetal myogenesis *in vivo*. It is well established that myoblasts increase proliferation in response to insulin and IGF-1 (275–278), and circulating levels of both growth factors are consistently reduced in FGR fetuses (114, 279). Additional evidence implicates IGF-1 in promoting myoblast differentiation via the same receptor that activates signaling pathways for myoblast proliferation (114, 280, 281). Previous studies identify positive correlations between fetal insulin and IGF-1 concentrations and the proportion of actively cycling myonuclei as well as the total number of myofibers across all FGR and CON sheep (131). Additionally, earlier research supports that deficits in myoblast proliferation are attributable to the non-nutritional components of the FGR intrauterine environment, as increasing glucose, oxygen, and amino acid concentrations *in vitro* was not sufficient to rescue proliferation rates in FGR myoblasts (270). Further, primary myoblasts from CON fetuses experienced reductions in proliferation when exposed to serum from FGR fetuses (270). Evidence that insulin supplementation can restore FGR

myoblast proliferation rates *in vitro* suggests that the relationships observed in Chang et al., 2019 are likely the result of growth factor-mediated enhancements in myoblast proliferation (124), and the cross-reactivity between insulin and IGF-1 receptors has been widely documented. However, the present study is the first to investigate whether fetal growth factors promote skeletal muscle growth solely by stimulating myoblast proliferation or through additional interactions with signaling pathways that regulate terminal differentiation and myoblast fusion *in vivo*. We propose that the relationship observed between fetal IGF-1 and *Mymk* abundance is mediated by interactions with MyoD, as IGF-1 has not been shown to directly regulate *Mymk* expression in skeletal muscle (281–283). Our results imply a central role for IGF-1 in regulating fetal myoblast function and suggest that deficits in FGR skeletal muscle likely result from limitations in growth factor availability during a critical window of development. Moreover, findings reported by Brown et al. (2016), Chang et al. (2021), and Stremming et al. (2022, 2024) suggest that fetal growth factor supplementation may be sufficient to restore myoblast proliferation and potentially support skeletal muscle growth in FGR fetuses (218, 221, 284, 285).

Given that the total population of quiescent satellite cells is formed during prenatal development (226, 286), reductions in fetal myoblast proliferation rates may limit the availability of muscle progenitor cells to support postnatal growth and repair (287, 288). Although deficits in satellite cell numbers have not been observed in FGR sheep (124, 270), the signaling pathways that regulate fetal cell cycle suppression are subject to epigenetic programming, which may permanently restrict the regenerative capacity of FGR skeletal muscle across the lifespan (289, 290). The total number of myofibers is also set *in utero*, so adequate myofiber formation during fetal development is essential for establishing a scaffold to support future skeletal muscle growth.

Myoblasts proliferate, differentiate, and fuse to form new multinucleated myofibers (286). Therefore, disruptions to any of these processes could cause permanent deficits in the total number of fibers in FGR skeletal muscle (131, 218, 270). Deficits in myogenesis also restrict the potential for fetal skeletal muscle hypertrophy, as myofiber enlargement is dependent on the number of myonuclei available to support an increase in cytoplasmic volume, especially during periods of rapid growth (131, 287). In an attempt to compensate for reductions in intrauterine growth, low birthweight infants often experience a postnatal "catch-up" period of rapid adipose tissue expansion, which can have significant implications for future metabolic health (104).

A primary limitation of this study was that we were not powered to test for sex differences due to the unequal distribution of male and female fetuses. Additional research is needed to identify interactions between FGR and fetal sex. However, male fetuses are often reported to be more severely affected by intrauterine exposures compared to females, so our comparisons should not be skewed by the primarily female CON group (291–293). Another limitation was that our measures of *Mymk* protein abundance were performed on whole skeletal muscle tissue, which contains myoblasts and various other cell types that could potentially influence our results. For the remaining analyses, we used flow cytometry to focus our assessments of proliferation and differentiation on only the unfused myogenic progenitor cells isolated from skeletal muscle of FGR and CON fetuses. Because each subpopulation of proliferating/differentiating myoblasts was normalized to a single parent population of CD56+ and/or Pax7+ cells, it is possible for changes in one subset of cells to skew perceived differences in another. Thus, careful consideration was given to minimize potential discrepancies through experimental design, appropriate controls, and reproducible gating strategies. Moreover, comparable changes in myoblast subpopulations were

noted in the absolute cell counts obtained prior to normalization. Still, future studies should employ alternative methods to confirm our results in isolated myoblasts and provide a more comprehensive understanding of FGR skeletal muscle dynamics. Lastly, there is some disagreement about whether MyoD is expressed in proliferating myoblasts or upregulated to initiate cell cycle exit for terminal differentiation (281–283, 294–297). Our explanation is based on the latter, but either interpretation is consistent with our findings of decreased proliferation and early differentiation in FGR myoblasts.

In summary, our findings uniquely identify stage-specific impairments in the myogenic programs of unfused muscle progenitor cells from FGR and CON fetuses. We observed that myoblasts from FGR skeletal muscle exhibit reduced proliferation rates, which directly correlate with deficits in fetal growth. Decreased percentages of myoblasts in the early stages of terminal differentiation suggest that myogenic induction is compromised in FGR. This may indicate a shift in progenitor cell trajectories away from myogenic lineage commitment. Reductions in the proportion of unfused yet differentiated myocytes, coupled with deficits in *Mymk*, imply that myoblast fusion processes are impaired in FGR. This is likely restricting myonuclear accretion and impeding skeletal muscle growth *in utero*. However, correlations with IGF-1 highlight potential avenues for preventing lasting deficits in skeletal muscle function with therapeutic interventions that enhance growth factor availability during fetal development. To further inform effective strategies for restoring skeletal muscle growth in FGR fetuses, future studies should investigate the mechanisms by which fetal growth factors regulate myoblast proliferation and differentiation *in utero*.

Figures

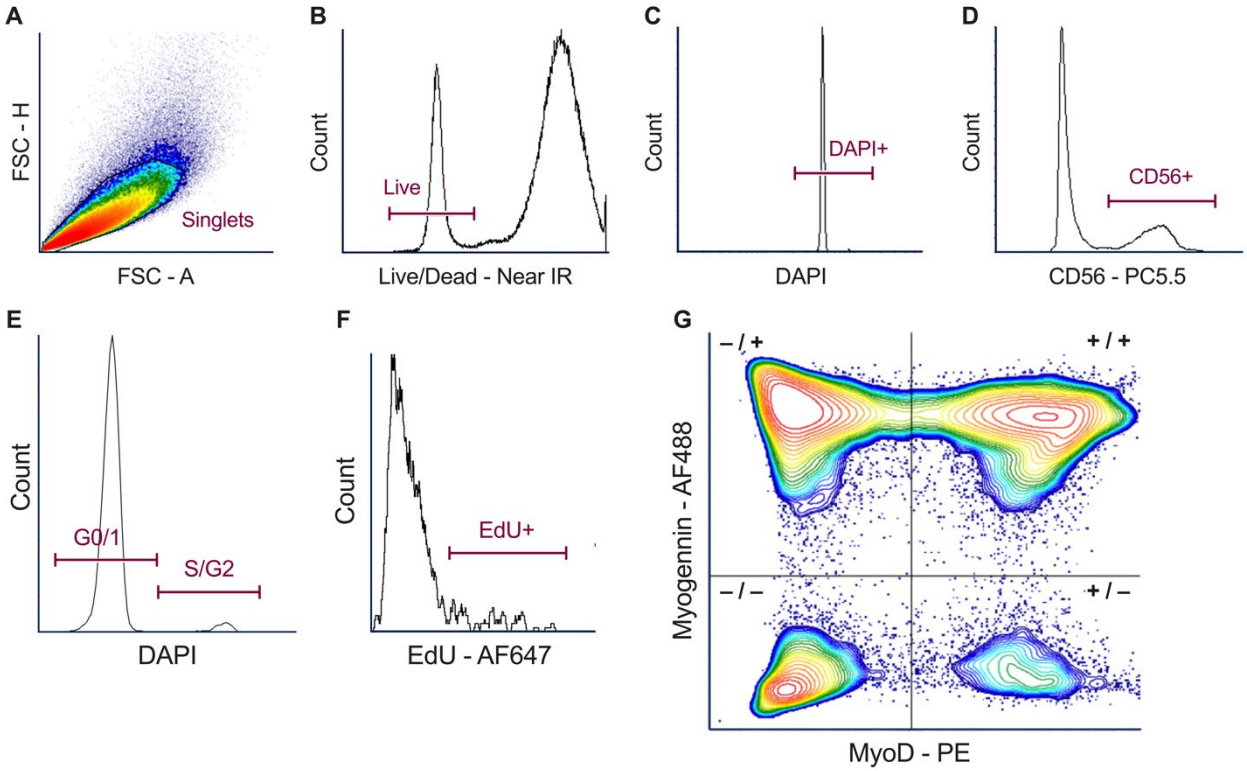

Figure 4.1. Gating strategy for analysis of myoblast proliferation and differentiation by flow cytometry. Representative plots of skeletal myoblast identification by (A) forward scatter height versus area, (B) Live/Dead Near-IR, (C) DAPI, and (D) CD56-PC5.5 antibody. (E) Gating of myoblasts in G0/1 and S/G2 phase based on DAPI fluorescence intensity. (F) Representative plot of EdU-AF647 signal and gating to quantify the percentage of EdU-positive myoblasts. (G) Flow cytometry plot of MyoD and Myogenin staining for myogenic regulatory factor analysis.

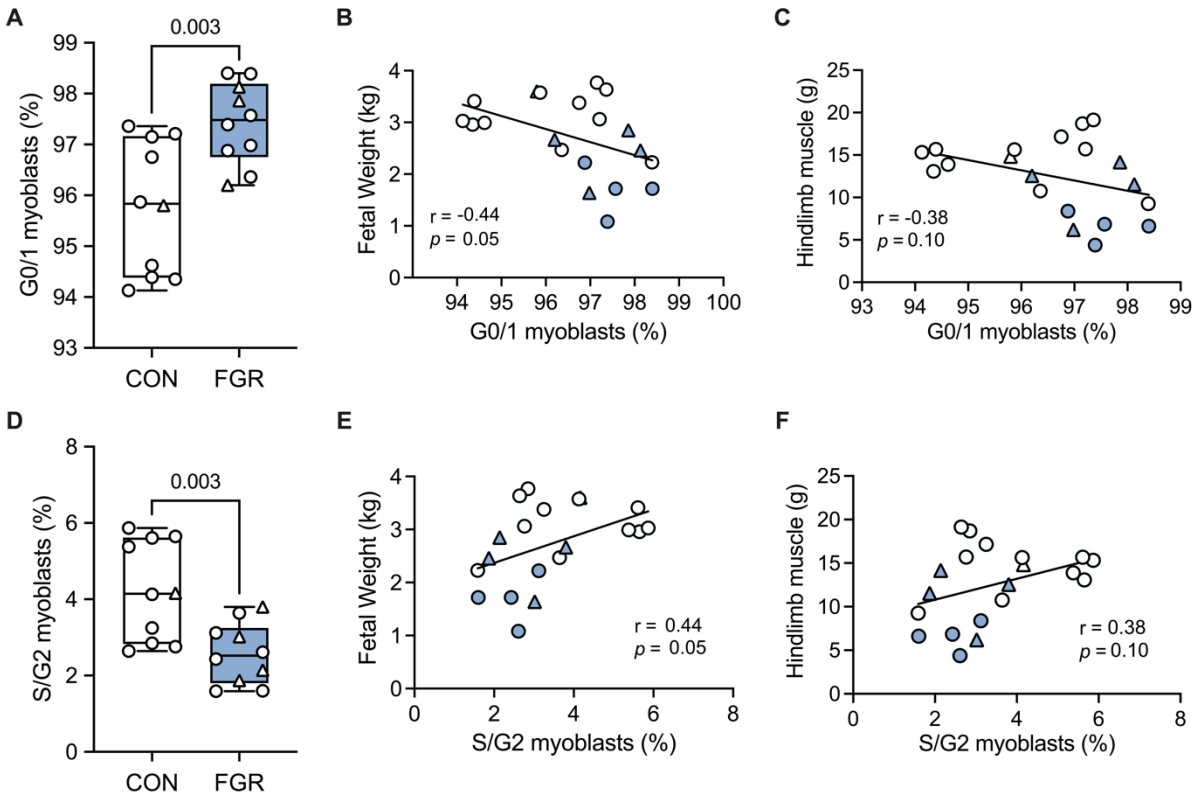

Figure 4.2. Myoblast cell cycle progression in FGR and CON fetuses. (A) The percentage of myoblasts in G0/1 is higher in FGR fetuses and correlates negatively with (B) fetal weight and (C) hindlimb muscle mass. (D) The fraction of replicating myoblasts in S/G2 is reduced in FGR and (E) correlates positively with fetal weight and (F) hindlimb muscle mass. Data are shown as mean ± SEM. Student's t-test with $\alpha = 0.05$ was used to determine differences between FGR (n=10) and CON (n=10) groups. Pearson's correlation coefficients (r) and *p*-values are listed (n=20). Simple linear regressions were fit to each correlation, and best fit lines are plotted with raw data. FGR fetuses are indicated by blue/closed symbols, CON fetuses by white/open symbols, and males and females are represented by triangles and circles, respectively.

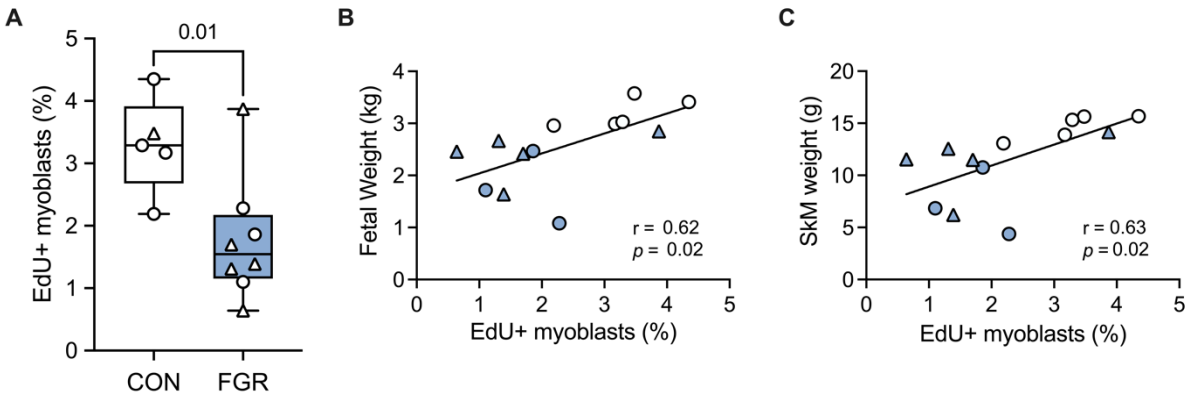

Figure 4.3. Fetal myoblast replication and EdU incorporation in utero. (A) FGR myoblasts have lower rates of EdU incorporation compared to CON. The percentage of EdU+ myoblasts correlates positively with (B) total body weight and (C) hindlimb muscle mass across all fetuses. Data are shown as mean ± SEM. Student's t-test with $\alpha = 0.05$ was used to determine differences between FGR (n=5) and CON (n=9) groups. Pearson's correlation coefficients (r) and p-values are listed (n=13). Simple linear regressions were fit to each correlation, and best fit lines are plotted with raw data. FGR fetuses are indicated by blue/closed symbols, CON fetuses by white/open symbols, and males and females are represented by triangles and circles, respectively.

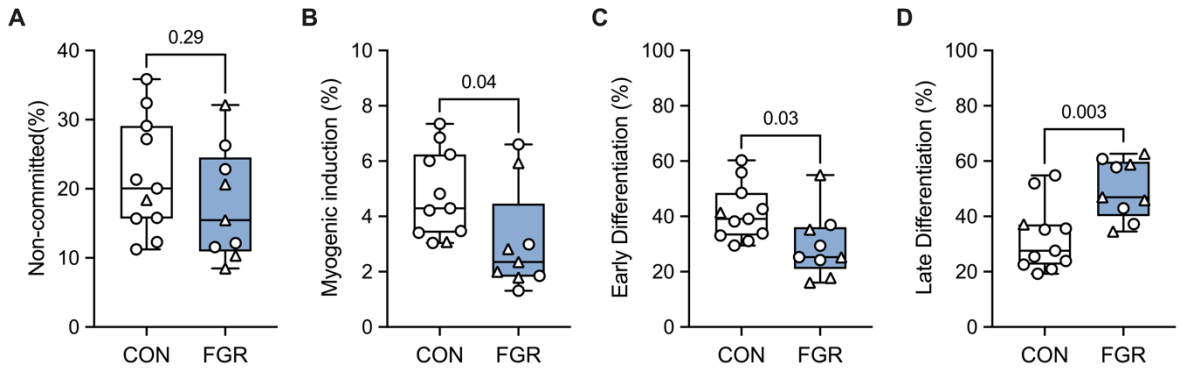

Figure 4.4. Stages of myogenesis in skeletal myoblasts from FGR and CON fetuses. (A) The percentage of non-committed myoblasts (MyoD-/MyoG-) is similar between FGR and CON groups. FGR fetuses have lower percentages of (B) activated (MyoD+/MyoG-) and (C) early differentiation (MyoD+/MyoG+) myoblasts compared to CON. (D) The proportion of myoblasts in final the stages of terminal differentiation (MyoD-/MyoG+) is increased in FGR skeletal muscle. Data are shown as mean ± SEM. Student's t-test with $\alpha = 0.05$ was used to determine differences between FGR (n=11) and CON (n=9) groups. Males and females are represented by triangles and circles, respectively.

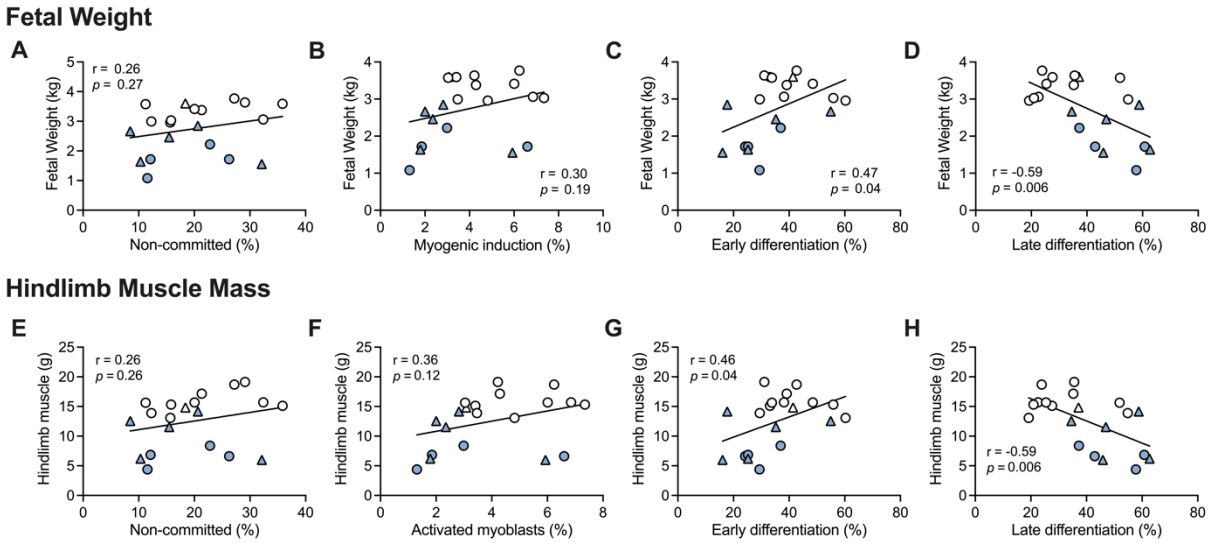

Figure 4.5. Associations between stages of myogenesis and fetal growth. Non-committed (MyoD-/MyoG-) and activated (MyoD+/MyoG-) myoblasts were not associated with (A-B) fetal weight or (E-F) hindlimb muscle mass across FGR and CON animals. The proportion of myoblasts in early differentiation (MyoD+/MyoG+) correlated positively with (C) fetal weight as well as (G) hindlimb muscle mass. The percentage of late differentiation myoblasts (MyoD-/MyoG+) correlated negatively with (D) total body mass and (H) hindlimb muscle mass in all fetuses. Simple linear regressions were fit to each correlation, and best fit lines are plotted with raw data. Pearson's correlation coefficients (r) and p-values are listed (n=20). FGR fetuses are indicated by blue/closed symbols, CON fetuses by white/open symbols, and males and females are represented by triangles and circles, respectively.

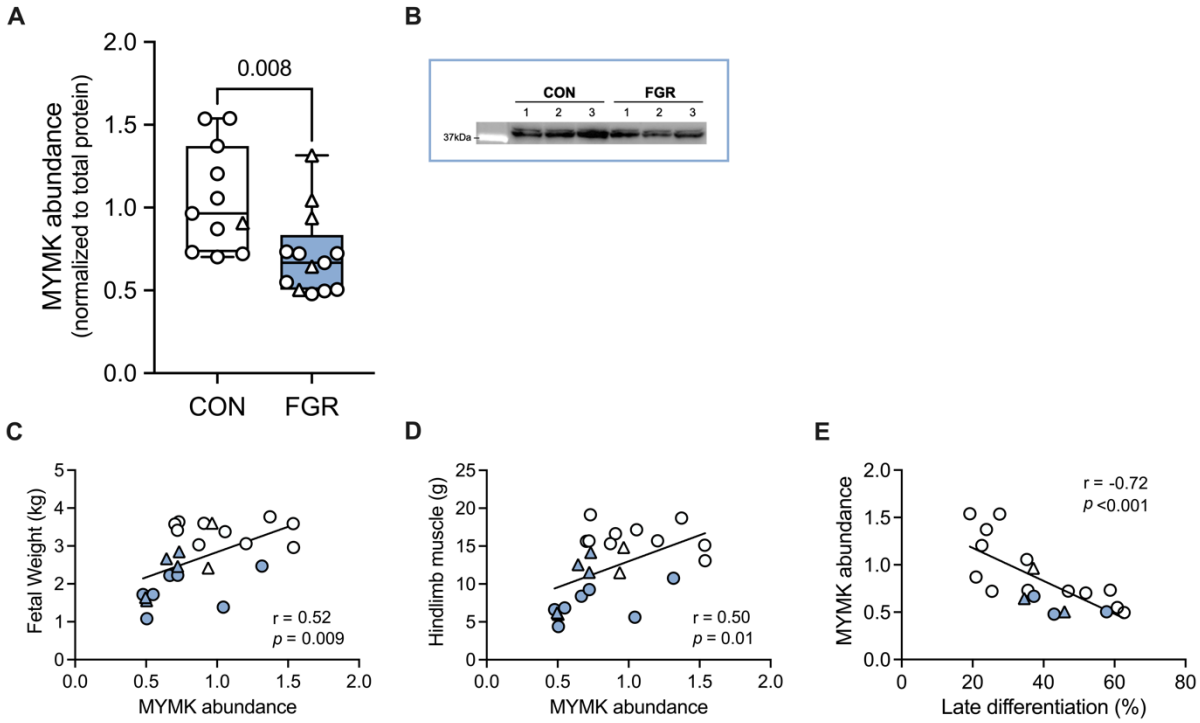

Figure 4.6. Myomaker protein abundance in fetal skeletal muscle. (A) The relative abundance of Myomaker (Mymk) protein was reduced in FGR fetuses compared to CON. (B) Representative Western blots of Mymk in biceps femoris muscle of FGR (n=3) and CON (n=3). Mymk abundance correlated positively with (C) fetal weight and (D) hindlimb muscle mass in all fetuses. (E) The percentage of myoblasts in late differentiation (MyoD-/MyoG+) correlated negatively with Mymk abundance across groups (n=10). Data are shown as mean ± SEM. Student's t-test with $\alpha = 0.05$ was used to determine differences between FGR (n=8) and CON (n=7) groups. Pearson's correlation coefficients (r) and p-values are listed (n=15). Simple linear regressions were fit to each correlation, and best fit lines are plotted with raw data. FGR fetuses are indicated by blue/closed symbols, CON fetuses by white/open symbols, and males and females are represented by triangles and circles, respectively.

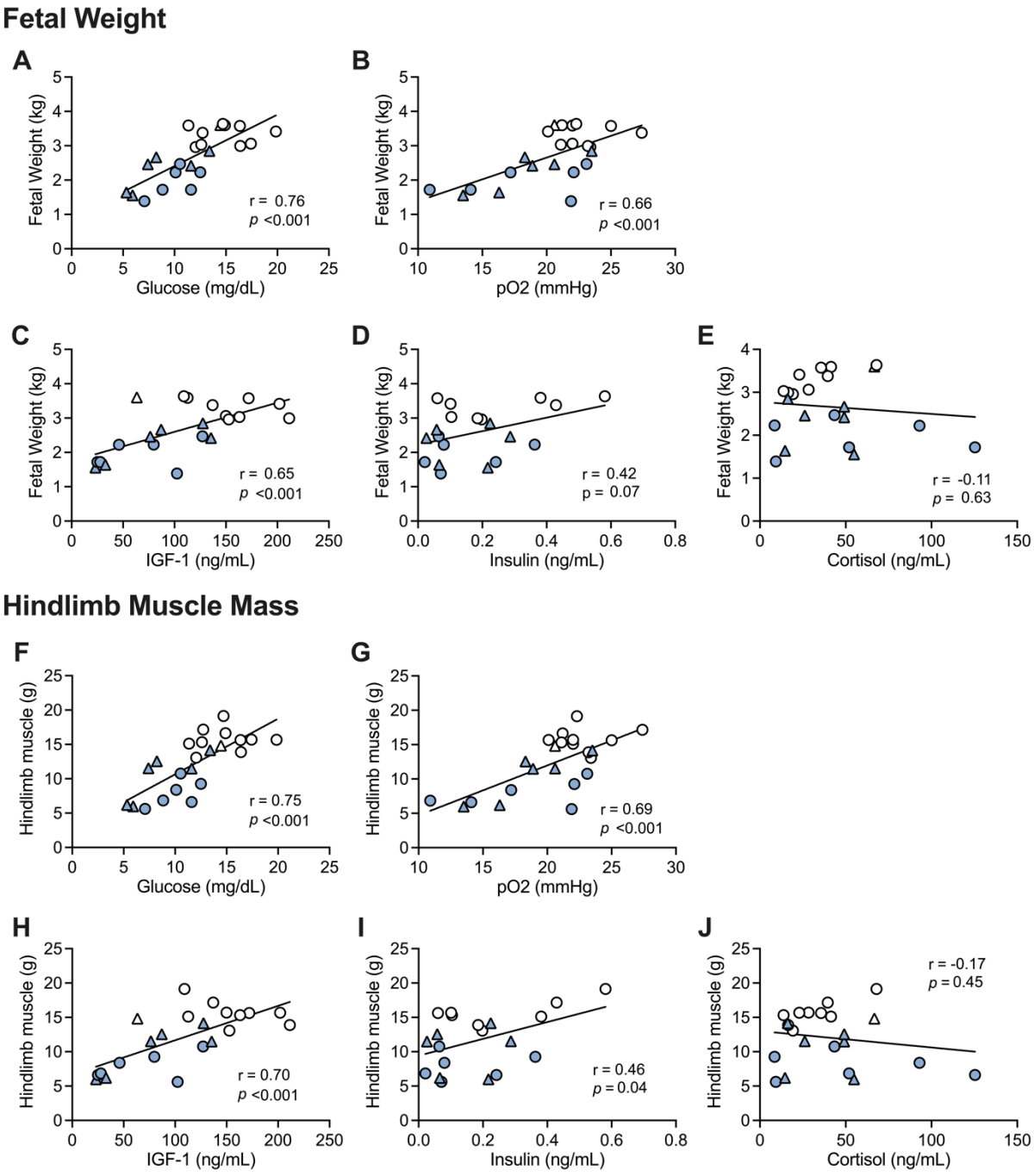

Figure 4.7. Associations between circulating factors and fetal growth. Fetal glucose (n=23), PaO_2 (n=23), and IGF-1 (n=22) correlated positively with (A-C) fetal weight and (F-G) hindlimb muscle mass in all FGR and CON sheep. (D) Insulin levels tended to increase with fetal weight

and (I) correlated positively with hindlimb mass (n=20). Fetal cortisol concentrations were not associated with (E) total body mass or (J) hindlimb mass across groups (n=22). Simple linear regressions were fit to each correlation, and best fit lines are plotted with raw data. Pearson's correlation coefficients (r) and p-values are listed. FGR fetuses are indicated by blue/closed symbols, CON fetuses by white/open symbols, and males and females are noted by triangles and circles, respectively.

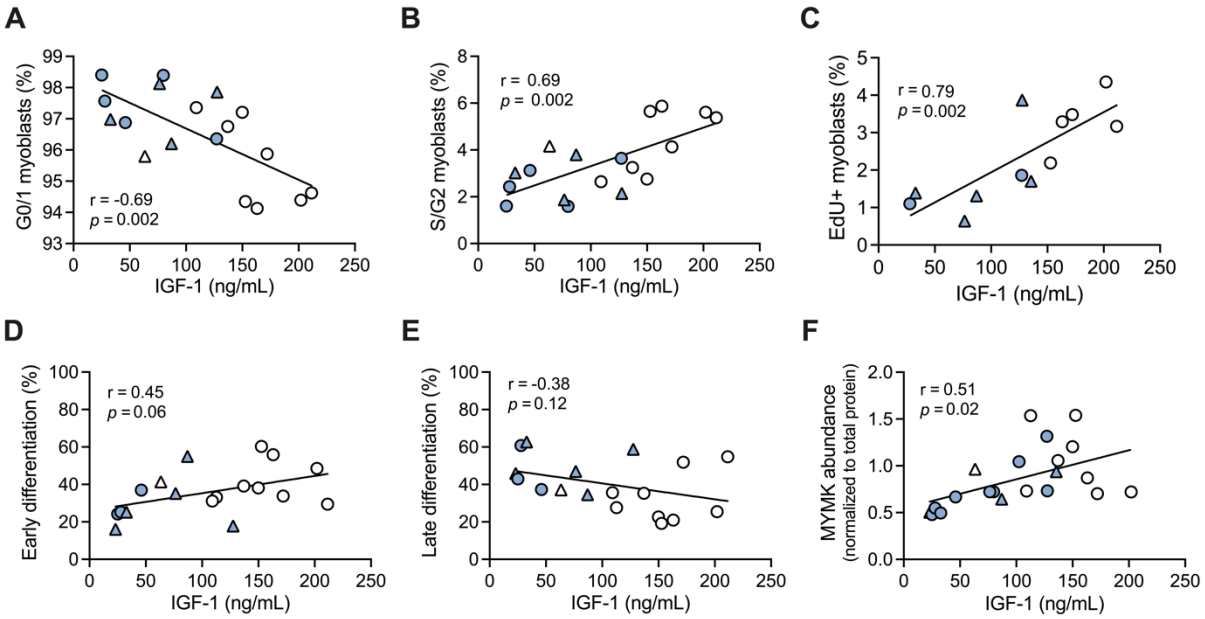

Figure 4.8. Associations between fetal IGF-1 and myoblast proliferation and differentiation rates. (A) Circulating IGF-1 levels correlated negatively with the proportion of myoblasts resting in G0/1 phase and (B) positively with the percentage of proliferative myoblasts in S/G2 (n=18). (C) Fetal IGF-1 also correlated positively with the proportion of EdU+ myoblasts across all FGR and CON animals (n=12). (D) The concentration of IGF-1 tended to increase with the proportion of myoblasts in early differentiation (MyoD+/MyoG+) and (E) decrease with the percentage of late differentiation (MyoD-/MyoG+) myoblasts (n=18). (F) There was a positive linear relationship between fetal IGF-1 and Mymk abundance across groups (n=12). Simple linear regressions were fit to each correlation, and best fit lines are plotted with raw data. Pearson's correlation coefficients (r) and p-values are listed. FGR fetuses are indicated by blue/closed symbols, CON fetuses by white/open symbols, and males and females are represented by triangles and circles, respectively.

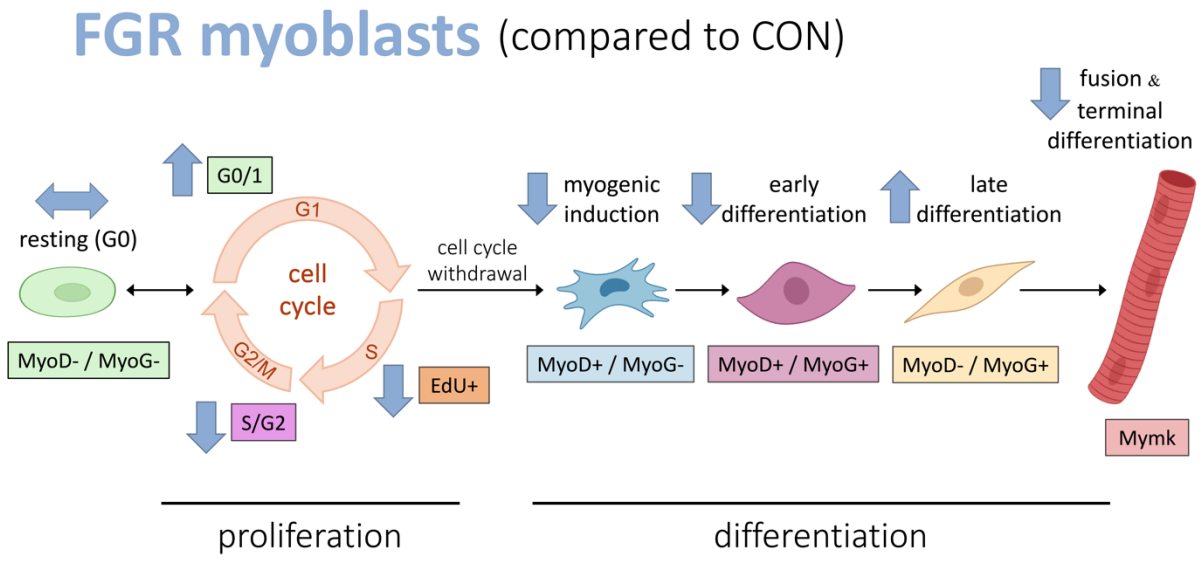

Figure 4.9. Schematic representation of skeletal myoblast growth programs in FGR fetuses compared to CON. While the proportion of non-committed progenitor cells is similar between FGR and CON groups, FGR fetuses had decreased rates of myoblast proliferation, indicated by reductions in the percentages of S/G2 and EdU+ myoblasts. FGR fetuses also had a lower percentage of cells in the initial stages of myogenesis, including activation and myogenic lineage commitment as well as early terminal differentiation. The proportion of unfused, late differentiation myoblasts was increased in FGR, which may result from impairments in myoblast fusion due to deficits in Mymk protein in FGR skeletal muscle.

V. CONCLUSION

Key Findings

Using an innovative flow cytometry approach to evaluate cardiomyocyte and skeletal myoblast development in FGR and CON fetuses, I identified impairments in FGR progenitor cell programming that likely precede lifelong deficits in cardiac and skeletal muscle growth and function. LV cardiomyocytes from FGR fetuses had impairments in terminal differentiation and maturation, indicated by reductions in the percentage of binucleated, non-replicating cells. In FGR hearts, a greater proportion of binucleated LV cardiomyocytes continued endocycling instead of progressing to terminal differentiation or cytokinesis. In the RV, cardiomyocytes from FGR fetuses displayed significant reductions in proliferation compared to CON. Similar to the LV, endocycling was upregulated in RV cardiomyocytes from FGR hearts, indicating that the processes regulating cytokinesis are likely disrupted in FGR. These finding reflect significant shifts in fetal cardiomyocyte programming in favor of endocycling and polyploidy over proliferation and terminal differentiation.

In the skeletal muscle, I observed lower rates of myoblast proliferation in FGR fetuses, indicated by reductions in the percentage of muscle progenitor cells that engaged in cell cycle activity *in utero*. FGR and CON fetuses had similar percentages of non-committed muscle progenitor cells, but the proportions of myoblasts in the initial stages of terminal differentiation were decreased in FGR. Surprisingly, the percentage of unfused, late-differentiation myoblasts was increased in FGR, despite lower rates of myogenic induction and early differentiation. However, reductions in the abundance of *Mymk* protein suggest that impairments in myoblast fusion may be limiting the contribution of late-differentiation myocytes to myofiber hypertrophy.

This disruption to terminal differentiation may be causing myocytes to accumulate beneath the basal lamina of mature muscle fibers, and likely plays a critical role in mediating the skeletal muscle deficits observed in FGR fetuses.

Biomedical Impact

This study is among the first to investigate the mechanisms underlying deficits in FGR cardiac and skeletal muscle development using dynamic measures of cardiomyocyte and skeletal myoblast proliferation and maturation *in vivo.* In FGR fetuses, cardiomyocyte endoreplication was markedly increased, reflecting a shift from cellular proliferation and maturation toward ploidy enhancement. This adaptation, while potentially compensatory under hypoxic and nutrient-restricted conditions, comes at the expense of cardiomyocyte expansion, terminal differentiation, and cardiac muscle growth during fetal development. Strong positive correlations between LV mass and measures of cardiomyocyte maturation suggest that FGR hearts may increase polyploidy to support cellular enlargement, potentially as a strategy to manage current or anticipated hemodynamic stress. This adaptation could contribute to pathological cardiac hypertrophy and is consistent with previous reports linking FGR to cardiovascular dysfunction later in life. Further, positive associations between cardiomyocyte division and RV mass imply that cardiac growth in FGR fetuses is also restricted by disruptions in cytokinesis. As in the LV, RV cardiomyocytes appear to engage in endoreplication without cell division, potentially to support growth under energy constraints by avoiding the demands of cytoskeletal reorganization. This novel finding suggests an adaptive mechanism through which both ventricles attempt to compensate for reductions in substrate availability *in utero*. However, because cardiomyocyte expansion and

maturation are restricted to the finite window of fetal development, these adaptations may ultimately compromise cardiac function later in life.

In skeletal muscle, my findings reveal a clear association between fetal growth and the rates of myoblast proliferation and terminal differentiation *in utero.* Deficits in muscle progenitor cell proliferation and differentiation in FGR may reflect both an adaptive intrauterine response to reductions in growth factor and substrate availability as well as potential epigenetic programming that could limit muscle growth and repair throughout postnatal life. The results in this dissertation identify that stimulation of cell cycle activity or myogenic induction alone is not sufficient to restore deficits in FGR skeletal muscle mass. Instead, my findings reveal that reductions fetal muscle growth may primarily be mediated by impairments in myoblast fusion, which restrict myonuclear accretion and the capacity to support myofiber hypertrophy in FGR.

Limitations

A primary limitation of this study was that we were not powered to test for sex differences due to the unequal distribution of males and females in FGR and CON groups. Additional research is needed to investigate interactions between FGR and fetal sex. However, our analysis should not be skewed by the predominantly female control group as female fetuses are reported to have smaller hearts and skeletal muscle compared to age-matched males (116, 292). While flow cytometry enabled the detailed investigation of fetal muscle progenitor cell dynamics, it is important to note that each reported subpopulation was calculated as a percentage of a single parent population of cardiomyocytes or skeletal muscle cells isolated from fetal tissue biopsies. Thus, changes in one subset could potentially influence perceived differences in others. To prevent this from skewing the results, careful attention was given to experimental design, appropriate controls,

and reproducible gating strategies. Moreover, similar trends in cardiac and skeletal myocyte dynamics were observed in absolute cell counts before normalization. Still, future studies should incorporate alternative methods, such as single cell RNA sequencing and imaging flow cytometry, to confirm these findings and provide a more comprehensive understanding of muscle progenitor cell dynamics in FGR fetuses.

Future Directions

Fetal IGF-1 levels predicted LV and RV growth, as well as the frequency of cardiomyocyte division, polyploidy, and LV myocyte binucleation across all fetuses. Our findings suggest that deficits in FGR cardiac muscle development may result from decreased cardiomyocyte proliferation, linked to reductions in circulating IGF-1. The critical role of IGF-1 in regulating fetal cardiomyocyte proliferation and maturation positions it as a promising therapeutic target for enhancing cardiac growth during intrauterine development. However, further research is needed to directly assess how IGF-1 modulates proliferation and differentiation in cardiomyocytes. The differences between LV and RV cardiomyocyte responses to FGR highlight the need for future work to determine the optimal timing to administer therapeutic interventions that target impairments in fetal cardiomyocyte development. Additionally, follow up studies should focus on targeted strategies to ensure cytokinesis or permanent withdrawal from the cell cycle after DNA synthesis is complete.

I observed strong positive correlations between fetal IGF-1 concentrations and skeletal myoblast proliferation rates *in utero*. It is well established that myoblast proliferation is stimulated by insulin and IGF-1, and IGF-1 has been shown to promote terminal differentiation through the same receptor that activates signaling for myoblast proliferation. Further, previous studies

demonstrate that augmenting growth factor concentrations *in vitro* can effectively restore proliferation rates in FGR myoblasts. This capacity for recovery is likely contingent upon modifying environmental conditions before the cells lose their developmental plasticity. Therefore, supplementing IGF-1 levels *in utero* may be both necessary and sufficient to alleviate deficits in myoblast proliferation and promote skeletal muscle growth in FGR fetuses, but further work is needed to test this hypothesis.

My findings suggest a central role for IGF-1 in regulating specific aspects of fetal cardiomyocyte and skeletal myoblast development. Further, the results of this research indicate that deficits in FGR cardiac and skeletal muscle growth may result from limitations in growth factor availability *in utero.* Findings reported by Brown et al. (2016), Chang et al. (2021), and Stremming et al. (2022, 2024) suggest that intrauterine growth factor supplementation enhances cardiac and skeletal muscle growth in CON fetuses. Additionally, my preliminary data indicate that administering a combination of IGF-1 and insulin to CON fetuses significantly increases myoblast proliferation rates *in utero* (***Supplemental Fig. 5.1A-B***). Therefore, additional research is warranted to determine whether exogenous growth factor stimulation can improve cardiomyocyte and skeletal myoblast dynamics in FGR fetuses and recover cardiac and skeletal muscle growth *in utero.*

VI. APPENDIX: SUPPLEMENTAL MATERIALS

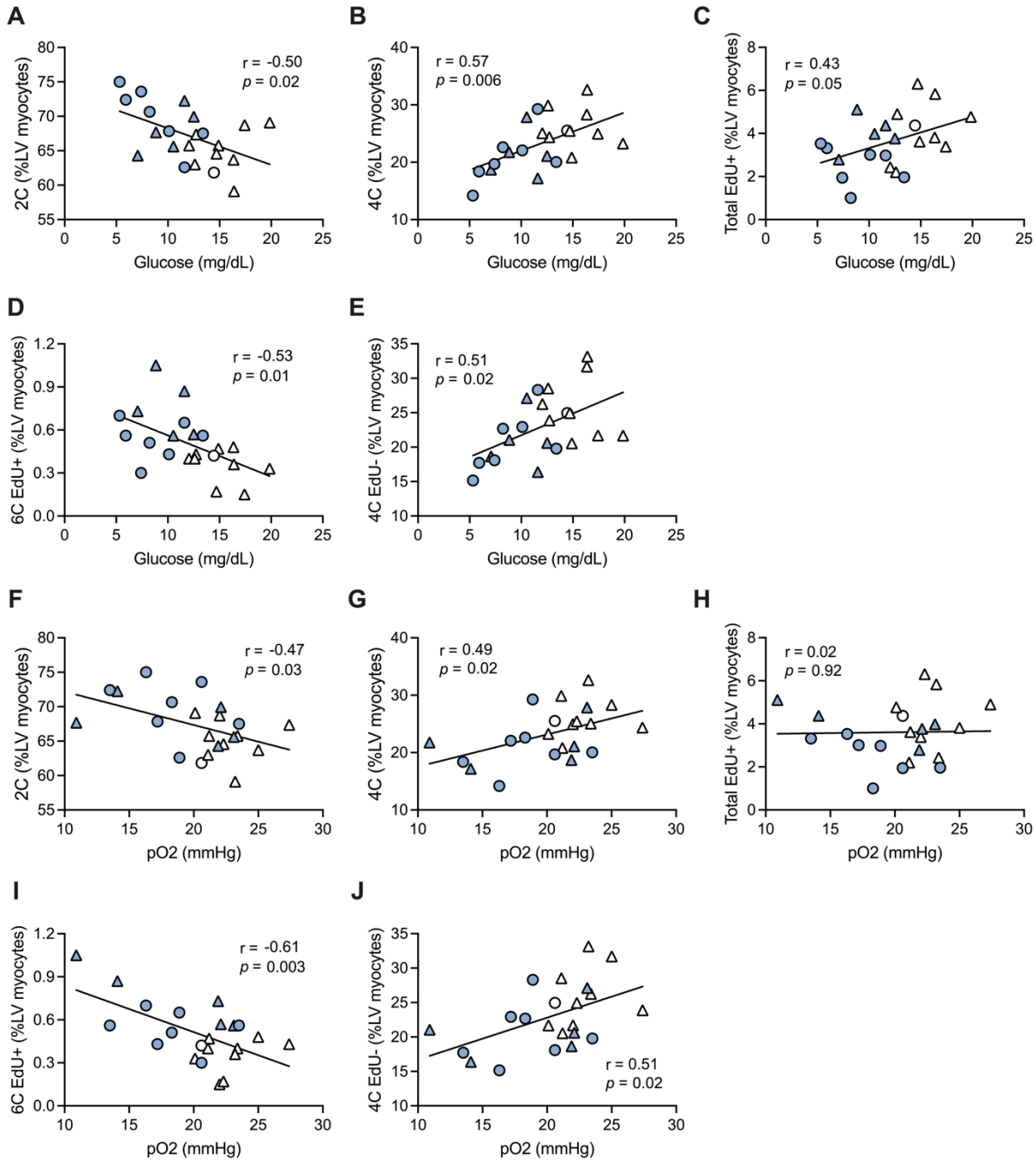

Supplemental Figure 3.1. Associations between LV cardiomyocyte measures and circulating levels of glucose and PaO_2.

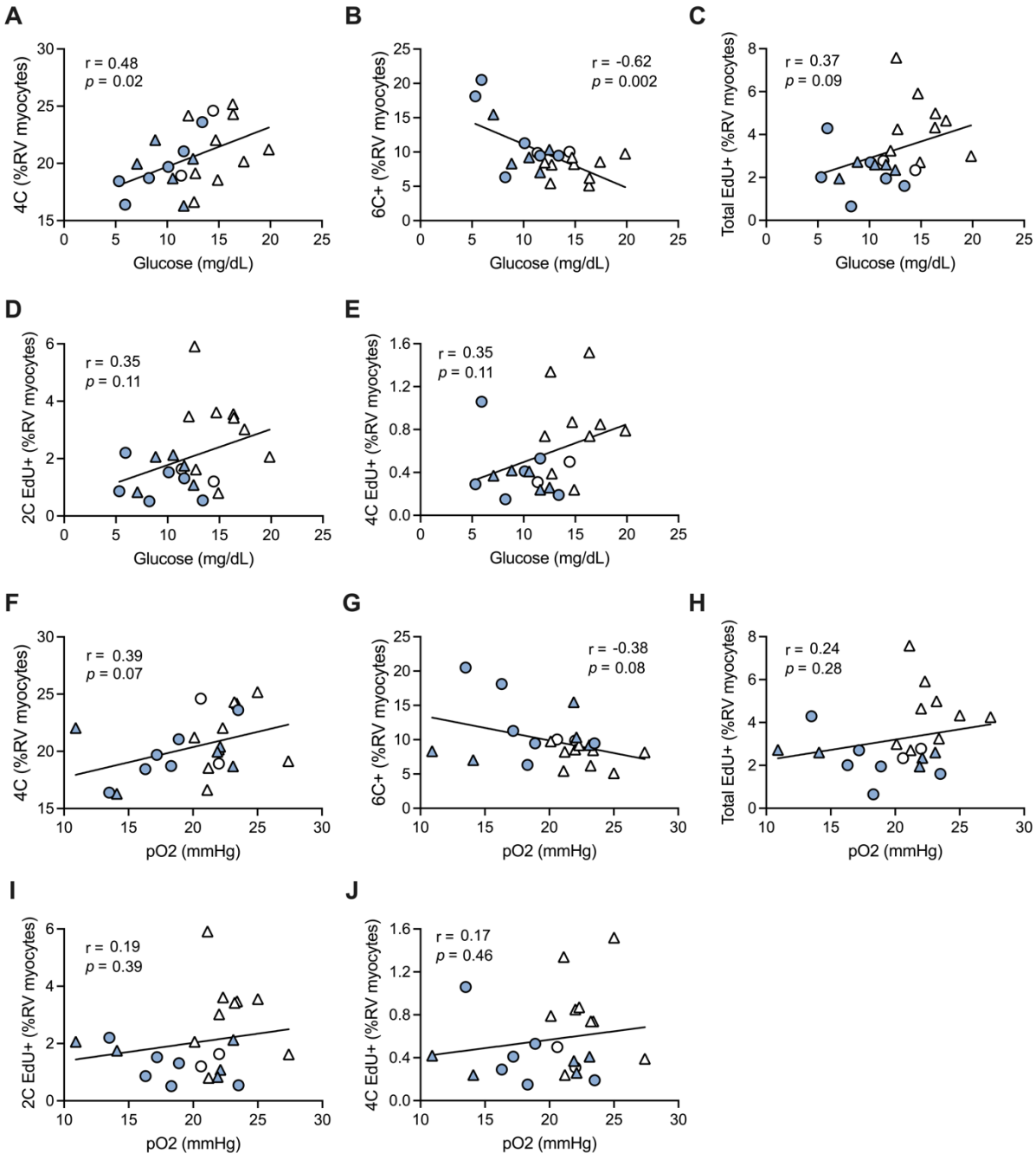

Supplemental Figure 3.2. Associations between RV cardiomyocyte measures and circulating levels of glucose and PaO_2.

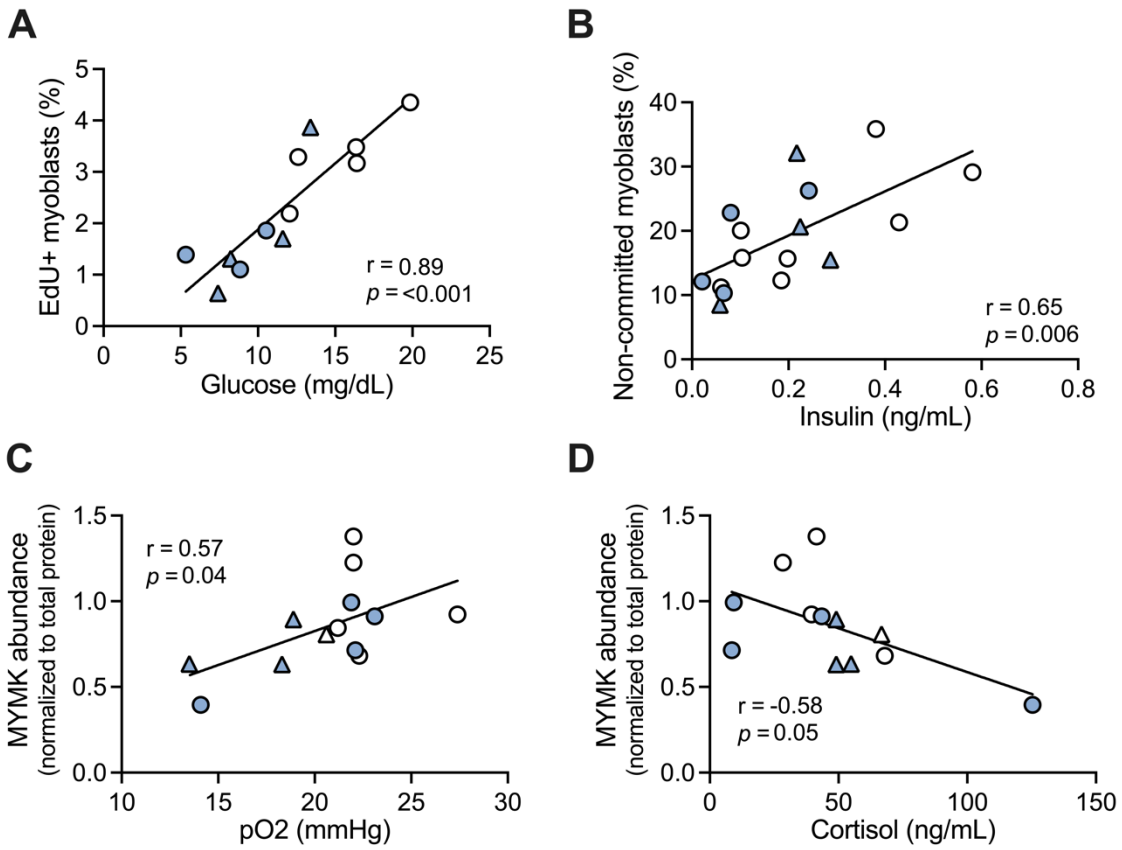

Supplemental Figure 4.1. Associations between circulating factors and fetal myoblast and skeletal muscle dynamics in FGR and CON sheep.

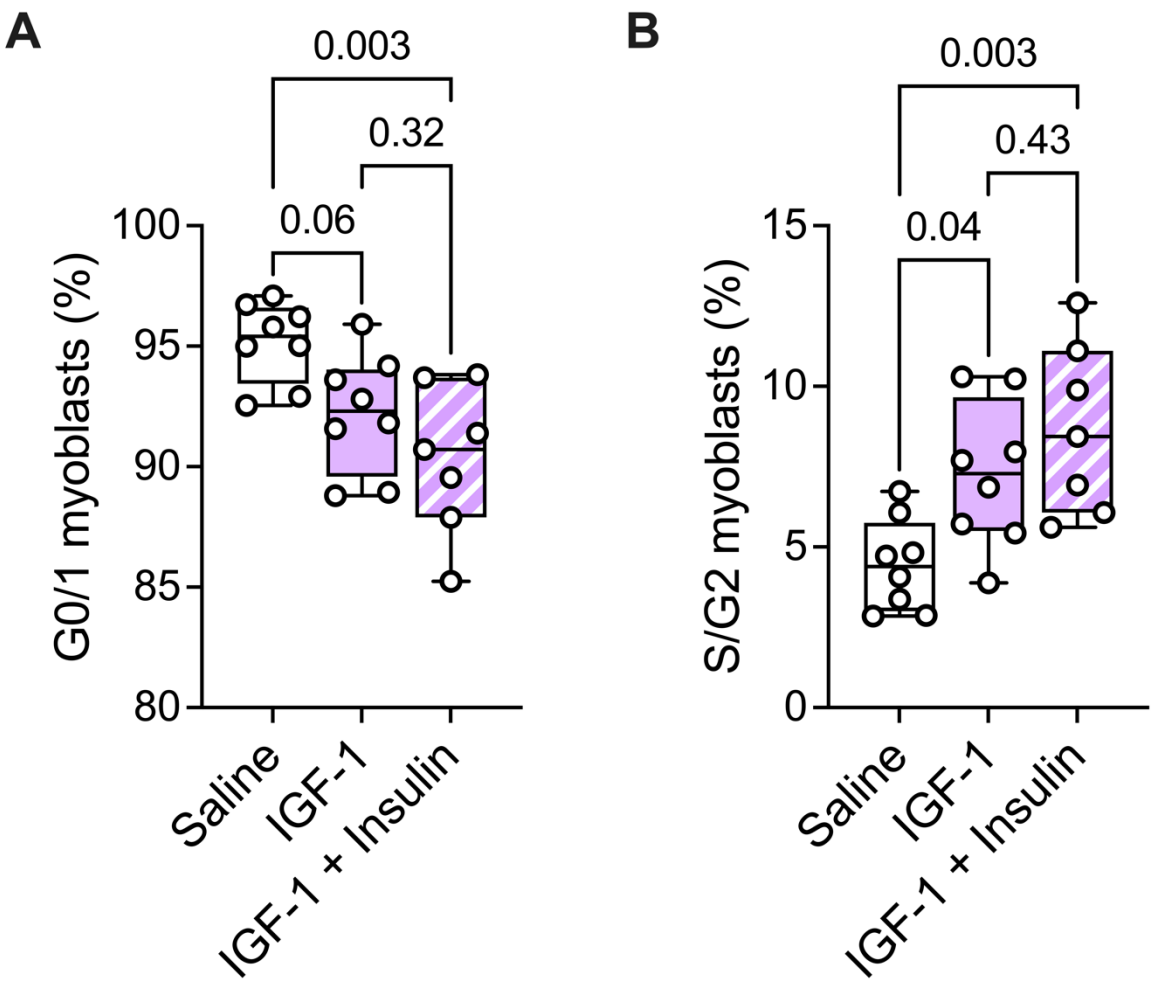

Supplemental Figure 5.1. Intrauterine supplementation of IGF-1 + Insulin increases skeletal myoblast proliferation rates in normally grown fetal sheep from healthy pregnancies.

VII. REFERENCES

1. **Barker DJ**, **Osmond C**. Diet and coronary heart disease in England and Wales during and after the second world war. *J Epidemiol Community Health* 40: 37–44, 1986.

2. **Barker DJP**, **Osmond C**. INFANT MORTALITY, CHILDHOOD NUTRITION, AND ISCHAEMIC HEART DISEASE IN ENGLAND AND WALES. *The Lancet* 327: 1077–1081, 1986. doi: 10.1016/S0140-6736(86)91340-1.

3. **Barker DJP**, **Osmond C**, **Winter PD**, **Margetts B**, **Simmonds SJ**. WEIGHT IN INFANCY AND DEATH FROM ISCHAEMIC HEART DISEASE. *The Lancet* 334: 577–580, 1989. doi: 10.1016/S0140-6736(89)90710-1.

4. **Barker DJ**, **Osmond C**, **Golding J**, **Kuh D**, **Wadsworth ME**. Growth in utero, blood pressure in childhood and adult life, and mortality from cardiovascular disease. *BMJ* 298: 564–567, 1989.

5. **Osmond C**, **Barker DJ**, **Slattery JM**. Risk of death from cardiovascular disease and chronic bronchitis determined by place of birth in England and Wales. *J Epidemiol Community Health* 44: 139–141, 1990.

6. **Barker DJ**, **Winter PD**, **Osmond C**, **Margetts B**, **Simmonds SJ**. Weight in infancy and death from ischaemic heart disease. *Lancet Lond Engl* 2: 577–580, 1989. doi: 10.1016/s0140-6736(89)90710-1.

7. **Barker DJ**, **Osmond C**, **Law CM**. The intrauterine and early postnatal origins of cardiovascular disease and chronic bronchitis. *J Epidemiol Community Health* 43: 237–240, 1989.

8. **Barker DJ**, **Gluckman PD**, **Godfrey KM**, **Harding JE**, **Owens JA**, **Robinson JS**. Fetal nutrition and cardiovascular disease in adult life. *Lancet Lond Engl* 341: 938–941, 1993. doi: 10.1016/0140-6736(93)91224-a.

9. **Barker DJ**. Fetal origins of coronary heart disease. *BMJ* 311: 171–174, 1995.

10. **Rich-Edwards JW**, **Stampfer MJ**, **Manson JE**, **Rosner B**, **Hankinson SE**, **Colditz GA**, **Willett WC**, **Hennekens CH**. Birth weight and risk of cardiovascular disease in a cohort of women followed up since 1976. *BMJ* 315: 396–400, 1997.

11. **Roseboom TJ**, **van der Meulen JHP**, **Ravelli ACJ**, **Osmond C**, **Barker DJP**, **Bleker OP**. Effects of prenatal exposure to the Dutch famine on adult disease in later life: an overview. *Mol Cell Endocrinol* 185: 93–98, 2001. doi: 10.1016/S0303-7207(01)00721-3.

12. **Eriksson JG**, **Forsén T**, **Tuomilehto J**, **Osmond C**, **Barker DJ**. Early growth, adult income, and risk of stroke. *Stroke* 31: 869–874, 2000. doi: 10.1161/01.str.31.4.869.

13. **Eriksson JG**, **Forsén T**, **Tuomilehto J**, **Osmond C**, **Barker DJP**. Early growth and coronary heart disease in later life: longitudinal study. *BMJ* 322: 949–953, 2001.

14. **Barker DJP**, **Forsén T**, **Uutela A**, **Osmond C**, **Eriksson JG**. Size at birth and resilience to effects of poor living conditions in adult life: longitudinal study. *BMJ* 323: 1273, 2001.

15. **Hyppönen E**, **Leon DA**, **Kenward MG**, **Lithell H**. Prenatal growth and risk of occlusive and haemorrhagic stroke in Swedish men and women born 1915-29: historical cohort study. *BMJ* 323: 1033–1034, 2001.

16. **Lawlor DA**, **Ronalds G**, **Clark H**, **Smith GD**, **Leon DA**. Birth weight is inversely associated with incident coronary heart disease and stroke among individuals born in the 1950s: findings from the Aberdeen Children of the 1950s prospective cohort study. *Circulation* 112: 1414–1418, 2005. doi: 10.1161/CIRCULATIONAHA.104.528356.

17. **Stein AD**, **Zybert PA**, **van der Pal-de Bruin K**, **Lumey LH**. Exposure to famine during gestation, size at birth, and blood pressure at age 59 y: evidence from the dutch famine. *Eur J Epidemiol* 21: 759–765, 2006. doi: 10.1007/s10654-006-9065-2.

18. **Osmond C**, **Kajantie E**, **Forsén TJ**, **Eriksson JG**, **Barker DJP**. Infant Growth and Stroke in Adult Life. *Stroke* 38: 264–270, 2007. doi: 10.1161/01.STR.0000254471.72186.03.

19. **Frankel S**, **Elwood P**, **Sweetnam P**, **Yarnell J**, **Smith GD**. Birthweight, body-mass index in middle age, and incident coronary heart disease. *Lancet Lond Engl* 348: 1478–1480, 1996. doi: 10.1016/S0140-6736(96)03482-4.

20. **Stein CE**, **Fall CH**, **Kumaran K**, **Osmond C**, **Cox V**, **Barker DJ**. Fetal growth and coronary heart disease in south India. *Lancet Lond Engl* 348: 1269–1273, 1996. doi: 10.1016/s0140-6736(96)04547-3.

21. **Leon DA**, **Lithell HO**, **Vâgerö D**, **Koupilová I**, **Mohsen R**, **Berglund L**, **Lithell UB**, **McKeigue PM**. Reduced fetal growth rate and increased risk of death from ischaemic heart disease: cohort study of 15 000 Swedish men and women born 1915-29. *BMJ* 317: 241–245, 1998. doi: 10.1136/bmj.317.7153.241.

22. **Forsén T**, **Eriksson JG**, **Tuomilehto J**, **Teramo K**, **Osmond C**, **Barker DJ**. Mother's weight in pregnancy and coronary heart disease in a cohort of Finnish men: follow up study. *BMJ* 315: 837–840, 1997. doi: 10.1136/bmj.315.7112.837.

23. **Eriksson J**, **Forsén T**, **Tuomilehto J**, **Osmond C**, **Barker D**. Size at birth, childhood growth and obesity in adult life. *Int J Obes Relat Metab Disord J Int Assoc Study Obes* 25: 735–740, 2001. doi: 10.1038/sj.ijo.0801602.

24. **Oken E**, **Gillman MW**. Fetal origins of obesity. *Obes Res* 11: 496–506, 2003. doi: 10.1038/oby.2003.69.

25. **Gluckman PD**, **Hanson MA**, **Pinal C**. The developmental origins of adult disease. *Matern Child Nutr* 1: 130–141, 2005. doi: 10.1111/j.1740-8709.2005.00020.x.

26. **Painter RC**, **Osmond C**, **Gluckman P**, **Hanson M**, **Phillips DIW**, **Roseboom TJ**. Transgenerational effects of prenatal exposure to the Dutch famine on neonatal adiposity and health in later life. *BJOG Int J Obstet Gynaecol* 115: 1243–1249, 2008. doi: 10.1111/j.1471-0528.2008.01822.x.

27. **Hales CN**, **Barker DJ**, **Clark PM**, **Cox LJ**, **Fall C**, **Osmond C**, **Winter PD**. Fetal and infant growth and impaired glucose tolerance at age 64. *Br Med J* 303: 1019–1022, 1991. doi: 10.1136/bmj.303.6809.1019.

28. **Ravelli A**, **van der Meulen J**, **Michels R**, **Osmond C**, **Barker D**, **Hales C**, **Bleker O**. Glucose tolerance in adults after prenatal exposure to famine. *The Lancet* 351: 173–177, 1998. doi: 10.1016/S0140-6736(97)07244-9.

29. **Barker DJP**. The developmental origins of insulin resistance. *Horm Res* 64 Suppl 3: 2–7, 2005. doi: 10.1159/000089311.

30. **Hales CN**, **Barker DJ**. Type 2 (non-insulin-dependent) diabetes mellitus: the thrifty phenotype hypothesis. *Diabetologia* 35: 595–601, 1992. doi: 10.1007/BF00400248.

31. **Eriksson JG**, **Forsen TJ**, **Osmond C**, **Barker DJP**. Pathways of infant and childhood growth that lead to type 2 diabetes. *Diabetes Care* 26: 3006–3010, 2003. doi: 10.2337/diacare.26.11.3006.

32. **Bateson P**, **Barker D**, **Clutton-Brock T**, **Deb D**, **D'Udine B**, **Foley RA**, **Gluckman P**, **Godfrey K**, **Kirkwood T**, **Lahr MM**, **McNamara J**, **Metcalfe NB**, **Monaghan P**, **Spencer HG**, **Sultan SE**. Developmental plasticity and human health. *Nature* 430: 419–421, 2004. doi: 10.1038/nature02725.

33. **Gluckman PD**, **Hanson MA**, **Spencer HG**, **Bateson P**. Environmental influences during development and their later consequences for health and disease: implications for the interpretation of empirical studies. *Proc R Soc B Biol Sci* 272: 671–677, 2005. doi: 10.1098/rspb.2004.3001.

34. **Sandman CA**, **Glynn LM**, **Davis EP**. Is there a viability–vulnerability tradeoff? Sex differences in fetal programming. *J Psychosom Res* 75: 327–335, 2013. doi: 10.1016/j.jpsychores.2013.07.009.

35. **Hanson MA**, **Gluckman PD**. Early Developmental Conditioning of Later Health and Disease: Physiology or Pathophysiology? *Physiol Rev* 94: 1027–1076, 2014. doi: 10.1152/physrev.00029.2013.

36. **Godfrey KM**, **Reynolds RM**, **Prescott SL**, **Nyirenda M**, **Jaddoe VWV**, **Eriksson JG**, **Broekman BFP**. Influence of maternal obesity on the long-term health of offspring. *Lancet Diabetes Endocrinol* 5: 53–64, 2017. doi: 10.1016/S2213-8587(16)30107-3.

37. **Godfrey K**, **Robinson S**, **Barker DJ**, **Osmond C**, **Cox V**. Maternal nutrition in early and late pregnancy in relation to placental and fetal growth. *BMJ* 312: 410–414, 1996.

38. **Gluckman PD**, **Hanson MA**. Maternal constraint of fetal growth and its consequences. *Semin Fetal Neonatal Med* 9: 419–425, 2004. doi: 10.1016/j.siny.2004.03.001.

39. **Barker DJ**, **Martyn CN**. The maternal and fetal origins of cardiovascular disease. *J Epidemiol Community Health* 46: 8–11, 1992.

40. **Agarwal P**, **Morriseau TS**, **Kereliuk SM**, **Doucette CA**, **Wicklow BA**, **Dolinsky VW**. Maternal obesity, diabetes during pregnancy and epigenetic mechanisms that influence the developmental origins of cardiometabolic disease in the offspring. *Crit Rev Clin Lab Sci* 55: 71–101, 2018. doi: 10.1080/10408363.2017.1422109.

41. **Barbour LA**, **Hernandez TL**. Maternal Non-glycemic Contributors to Fetal Growth in Obesity and Gestational Diabetes: Spotlight on Lipids. *Curr Diab Rep* 18: 37, 2018. doi: 10.1007/s11892-018-1008-2.

42. **Berglund SK**, **García-Valdés L**, **Torres-Espinola FJ**, **Segura MT**, **Martínez-Zaldívar C**, **Aguilar MJ**, **Agil A**, **Lorente JA**, **Florido J**, **Padilla C**, **Altmäe S**, **Marcos A**, **López-Sabater MC**, **Campoy C**, **on behalf of the PREOBE team**. Maternal, fetal and perinatal alterations associated with obesity, overweight and gestational diabetes: an observational cohort study (PREOBE). *BMC Public Health* 16: 207, 2016. doi: 10.1186/s12889-016-2809-3.

43. **Barbour LA**, **McCurdy CE**, **Hernandez TL**, **Kirwan JP**, **Catalano PM**, **Friedman JE**. Cellular Mechanisms for Insulin Resistance in Normal Pregnancy and Gestational Diabetes. *Diabetes Care* 30: S112–S119, 2007. doi: 10.2337/dc07-s202.

44. **Barrea L**, **Vetrani C**, **Verde L**, **Frias-Toral E**, **Garcia-Velasquez E**, **Ranasinghe P**, **Mendez V**, **Jayawardena R**, **Savastano S**, **Colao A**, **Muscogiuri G**. Gestational obesity: An unconventional endocrine disruptor for the fetus. *Biochem Pharmacol* 198: 114974, 2022. doi: 10.1016/j.bcp.2022.114974.

45. **Du M**, **Yan X**, **Tong JF**, **Zhao J**, **Zhu MJ**. Maternal Obesity, Inflammation, and Fetal Skeletal Muscle Development. *Biol Reprod* 82: 4–12, 2010. doi: 10.1095/biolreprod.109.077099.

46. **Perng W**, **Oken E**. Maternal obesity and associated offspring diabetes mellitus. *Nat Rev Endocrinol* 15: 630–632, 2019. doi: 10.1038/s41574-019-0249-8.

47. **Heslehurst N**, **Vieira R**, **Akhter Z**, **Bailey H**, **Slack E**, **Ngongalah L**, **Pemu A**, **Rankin J**. The association between maternal body mass index and child obesity: A systematic review and meta-analysis. *PLoS Med* 16: e1002817, 2019. doi: 10.1371/journal.pmed.1002817.

48. **Gallardo JM**, **Gómez-López J**, **Medina-Bravo P**, **Juárez-Sánchez F**, **Contreras-Ramos A**, **Galicia-Esquivel M**, **Sánchez-Urbina R**, **Klünder-Klünder M**. Maternal obesity increases oxidative stress in the newborn. *Obesity* 23: 1650–1654, 2015. doi: 10.1002/oby.21159.

49. **McCurdy CE**, **Schenk S**, **Hetrick B**, **Houck J**, **Drew BG**, **Kaye S**, **Lashbrook M**, **Bergman BC**, **Takahashi DL**, **Dean TA**, **Nemkov T**, **Gertsman I**, **Hansen KC**, **Philp A**, **Hevener AL**, **Chicco AJ**, **Aagaard KM**, **Grove KL**, **Friedman JE**. Maternal obesity reduces oxidative capacity in fetal skeletal muscle of Japanese macaques. *JCI Insight* 1: e86612, 2016. doi: 10.1172/jci.insight.86612.

50. **Zhu M-J**, **Ford SP**, **Nathanielsz PW**, **Du M**. Effect of Maternal Nutrient Restriction in Sheep on the Development of Fetal Skeletal Muscle. *Biol Reprod* 71: 1968–1973, 2004. doi: 10.1095/biolreprod.104.034561.

51. **Zhu MJ**, **Ford SP**, **Means WJ**, **Hess BW**, **Nathanielsz PW**, **Du M**. Maternal nutrient restriction affects properties of skeletal muscle in offspring. *J Physiol* 575: 241–250, 2006. doi: 10.1113/jphysiol.2006.112110.

52. **Campodonico-Burnett W**, **Hetrick B**, **Wesolowski SR**, **Schenk S**, **Takahashi DL**, **Dean TA**, **Sullivan EL**, **Kievit P**, **Gannon M**, **Aagaard K**, **Friedman JE**, **McCurdy CE**. Maternal Obesity and Western-Style Diet Impair Fetal and Juvenile Offspring Skeletal Muscle Insulin-Stimulated Glucose Transport in Nonhuman Primates. *Diabetes* 69: 1389–1400, 2020. doi: 10.2337/db19-1218.

53. **Greyslak KT**, **Hetrick B**, **Bergman BC**, **Dean TA**, **Wesolowski SR**, **Gannon M**, **Schenk S**, **Sullivan EL**, **Aagaard KM**, **Kievit P**, **Chicco AJ**, **Friedman JE**, **McCurdy CE**. A Maternal Western-Style Diet Impairs Skeletal Muscle Lipid Metabolism in Adolescent Japanese Macaques. *Diabetes* 72: 1766–1780, 2023. doi: 10.2337/db23-0289.

54. **Bertossa MR**, **Darby JRT**, **Holman SL**, **Meakin AS**, **Li C**, **Huber HF**, **Wiese MD**, **Nathanielsz PW**, **Morrison JL**. Maternal high fat–high energy diet alters metabolic factors in the non-human primate fetal heart. *J Physiol* n/a, [date unknown]. doi: 10.1113/JP286861.

55. **Keleher MR**, **Zaidi R**, **Shah S**, **Oakley ME**, **Pavlatos C**, **Idrissi SE**, **Xing X**, **Li D**, **Wang T**, **Cheverud JM**. Maternal high-fat diet associated with altered gene expression, DNA methylation, and obesity risk in mouse offspring. *PLOS ONE* 13: e0192606, 2018. doi: 10.1371/journal.pone.0192606.

56. **Litzenburger T**, **Huber E-K**, **Dinger K**, **Wilke R**, **Vohlen C**, **Selle J**, **Kadah M**, **Persigehl T**, **Heneweer C**, **Dötsch J**, **Alejandre Alcazar MA**. Maternal high-fat diet induces long-term obesity with sex-dependent metabolic programming of adipocyte differentiation,

hypertrophy and dysfunction in the offspring. *Clin Sci* 134: 921–939, 2020. doi: 10.1042/CS20191229.

57. **McCurdy CE**, **Bishop JM**, **Williams SM**, **Grayson BE**, **Smith MS**, **Friedman JE**, **Grove KL**. Maternal high-fat diet triggers lipotoxicity in the fetal livers of nonhuman primates. *J Clin Invest* 119: 323–335, 2009. doi: 10.1172/JCI32661.

58. **Nash MJ**, **Dobrinskikh E**, **Soderborg TK**, **Janssen RC**, **Takahashi DL**, **Dean TA**, **Varlamov O**, **Hennebold JD**, **Gannon M**, **Aagaard KM**, **McCurdy CE**, **Kievit P**, **Bergman BC**, **Jones KL**, **Pietras EM**, **Wesolowski SR**, **Friedman JE**. Maternal diet alters long-term innate immune cell memory in fetal and juvenile hematopoietic stem and progenitor cells in nonhuman primate offspring. *Cell Rep* 42: 112393, 2023. doi: 10.1016/j.celrep.2023.112393.

59. **Ross EJ**, **Graham DL**, **Money KM**, **Stanwood GD**. Developmental Consequences of Fetal Exposure to Drugs: What We Know and What We Still Must Learn. *Neuropsychopharmacology* 40: 61–87, 2015. doi: 10.1038/npp.2014.147.

60. **Abbott LC**, **Winzer-Serhan UH**. Smoking during pregnancy: lessons learned from epidemiological studies and experimental studies using animal models. *Crit Rev Toxicol* 42: 279–303, 2012. doi: 10.3109/10408444.2012.658506.

61. **Padula AM**, **Monk C**, **Brennan PA**, **Borders A**, **Barrett ES**, **McEvoy C**, **Foss S**, **Desai P**, **Alshawabkeh A**, **Wurth R**, **Salafia C**, **Fichorova R**, **Varshavsky J**, **Kress A**, **Woodruff TJ**, **Morello-Frosch R**. Maternal prenatal exposures to environmental chemicals and psychosocial stressors in the ECHO Program - implications for research on perinatal outcomes. *J Perinatol Off J Calif Perinat Assoc* 40: 10–24, 2020. doi: 10.1038/s41372-019-0510-y.

62. **Vesterinen HM**, **Morello-Frosch R**, **Sen S**, **Zeise L**, **Woodruff TJ**. Cumulative effects of prenatal-exposure to exogenous chemicals and psychosocial stress on fetal growth: Systematic-review of the human and animal evidence. *PLoS ONE* 12: e0176331, 2017. doi: 10.1371/journal.pone.0176331.

63. **Chen Y-P**, **Xiao X-M**, **Li J**, **Reichetzeder C**, **Wang Z-N**, **Hocher B**. Paternal body mass index (BMI) is associated with offspring intrauterine growth in a gender dependent manner. *PloS One* 7: e36329, 2012. doi: 10.1371/journal.pone.0036329.

64. **Fullston T**, **Teague EMCO**, **Palmer NO**, **DeBlasio MJ**, **Mitchell M**, **Corbett M**, **Print CG**, **Owens JA**, **Lane M**. Paternal obesity initiates metabolic disturbances in two generations of mice with incomplete penetrance to the F2 generation and alters the transcriptional profile of testis and sperm microRNA content. *FASEB J* 27: 4226–4243, 2013. doi: 10.1096/fj.12-224048.

65. **Cropley JE**, **Eaton SA**, **Aiken A**, **Young PE**, **Giannoulatou E**, **Ho JWK**, **Buckland ME**, **Keam SP**, **Hutvagner G**, **Humphreys DT**, **Langley KG**, **Henstridge DC**, **Martin DIK**,

Febbraio MA, **Suter CM**. Male-lineage transmission of an acquired metabolic phenotype induced by grand-paternal obesity. *Mol Metab* 5: 699–708, 2016. doi: 10.1016/j.molmet.2016.06.008.

66. **Sharp GC**, **Lawlor DA**. Paternal impact on the life course development of obesity and type 2 diabetes in the offspring. *Diabetologia* 62: 1802–1810, 2019. doi: 10.1007/s00125-019-4919-9.

67. **Dimasuay KG**, **Boeuf P**, **Powell TL**, **Jansson T**. Placental Responses to Changes in the Maternal Environment Determine Fetal Growth [Online]. *Front Physiol* 7, 2016. https://www.frontiersin.org/article/10.3389/fphys.2016.00012 [25 Feb. 2022].

68. **Barker DJ**, **Larsen G**, **Osmond C**, **Thornburg KL**, **Kajantie E**, **Eriksson JG**. The placental origins of sudden cardiac death. *Int J Epidemiol* 41: 1394–1399, 2012. doi: 10.1093/ije/dys116.

69. **Keleher MR**, **Erickson K**, **Smith HA**, **Kechris KJ**, **Yang IV**, **Dabelea D**, **Friedman JE**, **Boyle KE**, **Jansson T**. Placental Insulin/IGF-1 Signaling, PGC-1α, and Inflammatory Pathways Are Associated With Metabolic Outcomes at 4–6 Years of Age: The ECHO Healthy Start Cohort. *Diabetes* 70: 745–751, 2021. doi: 10.2337/db20-0902.

70. **Andrews C**, **Monthé-Drèze C**, **Sacks DA**, **Ma RCW**, **Tam WH**, **McIntyre HD**, **Lowe J**, **Catalano P**, **Sen S**. Role of maternal glucose metabolism in the association between maternal BMI and neonatal size and adiposity. *Int J Obes* 45: 515–524, 2021. doi: 10.1038/s41366-020-00705-1.

71. **Bianco ME**, **Kuang A**, **Josefson JL**, **Catalano PM**, **Dyer AR**, **Lowe LP**, **Metzger BE**, **Scholtens DM**, **Lowe WL**, **HAPO Follow-Up Study Cooperative Research Group**. Hyperglycemia and Adverse Pregnancy Outcome Follow-Up Study: newborn anthropometrics and childhood glucose metabolism. *Diabetologia* 64: 561–570, 2021. doi: 10.1007/s00125-020-05331-0.

72. **Cadaret CN**, **Merrick EM**, **Barnes TL**, **Beede KA**, **Posont RJ**, **Petersen JL**, **Yates DT**. Sustained maternal inflammation during the early third-trimester yields intrauterine growth restriction, impaired skeletal muscle glucose metabolism, and diminished β-cell function in fetal sheep,. *J Anim Sci* 97: 4822–4833, 2019. doi: 10.1093/jas/skz321.

73. **Pantham P**, **Aye ILMH**, **Powell TL**. Inflammation in Maternal Obesity and Gestational Diabetes Mellitus. *Placenta* 36: 709–715, 2015. doi: 10.1016/j.placenta.2015.04.006.

74. **Aye ILMH**, **Lager S**, **Ramirez VI**, **Gaccioli F**, **Dudley DJ**, **Jansson T**, **Powell TL**. Increasing Maternal Body Mass Index Is Associated with Systemic Inflammation in the Mother and the Activation of Distinct Placental Inflammatory Pathways. *Biol Reprod* 90: 129, 2014. doi: 10.1095/biolreprod.113.116186.

75. **Chang E**, **Hafner H**, **Varghese M**, **Griffin C**, **Clemente J**, **Islam M**, **Carlson Z**, **Zhu A**, **Hak L**, **Abrishami S**, **Gregg B**, **Singer K**. Programming effects of maternal and gestational obesity on offspring metabolism and metabolic inflammation. *Sci Rep* 9: 16027, 2019. doi: 10.1038/s41598-019-52583-x.

76. **Challier JC**, **Basu S**, **Bintein T**, **Minium J**, **Hotmire K**, **Catalano PM**, **Hauguel-de Mouzon S**. Obesity in Pregnancy Stimulates Macrophage Accumulation and Inflammation in the Placenta. *Placenta* 29: 274–281, 2008. doi: 10.1016/j.placenta.2007.12.010.

77. **Shook LL**, **James KE**, **Roberts DJ**, **Powe CE**, **Perlis RH**, **Thornburg KL**, **O'Tierney-Ginn PF**, **Edlow AG**. Sex-specific impact of maternal obesity on fetal placental macrophages and cord blood triglycerides. *Placenta* 140: 100–108, 2023. doi: 10.1016/j.placenta.2023.08.001.

78. **Waldrop SW**, **Niemiec S**, **Wood C**, **Gyllenhammer LE**, **Jansson T**, **Friedman JE**, **Tryggestad JB**, **Borengasser SJ**, **Davidson EJ**, **Yang IV**, **Kechris K**, **Dabelea D**, **Boyle KE**. Cord blood DNA methylation of immune and lipid metabolism genes is associated with maternal triglycerides and child adiposity. *Obesity* 32: 187–199, 2024. doi: 10.1002/oby.23915.

79. **DeLacey S**, **Gurra M**, **Arzu J**, **Lowe LP**, **Lowe WL**, **Scholtens DM**, **Josefson JL**. Leptin and adiposity measures from birth to later childhood: Findings from the Hyperglycemia and Adverse Pregnancy Outcomes Follow-Up Study. *Pediatr Obes* 19: e13087, 2024. doi: 10.1111/ijpo.13087.

80. **Josefson JL**, **Zeiss DM**, **Rademaker AW**, **Metzger BE**. Maternal Leptin Predicts Adiposity of the Neonate. *Horm Res Paediatr* 81: 13–19, 2013. doi: 10.1159/000355387.

81. **Saben J**, **Lindsey F**, **Zhong Y**, **Thakali K**, **Badger TM**, **Andres A**, **Gomez-Acevedo H**, **Shankar K**. Maternal Obesity is Associated with a Lipotoxic Placental Environment. *Placenta* 35: 171–177, 2014. doi: 10.1016/j.placenta.2014.01.003.

82. **Christensen SH**, **Rom AL**, **Greve T**, **Lewis JI**, **Frøkiær H**, **Allen LH**, **Mølgaard C**, **Renault KM**, **Michaelsen KF**. Maternal inflammatory, lipid and metabolic markers and associations with birth and breastfeeding outcomes [Online]. *Front Nutr* 10, 2023. https://www.frontiersin.org/articles/10.3389/fnut.2023.1223753 [26 Feb. 2024].

83. **Zambrano E**, **Nathanielsz PW**. Mechanisms by which maternal obesity programs offspring for obesity: evidence from animal studies. *Nutr Rev* 71: S42–S54, 2013. doi: 10.1111/nure.12068.

84. **Calvo MJ**, **Parra H**, **Santeliz R**, **Bautista J**, **Luzardo E**, **Villasmil N**, **Martínez MS**, **Chacín M**, **Cano C**, **Checa-Ros A**, **D'Marco L**, **Bermúdez V**, **De Sanctis JB**. The Placental Role in Gestational Diabetes Mellitus: A Molecular Perspective. *TouchREVIEWS Endocrinol* 20: 10–18, 2024. doi: 10.17925/EE.2024.20.1.5.

85. **Higgins L**, **Greenwood SL**, **Wareing M**, **Sibley CP**, **Mills TA**. Obesity and the placenta: A consideration of nutrient exchange mechanisms in relation to aberrant fetal growth. *Placenta* 32: 1–7, 2011. doi: 10.1016/j.placenta.2010.09.019.

86. **Vuppaladhadiam L**, **Lager J**, **Fiehn O**, **Weiss S**, **Chesney M**, **Hasdemir B**, **Bhargava A**. Human Placenta Buffers the Fetus from Adverse Effects of Perceived Maternal Stress. *Cells* 10: 379, 2021. doi: 10.3390/cells10020379.

87. **Oke SL**, **Hardy DB**. The Role of Cellular Stress in Intrauterine Growth Restriction and Postnatal Dysmetabolism. *Int J Mol Sci* 22: 6986, 2021. doi: 10.3390/ijms22136986.

88. **Rashid CS**, **Bansal A**, **Simmons RA**. Oxidative Stress, Intrauterine Growth Restriction, and Developmental Programming of Type 2 Diabetes. *Physiology* 33: 348–359, 2018. doi: 10.1152/physiol.00023.2018.

89. **Mao Q**, **Chen X**. An update on placental drug transport and its relevance to fetal drug exposure. *Med Rev* 2: 501–511, [date unknown]. doi: 10.1515/mr-2022-0025.

90. **Jones HE**, **Fielder A**. Neonatal abstinence syndrome: Historical perspective, current focus, future directions. *Prev Med* 80: 12–17, 2015. doi: 10.1016/j.ypmed.2015.07.017.

91. **Dong N**, **Zhu J**, **Wang R**, **Wang S**, **Chen Y**, **Wang C**, **Goh ELK**, **Chen T**. Maternal Methamphetamine Exposure Influences Behavioral Sensitization and Nucleus Accumbens DNA Methylation in Subsequent Generation. *Front Pharmacol* 13: 940798, 2022. doi: 10.3389/fphar.2022.940798.

92. **Lee CT-C**, **Chen VC-H**, **Lee JK-W**, **Wu S-I**, **Cheng G**, **Kao T-M**, **Wang S-Y**, **Gossop M**. Substance use before or during pregnancy and the risk of child mortality, perinatal morbidities and congenital anomalies. *Epidemiol Psychiatr Sci* 32: e43, 2023. doi: 10.1017/S2045796023000549.

93. **Rani P**, **Dhok A**. Effects of Pollution on Pregnancy and Infants. *Cureus* 15: e33906, [date unknown]. doi: 10.7759/cureus.33906.

94. **Segal TR**, **Giudice LC**. Before the beginning: environmental exposures and reproductive and obstetrical outcomes. *Fertil Steril* 112: 613–621, 2019. doi: 10.1016/j.fertnstert.2019.08.001.

95. **Lumey LH**, **Stein AD**. Offspring Birth Weights after Maternal Intrauterine Undernutrition: A Comparison within Sibships. *Am J Epidemiol* 146: 810–819, 1997. doi: 10.1093/oxfordjournals.aje.a009198.

96. **Gaccioli F**, **Lager S**. Placental Nutrient Transport and Intrauterine Growth Restriction. *Front Physiol* 7: 40, 2016. doi: 10.3389/fphys.2016.00040.

97. **Gaccioli F**, **Lager S**. Placental Nutrient Transport and Intrauterine Growth Restriction. *Front Physiol* 7: 40, 2016. doi: 10.3389/fphys.2016.00040.

98. **Thornburg KL**, **Louey S**. Uteroplacental Circulation and Fetal Vascular Function and Development. *Curr Vasc Pharmacol* 11: 748, 2013. doi: 10.2174/1570161111311050012.

99. **Wallace JM**, **Regnault TRH**, **Limesand SW**, **Hay WW**, **Anthony RV**. Investigating the causes of low birth weight in contrasting ovine paradigms. *J Physiol* 565: 19–26, 2005. doi: 10.1113/jphysiol.2004.082032.

100. **Griffiths SK**, **Campbell JP**. Placental structure, function and drug transfer. *Contin Educ Anaesth Crit Care Pain* 15: 84–89, 2015. doi: 10.1093/bjaceaccp/mku013.

101. **Charalambous M**, **Da Rocha ST**, **Ferguson-Smith AC**. Genomic imprinting, growth control and the allocation of nutritional resources: consequences for postnatal life. *Curr Opin Endocrinol Diabetes Obes* 14: 3–12, 2007. doi: 10.1097/MED.0b013e328013daa2.

102. **Regnault TRH**, **Galan HL**, **Parker TA**, **Anthony RV**. Placental development in normal and compromised pregnancies-- a review. *Placenta* 23 Suppl A: S119-129, 2002. doi: 10.1053/plac.2002.0792.

103. **Thame M**, **Osmond C**, **Bennett F**, **Wilks R**, **Forrester T**. Fetal growth is directly related to maternal anthropometry and placental volume. *Eur J Clin Nutr* 58: 894–900, 2004. doi: 10.1038/sj.ejcn.1601909.

104. **Brown LD**, **Hay WW**. Impact of placental insufficiency on fetal skeletal muscle growth. *Mol Cell Endocrinol* 435: 69–77, 2016. doi: 10.1016/j.mce.2016.03.017.

105. **Eriksson JG**, **Kajantie E**, **Thornburg KL**, **Osmond C**, **Barker DJ**. Mother's body size and placental size predict coronary heart disease in men. *Eur Heart J* 32: 2297, 2011. doi: 10.1093/eurheartj/ehr147.

106. **Barker DJP**, **Gelow J**, **Thornburg K**, **Osmond C**, **Kajantie E**, **Eriksson JG**. The early origins of chronic heart failure: impaired placental growth and initiation of insulin resistance in childhood. *Eur J Heart Fail* 12: 819–825, 2010. doi: 10.1093/eurjhf/hfq069.

107. **Morrison JL**. Sheep models of intrauterine growth restriction: fetal adaptations and consequences. *Clin Exp Pharmacol Physiol* 35: 730–743, 2008. doi: 10.1111/j.1440-1681.2008.04975.x.

108. **Baker J**, **Workman M**, **Bedrick E**, **Frey MA**, **Hurtado M**, **Pearson O**. Brains versus brawn: an empirical test of Barker's brain sparing model. *Am J Hum Biol Off J Hum Biol Counc* 22: 206–215, 2010. doi: 10.1002/ajhb.20979.

109. **Beltrand J**, **Verkauskiene R**, **Nicolescu R**, **Sibony O**, **Gaucherand P**, **Chevenne D**, **Claris O**, **Lévy-Marchal C**. Adaptive changes in neonatal hormonal and metabolic profiles

induced by fetal growth restriction. *J Clin Endocrinol Metab* 93: 4027–4032, 2008. doi: 10.1210/jc.2008-0562.

110. **Kensara OA**, **Wootton SA**, **Phillips DI**, **Patel M**, **Jackson AA**, **Elia M**, **Hertfordshire Study Group**. Fetal programming of body composition: relation between birth weight and body composition measured with dual-energy X-ray absorptiometry and anthropometric methods in older Englishmen. *Am J Clin Nutr* 82: 980–987, 2005. doi: 10.1093/ajcn/82.5.980.

111. **Larciprete G**, **Valensise H**, **Di Pierro G**, **Vasapollo B**, **Casalino B**, **Arduini D**, **Jarvis S**, **Cirese E**. Intrauterine growth restriction and fetal body composition. *Ultrasound Obstet Gynecol Off J Int Soc Ultrasound Obstet Gynecol* 26: 258–262, 2005. doi: 10.1002/uog.1980.

112. **Aihie Sayer A**, **Syddall HE**, **Dennison EM**, **Gilbody HJ**, **Duggleby SL**, **Cooper C**, **Barker DJ**, **Phillips DI**. Birth weight, weight at 1 y of age, and body composition in older men: findings from the Hertfordshire Cohort Study123. *Am J Clin Nutr* 80: 199–203, 2004. doi: 10.1093/ajcn/80.1.199.

113. **Thorn SR**, **Rozance PJ**, **Brown LD**, **Hay WW**. The Intrauterine Growth Restriction Phenotype: Fetal Adaptations and Potential Implications for Later Life Insulin Resistance and Diabetes. *Semin Reprod Med* 29: 225–236, 2011. doi: 10.1055/s-0031-1275516.

114. **Brown LD**. Endocrine regulation of fetal skeletal muscle growth: impact on future metabolic health. *J Endocrinol* 221: R13–R29, 2014. doi: 10.1530/JOE-13-0567.

115. **Jonker SS**, **Kamna D**, **Loturco D**, **Kailey J**, **Brown LD**. IUGR impairs cardiomyocyte growth and maturation in fetal sheep. *J Endocrinol* 239: 253–265, 2018. doi: 10.1530/JOE-18-0382.

116. **Botting KJ**, **Loke XY**, **Zhang S**, **Andersen JB**, **Nyengaard JR**, **Morrison JL**. IUGR decreases cardiomyocyte endowment and alters cardiac metabolism in a sex- and cause-of-IUGR-specific manner. *Am J Physiol-Regul Integr Comp Physiol* 315: R48–R67, 2018. doi: 10.1152/ajpregu.00180.2017.

117. **Jonker SS**, **Zhang L**, **Louey S**, **Giraud GD**, **Thornburg KL**, **Faber JJ**. Myocyte enlargement, differentiation, and proliferation kinetics in the fetal sheep heart. *J Appl Physiol* 102: 1130–1142, 2007. doi: 10.1152/japplphysiol.00937.2006.

118. **Jonker SS**, **Louey S**, **Giraud GD**, **Thornburg KL**, **Faber JJ**. Timing of cardiomyocyte growth, maturation, and attrition in perinatal sheep. *FASEB J* 29: 4346–4357, 2015. doi: 10.1096/fj.15-272013.

119. **Bishop SP**, **Zhang J**, **Ye L**. Cardiomyocyte Proliferation from Fetal- to Adult- and from Normal- to Hypertrophy and Failing Hearts. *Biology* 11: 880, 2022. doi: 10.3390/biology11060880.

120. **Thornburg K**, **Jonker S**, **O'Tierney P**, **Chattergoon N**, **Louey S**, **Faber J**, **Giraud G**. Regulation of the Cardiomyocyte Population in the Developing Heart. *Prog Biophys Mol Biol* 106: 289–299, 2011. doi: 10.1016/j.pbiomolbio.2010.11.010.

121. **Brown LD**. Endocrine regulation of fetal skeletal muscle growth: impact on future metabolic health. *J Endocrinol* 221: R13–R29, 2014. doi: 10.1530/JOE-13-0567.

122. **Tong JF**, **Yan X**, **Zhu MJ**, **Ford SP**, **Nathanielsz PW**, **Du M**. Maternal obesity downregulates myogenesis and beta-catenin signaling in fetal skeletal muscle. *Am J Physiol Endocrinol Metab* 296: E917-924, 2009. doi: 10.1152/ajpendo.90924.2008.

123. **Mikovic J**, **Brightwell C**, **Lindsay A**, **Wen Y**, **Kowalski G**, **Russell AP**, **Fry CS**, **Lamon S**. An obesogenic maternal environment impairs mouse growth patterns, satellite cell activation, and markers of postnatal myogenesis. *Am J Physiol-Endocrinol Metab* 319: E1008–E1018, 2020. doi: 10.1152/ajpendo.00398.2020.

124. **Soto SM**, **Blake AC**, **Wesolowski SR**, **Rozance PJ**, **Barthels KB**, **Gao B**, **Hetrick B**, **McCurdy CE**, **Garza NG**, **Hay WW**, **Leinwand LA**, **Friedman JE**, **Brown LD**. Myoblast replication is reduced in the IUGR fetus despite maintained proliferative capacity in vitro. *J Endocrinol* 232: 475–491, 2017. doi: 10.1530/JOE-16-0123.

125. **Tong J**, **Zhu MJ**, **Underwood KR**, **Hess BW**, **Ford SP**, **Du M**. AMP-activated protein kinase and adipogenesis in sheep fetal skeletal muscle and 3T3-L1 cells1. *J Anim Sci* 86: 1296–1305, 2008. doi: 10.2527/jas.2007-0794.

126. **Yates DT**, **Clarke DS**, **Macko AR**, **Anderson MJ**, **Shelton LA**, **Nearing M**, **Allen RE**, **Rhoads RP**, **Limesand SW**. Myoblasts from intrauterine growth-restricted sheep fetuses exhibit intrinsic deficiencies in proliferation that contribute to smaller semitendinosus myofibres. *J Physiol* 592: 3113–3125, 2014. doi: 10.1113/jphysiol.2014.272591.

127. **Boyle KE**, **Patinkin ZW**, **Shapiro ALB**, **Baker PR**, **Dabelea D**, **Friedman JE**. Mesenchymal Stem Cells From Infants Born to Obese Mothers Exhibit Greater Potential for Adipogenesis: The Healthy Start BabyBUMP Project. *Diabetes* 65: 647–659, 2016. doi: 10.2337/db15-0849.

128. **DeFronzo RA**, **Tripathy D**. Skeletal Muscle Insulin Resistance Is the Primary Defect in Type 2 Diabetes. *Diabetes Care* 32: S157–S163, 2009. doi: 10.2337/dc09-S302.

129. **Merz KE**, **Thurmond DC**. Role of Skeletal Muscle in Insulin Resistance and Glucose Uptake. *Compr Physiol* 10: 785–809, 2020. doi: 10.1002/cphy.c190029.

130. **Petersen KF**, **Dufour S**, **Savage DB**, **Bilz S**, **Solomon G**, **Yonemitsu S**, **Cline GW**, **Befroy D**, **Zemany L**, **Kahn BB**, **Papademetris X**, **Rothman DL**, **Shulman GI**. The role of skeletal muscle insulin resistance in the pathogenesis of the metabolic syndrome. *Proc Natl Acad Sci* 104: 12587–12594, 2007. doi: 10.1073/pnas.0705408104.

131. **Chang EI**, **Rozance PJ**, **Wesolowski SR**, **Nguyen LM**, **Shaw SC**, **Sclafani RA**, **Bjorkman KK**, **Peter AK**, **Hay W**, **Brown LD**. Rates of myogenesis and myofiber numbers are reduced in late gestation IUGR fetal sheep. *J Endocrinol* 244: 339–352, 2019. doi: 10.1530/JOE-19-0273.

132. **Swanson AM**, **David AL**. Animal models of fetal growth restriction: Considerations for translational medicine. *Placenta* 36: 623–630, 2015. doi: 10.1016/j.placenta.2015.03.003.

133. **Coe BL**, **Kirkpatrick JR**, **Taylor JA**, **Vom Saal FS**. A New 'Crowded Uterine Horn' Mouse Model for Examining the Relationship Between Foetal Growth and Adult Obesity. *Basic Clin Pharmacol Toxicol* 102: 162–167, 2008. doi: 10.1111/j.1742-7843.2007.00195.x.

134. **Anthony R**, **Scheaffer A**, **Wright C**, **Regnault T**. Ruminant models of prenatal growth restriction. .

135. **Barry JS**, **Rozance PJ**, **Anthony RV**. An animal model of placental insufficiency-induced intrauterine growth restriction. *Semin Perinatol* 32: 225–230, 2008. doi: 10.1053/j.semperi.2007.11.004.

136. **Boddy K**, **Dawes GS**, **Fisher R**, **Pinter S**, **Robinson JS**. Foetal respiratory movements, electrocortical and cardiovascular responses to hypoxaemia and hypercapnia in sheep. *J Physiol* 243: 599–618, 1974. doi: 10.1113/jphysiol.1974.sp010768.

137. **Richardson BS**, **Bocking AD**. Metabolic and circulatory adaptations to chronic hypoxia in the fetus. *Comp Biochem Physiol A Mol Integr Physiol* 119: 717–723, 1998. doi: 10.1016/s1095-6433(98)01010-1.

138. **Block BS**, **Schlafer DH**, **Wentworth RA**, **Kreitzer LA**, **Nathanielsz PW**. Regional blood flow distribution in fetal sheep with intrauterine growth retardation produced by decreased umbilical placental perfusion. *J Dev Physiol* 13: 81–85, 1990.

139. **Sheldon RE**, **Peeters LL**, **Jones MD**, **Makowski EL**, **Meschia G**. Redistribution of cardiac output and oxygen delivery in the hypoxemic fetal lamb. *Am J Obstet Gynecol* 135: 1071–1078, 1979. doi: 10.1016/0002-9378(79)90739-7.

140. **Jonker SS**, **Louey S**. Endocrine and other physiologic modulators of perinatal cardiomyocyte endowment. *J Endocrinol* 228: R1–R18, 2016. doi: 10.1530/JOE-15-0309.

141. **Milani-Nejad N**, **Janssen PM**. Small and Large Animal Models in Cardiac Contraction Research: Advantages and Disadvantages. *Pharmacol Ther* 141: 235, 2013. doi: 10.1016/j.pharmthera.2013.10.007.

142. **Rudolph AM**. Congenital Diseases of the Heart: Clinical-Physiological Considerations. 1st ed. Wiley.

143. **Adler CP**. Relationship between deoxyribonucleic acid content and nucleoli in human heart muscle cells and estimation of cell number during cardiac growth and hyperfunction. *Recent Adv Stud Cardiac Struct Metab* 8: 373–386, 1975.

144. **Adler CP**, **Costabel U**. Myocardial DNA and cell number under the influence of cytostatics. I. Post mortem investigations of human hearts. *Virchows Arch B Cell Pathol Incl Mol Pathol* 32: 109–125, 1980. doi: 10.1007/BF02889020.

145. **Adler CP**, **Costabel U**. Cell number in human heart in atrophy, hypertrophy, and under the influence of cytostatics. *Recent Adv Stud Cardiac Struct Metab* 6: 343–355, 1975.

146. **Huttenbach Y**, **Ostrowski ML**, **Thaller D**, **Kim HS**. Cell proliferation in the growing human heart: MIB-1 immunostaining in preterm and term infants at autopsy. *Cardiovasc Pathol Off J Soc Cardiovasc Pathol* 10: 119–123, 2001. doi: 10.1016/s1054-8807(01)00065-5.

147. **Kim HD**, **Kim DJ**, **Lee IJ**, **Rah BJ**, **Sawa Y**, **Schaper J**. Human fetal heart development after mid-term: morphometry and ultrastructural study. *J Mol Cell Cardiol* 24: 949–965, 1992. doi: 10.1016/0022-2828(92)91862-y.

148. **Jonker SS**, **Faber JJ**, **Anderson DF**, **Thornburg KL**, **Louey S**, **Giraud GD**. Sequential growth of fetal sheep cardiac myocytes in response to simultaneous arterial and venous hypertension. *Am J Physiol-Regul Integr Comp Physiol* 292: R913–R919, 2007. doi: 10.1152/ajpregu.00484.2006.

149. **Burrell JH**, **Boyn AM**, **Kumarasamy V**, **Hsieh A**, **Head SI**, **Lumbers ER**. Growth and maturation of cardiac myocytes in fetal sheep in the second half of gestation. *Anat Rec A Discov Mol Cell Evol Biol* 274A: 952–961, 2003. doi: 10.1002/ar.a.10110.

150. **Bergmann O**, **Zdunek S**, **Felker A**, **Salehpour M**, **Alkass K**, **Bernard S**, **Sjostrom SL**, **Szewczykowska M**, **Jackowska T**, **Dos Remedios C**, **Malm T**, **Andrä M**, **Jashari R**, **Nyengaard JR**, **Possnert G**, **Jovinge S**, **Druid H**, **Frisén J**. Dynamics of Cell Generation and Turnover in the Human Heart. *Cell* 161: 1566–1575, 2015. doi: 10.1016/j.cell.2015.05.026.

151. **Rumyantsev PP**. *Growth and Hyperplasia of Cardiac Muscle Cells*. Taylor & Francis, 1991.

152. **Rumyantsev PP**. Interrelations of the proliferation and differentiation processes during cardiact myogenesis and regeneration. *Int Rev Cytol* 51: 186–273, 1977.

153. **Zebrowski DC**, **Becker R**, **Engel FB**. Towards regenerating the mammalian heart: challenges in evaluating experimentally induced adult mammalian cardiomyocyte proliferation. *Am J Physiol-Heart Circ Physiol* 310: H1045–H1054, 2016. doi: 10.1152/ajpheart.00697.2015.

154. **Adler CP**, **Friedburg H**, **Herget GW**, **Neuburger M**, **Schwalb H**. Variability of cardiomyocyte DNA content, ploidy level and nuclear number in mammalian hearts. *Virchows Arch Int J Pathol* 429: 159–164, 1996. doi: 10.1007/BF00192438.

155. **Bensley JG**, **Stacy VK**, **De Matteo R**, **Harding R**, **Black MJ**. Cardiac remodelling as a result of pre-term birth: implications for future cardiovascular disease. *Eur Heart J* 31: 2058–2066, 2010. doi: 10.1093/eurheartj/ehq104.

156. **Brodsky VY**, **Arefyeva AM**, **Gvasava IG**, **Sarkisov DS**, **Panova NW**. Polyploidy in cardiac myocytes of normal and hypertrophic human hearts; range of values. *Virchows Arch* 424: 429–435, 1994. doi: 10.1007/BF00190566.

157. **Schmid G**, **Pfitzer P**. Mitoses and binucleated cells in perinatal human hearts. *Virchows Arch B* 48: 59–67, 1985. doi: 10.1007/BF02890115.

158. **Rudolph AM**, **Roman C**, **Gournay V**. Perinatal Myocardial DNA and Protein Changes in the Lamb: Effect of Cortisol in the Fetus. *Pediatr Res* 46: 141–146, 1999. doi: 10.1203/00006450-199908000-00002.

159. **Vliegen HW**, **Eulderink F**, **Bruschke AV**, **van der Laarse A**, **Cornelisse CJ**. Polyploidy of myocyte nuclei in pressure overloaded human hearts: a flow cytometric study in left and right ventricular myocardium. *Am J Cardiovasc Pathol* 5: 27–31, 1995.

160. **Du M**, **Tong J**, **Zhao J**, **Underwood KR**, **Zhu M**, **Ford SP**, **Nathanielsz PW**. Fetal programming of skeletal muscle development in ruminant animals. *J Anim Sci* 88: E51-60, 2010. doi: 10.2527/jas.2009-2311.

161. **Davis TA**, **Fiorotto ML**. Regulation of muscle growth in neonates. *Curr Opin Clin Nutr Metab Care* 12: 78–85, 2009. doi: 10.1097/MCO.0b013e32831cef9f.

162. **Romero NB**, **Mezmezian M**, **Fidziańska A**. Main steps of skeletal muscle development in the human: morphological analysis and ultrastructural characteristics of developing human muscle. *Handb Clin Neurol* 113: 1299–1310, 2013. doi: 10.1016/B978-0-444-59565-2.00002-2.

163. **Padoan A**, **Rigano S**, **Ferrazzi E**, **Beaty BL**, **Battaglia FC**, **Galan HL**. Differences in fat and lean mass proportions in normal and growth-restricted fetuses. *Am J Obstet Gynecol* 191: 1459–1464, 2004. doi: 10.1016/j.ajog.2004.06.045.

164. **Yau KI**, **Chang MH**. Growth and body composition of preterm, small-for-gestational-age infants at a postmenstrual age of 37-40 weeks. *Early Hum Dev* 33: 117–131, 1993. doi: 10.1016/0378-3782(93)90207-b.

165. **Hediger ML**, **Overpeck MD**, **Kuczmarski RJ**, **McGlynn A**, **Maurer KR**, **Davis WW**. Muscularity and fatness of infants and young children born small- or large-for-gestational-age. *Pediatrics* 102: E60, 1998. doi: 10.1542/peds.102.5.e60.

166. **Lapillonne A**, **Braillon P**, **Claris O**, **Chatelain PG**, **Delmas PD**, **Salle BL**. Body composition in appropriate and in small for gestational age infants. *Acta Paediatr Oslo Nor 1992* 86: 196–200, 1997. doi: 10.1111/j.1651-2227.1997.tb08868.x.

167. **Fahey AJ**, **Brameld JM**, **Parr T**, **Buttery PJ**. The effect of maternal undernutrition before muscle differentiation on the muscle fiber development of the newborn lamb. *J Anim Sci* 83: 2564–2571, 2005. doi: 10.2527/2005.83112564x.

168. **Widdowson EM**, **Crabb DE**, **Milner RDG**. Cellular Development of Some Human Organs Before Birth. *Arch Dis Child* 47: 652, 1972. doi: 10.1136/adc.47.254.652.

169. **Wilson SJ**, **McEwan JC**, **Sheard PW**, **Harris AJ**. Early stages of myogenesis in a large mammal: formation of successive generations of myotubes in sheep tibialis cranialis muscle. *J Muscle Res Cell Motil* 13: 534–550, 1992. doi: 10.1007/BF01737996.

170. **Fahey AJ**, **Brameld JM**, **Parr T**, **Buttery PJ**. Ontogeny of factors associated with proliferation and differentiation of muscle in the ovine fetus. *J Anim Sci* 83: 2330–2338, 2005. doi: 10.2527/2005.83102330x.

171. **McCoard SA**, **McNabb WC**, **Peterson SW**, **McCutcheon SN**, **Harris PM**. Muscle growth, cell number, type and morphometry in single and twin fetal lambs during mid to late gestation. *Reprod Fertil Dev* 12: 319–327, 2000. doi: 10.1071/rd99059.

172. **McCoard SA**, **McNabb WC**, **Birtles MJ**, **Harris PM**, **McCutcheon SN**, **Peterson SW**. Immunohistochemical detection of myogenic cells in muscles of fetal and neonatal lambs. *Cells Tissues Organs* 169: 21–33, 2001. doi: 10.1159/000047857.

173. **Stickland NC**. Muscle development in the human fetus as exemplified by m. sartorius: a quantitative study. *J Anat* 132: 557–579, 1981.

174. **McLennan IS**. Neurogenic and myogenic regulation of skeletal muscle formation: A critical re-evaluation. *Prog Neurobiol* 44: 119–140, 1994. doi: 10.1016/0301-0082(94)90035-3.

175. **Regnault TRH**, **De Vrijer B**, **Galan HL**, **Wilkening RB**, **Battaglia FC**, **Meschia G**. Development and Mechanisms of Fetal Hypoxia in Severe Fetal Growth Restriction. *Placenta* 28: 714–723, 2007. doi: 10.1016/j.placenta.2006.06.007.

176. **Galan HL**, **Anthony RV**, **Rigano S**, **Parker TA**, **De Vrijer B**, **Ferrazzi E**, **Wilkening RB**, **Regnault TRH**. Fetal hypertension and abnormal Doppler velocimetry in an ovine model of intrauterine growth restriction. *Am J Obstet Gynecol* 192: 272–279, 2005. doi: 10.1016/j.ajog.2004.05.088.

177. **Regnault T**, **Orbus R**, **Battaglia F**, **Wilkening R**, **Anthony R**. Altered arterial concentrations of placental hormones during maximal placental growth in a model of placental insufficiency. *J Endocrinol* 162: 433–442, 1999. doi: 10.1677/joe.0.1620433.

178. **Bell AW**, **Wilkening RB**, **Meschia G**. Some aspects of placental function in chronically heat-stressed ewes. *J Dev Physiol* 9: 17–29, 1987.

179. **Hafez SA**, **Borowicz P**, **Reynolds LP**, **Redmer DA**. Maternal and fetal microvasculature in sheep placenta at several stages of gestation. *J Anat* 216: 292, 2010. doi: 10.1111/j.1469-7580.2009.01184.x.

180. **Boyd RD**, **Haworth C**, **Stacey TE**, **Ward HT**. Permeability of the sheep placenta to unmetabolized polar non-electrolytes. *J Physiol* 256: 617–634, 1976. doi: 10.1113/jphysiol.1976.sp011342.

181. **Pardi G**, **Cetin I**, **Marconi AM**, **Lanfranchi A**, **Bozzetti P**, **Ferrazzi E**, **Buscaglia M**, **Battaglia FC**. Diagnostic value of blood sampling in fetuses with growth retardation. *N Engl J Med* 328: 692–696, 1993. doi: 10.1056/NEJM199303113281004.

182. **Anthony RV**, **Scheaffer AN**, **Wright CD**, **Regnault TRH**. Ruminant models of prenatal growth restriction. *Reprod Camb Engl Suppl* 61: 183–194, 2003.

183. **Steyn C**, **Hawkins P**, **Saito T**, **Noakes DE**, **Kingdom JC**, **Hanson MA**. Undernutrition during the first half of gestation increases the predominance of fetal tissue in late-gestation ovine placentomes. *Eur J Obstet Gynecol Reprod Biol* 98: 165–170, 2001. doi: 10.1016/s0301-2115(01)00321-9.

184. **Wallace JM**, **Bourke DA**, **Aitken RP**, **Leitch N**, **Hay WW**. Blood flows and nutrient uptakes in growth-restricted pregnancies induced by overnourishing adolescent sheep. *Am J Physiol Regul Integr Comp Physiol* 282: R1027-1036, 2002. doi: 10.1152/ajpregu.00465.2001.

185. **Wallace JM**, **Bourke DA**, **Aitken RP**, **Milne JS**, **William W Hay J**. Placental glucose transport in growth-restricted pregnancies induced by overnourishing adolescent sheep. *J Physiol* 547: 85, 2002. doi: 10.1113/jphysiol.2002.023333.

186. **Julian CG**, **Vargas E**, **Browne VA**, **Wilson MJ**, **Bigham AW**, **Rodriguez C**, **McCord JM**, **Moore LG**. Potential role for elevated maternal enzymatic antioxidant status in Andean protection against altitude-associated SGA. *J Matern Fetal Neonatal Med* 25: 1233–1240, 2012. doi: 10.3109/14767058.2011.636102.

187. **Robinson JS**, **Jones CT**, **Kingston EJ**. Studies on experimental growth retardation in sheep. The effects of maternal hypoxaemia. *J Dev Physiol* 5: 89–100, 1983.

188. **Morrison JL**, **Botting KJ**, **Dyer JL**, **Williams SJ**, **Thornburg KL**, **McMillen IC**. Restriction of placental function alters heart development in the sheep fetus. *Am J Physiol-Regul Integr Comp Physiol* 293: R306–R313, 2007. doi: 10.1152/ajpregu.00798.2006.

189. **Alexander G**. STUDIES ON THE PLACENTA OF THE SHEEP (OVIS ARIES L.). EFFECT OF SURGICAL REDUCTION IN THE NUMBER OF CARUNCLES. *J Reprod Fertil* 7: 307–322, 1964. doi: 10.1530/jrf.0.0070307.

190. **Bowman CE**, **Arany Z**, **Wolfgang MJ**. Regulation of maternal–fetal metabolic communication. *Cell Mol Life Sci CMLS* 78: 1455, 2020. doi: 10.1007/s00018-020-03674-w.

191. **Kind KL**, **Owens JA**, **Robinson JS**, **Quinn KJ**, **Grant PA**, **Walton PE**, **Gilmour RS**, **Owens PC**. Effect of restriction of placental growth on expression of IGFs in fetal sheep: relationship to fetal growth, circulating IGFs and binding proteins. *J Endocrinol* 146: 23–34, 1995. doi: 10.1677/joe.0.1460023.

192. **Murotsuki J**, **Gagnon R**, **Matthews SG**, **Challis JR**. Effects of long-term hypoxemia on pituitary-adrenal function in fetal sheep. *Am J Physiol-Endocrinol Metab* 271: E678–E685, 1996. doi: 10.1152/ajpendo.1996.271.4.E678.

193. **Gagnon R**, **Challis J**, **Johnston L**, **Fraher L**. Fetal endocrine responses to chronic placental embolization in the late-gestation ovine fetus. *Am J Obstet Gynecol* 170: 929–938, 1994. doi: 10.1016/s0002-9378(94)70309-4.

194. **Murotsuki J**, **Challis JR**, **Han VK**, **Fraher LJ**, **Gagnon R**. Chronic fetal placental embolization and hypoxemia cause hypertension and myocardial hypertrophy in fetal sheep. *Am J Physiol-Regul Integr Comp Physiol* 272: R201–R207, 1997. doi: 10.1152/ajpregu.1997.272.1.R201.

195. **Gagnon R**, **Johnston L**, **Murotsuki J**. Fetal placental embolization in the late-gestation ovine fetus: alterations in umbilical blood flow and fetal heart rate patterns. *Am J Obstet Gynecol* 175: 63–72, 1996. doi: 10.1016/s0002-9378(96)70252-1.

196. **Oyama K**, **Padbury J**, **Chappell B**, **Martinez A**, **Stein H**, **Humme J**. Single umbilical artery ligation-induced fetal growth retardation: effect on postnatal adaptation. *Am J Physiol-Endocrinol Metab* 263: E575–E583, 1992. doi: 10.1152/ajpendo.1992.263.3.E575.

197. **Barry JS**, **Rozance PJ**, **Anthony RV**. An Animal Model of Placental Insufficiency-Induced Intrauterine Growth Restriction. *Semin Perinatol* 32: 225–230, 2008. doi: 10.1053/j.semperi.2007.11.004.

198. **Alexander G**, **Williams D**. Heat stress and development of the conceptus in domestic sheep. *J Agric Sci* 76: 53–72, 1971. doi: 10.1017/S0021859600015616.

199. **Arroyo JA**, **Brown LD**, **Galan HL**. Placental mTOR and related signaling pathways in an Ovine Model of Intrauterine Growth Restriction (IUGR). *Am J Obstet Gynecol* 201: 616.e1-616.e7, 2009. doi: 10.1016/j.ajog.2009.07.031.

200. **Thornburg KL**. The programming of cardiovascular disease. *J Dev Orig Health Dis* 6: 366–376, 2015. doi: 10.1017/S2040174415001300.

201. **Iwamoto HS**, **Teitel D**, **Rudolph AM**. Effects of Birth-Related Events on Blood Flow Distribution. *Pediatr Res* 22: 634–640, 1987. doi: 10.1203/00006450-198712000-00004.

202. **Teitel DF**, **Iwamoto HS**, **Rudolph AM**. Effects of Birth-Related Events on Central Blood Flow Patterns. *Pediatr Res* 22: 557–566, 1987. doi: 10.1203/00006450-198711000-00017.

203. **Rudolph AM**. Distribution and regulation of blood flow in the fetal and neonatal lamb. *Circ Res* 57: 811–821, 1985. doi: 10.1161/01.RES.57.6.811.

204. **Bubb KJ**, **Cock ML**, **Black MJ**, **Dodic M**, **Boon W-M**, **Parkington HC**, **Harding R**, **Tare M**. Intrauterine growth restriction delays cardiomyocyte maturation and alters coronary artery function in the fetal sheep. *J Physiol* 578: 871–881, 2007. doi: 10.1113/jphysiol.2006.121160.

205. **Crispi F**, **Bijnens B**, **Figueras F**, **Bartrons J**, **Eixarch E**, **Le Noble F**, **Ahmed A**, **Gratacós E**. Fetal growth restriction results in remodeled and less efficient hearts in children. *Circulation* 121: 2427–2436, 2010. doi: 10.1161/CIRCULATIONAHA.110.937995.

206. **Bjarnegård N**, **Morsing E**, **Cinthio M**, **Länne T**, **Brodszki J**. Cardiovascular function in adulthood following intrauterine growth restriction with abnormal fetal blood flow. *Ultrasound Obstet Gynecol Off J Int Soc Ultrasound Obstet Gynecol* 41: 177–184, 2013. doi: 10.1002/uog.12314.

207. **Sarvari SI**, **Rodriguez-Lopez M**, **Nuñez-Garcia M**, **Sitges M**, **Sepulveda-Martinez A**, **Camara O**, **Butakoff C**, **Gratacos E**, **Bijnens B**, **Crispi F**. Persistence of Cardiac Remodeling in Preadolescents With Fetal Growth Restriction. *Circ Cardiovasc Imaging* 10: e005270, 2017. doi: 10.1161/CIRCIMAGING.116.005270.

208. **Li F**, **Wang X**, **Capasso JM**, **Gerdes AM**. Rapid transition of cardiac myocytes from hyperplasia to hypertrophy during postnatal development. *J Mol Cell Cardiol* 28: 1737–1746, 1996. doi: 10.1006/jmcc.1996.0163.

209. **Vranas S**, **Heinemann GK**, **Liu H**, **De Blasio MJ**, **Owens JA**, **Gatford KL**, **Black MJ**. Small size at birth predicts decreased cardiomyocyte number in the adult ovine heart. *J Dev Orig Health Dis* 8: 618–625, 2017. doi: 10.1017/S2040174417000381.

210. **Jonker SS**, **Louey S**. Endocrine and other physiologic modulators of perinatal cardiomyocyte endowment. *J Endocrinol* 228: R1–R18, 2016. doi: 10.1530/JOE-15-0309.

211. **Paradis AN**, **Gay MS**, **Zhang L**. Binucleation of cardiomyocytes: the transition from a proliferative to a terminally differentiated state. *Drug Discov Today* 19: 602–609, 2014. doi: 10.1016/j.drudis.2013.10.019.

212. **Øvrebø JI**, **Edgar BA**. Polyploidy in tissue homeostasis and regeneration. *Dev Camb Engl* 145: dev156034, 2018. doi: 10.1242/dev.156034.

213. **Derks W**, **Bergmann O**. Polyploidy in Cardiomyocytes. *Circ Res* 126: 552–565, 2020. doi: 10.1161/CIRCRESAHA.119.315408.

214. **Anatskaya OV**, **Sidorenko NV**, **Beyer TV**, **Vinogradov AE**. Neonatal cardiomyocyte ploidy reveals critical windows of heart development. *Int J Cardiol* 141: 81–91, 2010. doi: 10.1016/j.ijcard.2008.11.158.

215. **Louey S**, **Jonker SS**, **Giraud GD**, **Thornburg KL**. Placental insufficiency decreases cell cycle activity and terminal maturation in fetal sheep cardiomyocytes. *J Physiol* 580: 639–648, 2007. doi: 10.1113/jphysiol.2006.122200.

216. **Botting KJ**, **McMillen IC**, **Forbes H**, **Nyengaard JR**, **Morrison JL**. Chronic Hypoxemia in Late Gestation Decreases Cardiomyocyte Number but Does Not Change Expression of Hypoxia-Responsive Genes. *J Am Heart Assoc Cardiovasc Cerebrovasc Dis* 3: e000531, 2014. doi: 10.1161/JAHA.113.000531.

217. **van Amerongen MJ**, **Engel FB**. Features of cardiomyocyte proliferation and its potential for cardiac regeneration. *J Cell Mol Med* 12: 2233–2244, 2008. doi: 10.1111/j.1582-4934.2008.00439.x.

218. **Chang EI**, **Hetrick B**, **Wesolowski SR**, **McCurdy CE**, **Rozance PJ**, **Brown LD**. A Two-Week Insulin Infusion in Intrauterine Growth Restricted Fetal Sheep at 75% Gestation Increases Skeletal Myoblast Replication but Did Not Restore Muscle Mass or Increase Fiber Number. *Front Endocrinol* 12: 785242, 2021. doi: 10.3389/fendo.2021.785242.

219. **Chang EI**, **Stremming J**, **Knaub LA**, **Wesolowski SR**, **Rozance PJ**, **Sucharov CC**, **Reusch JEB**, **Brown LD**. Mitochondrial respiration is lower in the intrauterine growth-restricted fetal sheep heart. .

220. **Percie du Sert N**, **Hurst V**, **Ahluwalia A**, **Alam S**, **Avey MT**, **Baker M**, **Browne WJ**, **Clark A**, **Cuthill IC**, **Dirnagl U**, **Emerson M**, **Garner P**, **Holgate ST**, **Howells DW**, **Karp NA**, **Lazic SE**, **Lidster K**, **MacCallum CJ**, **Macleod M**, **Pearl EJ**, **Petersen OH**, **Rawle F**, **Reynolds P**, **Rooney K**, **Sena ES**, **Silberberg SD**, **Steckler T**, **Würbel H**. The ARRIVE guidelines 2.0: Updated guidelines for reporting animal research. *PLoS Biol* 18: e3000410, 2020. doi: 10.1371/journal.pbio.3000410.

221. **Brown LD**, **Wesolowski SR**, **Kailey J**, **Bourque S**, **Wilson A**, **Andrews SE**, **Hay WW**, **Rozance PJ**. Chronic Hyperinsulinemia Increases Myoblast Proliferation in Fetal Sheep Skeletal Muscle. *Endocrinology* 157: 2447–2460, 2016. doi: 10.1210/en.2015-1744.

222. **Brown LD**, **Hay WW**. Effect of hyperinsulinemia on amino acid utilization and oxidation independent of glucose metabolism in the ovine fetus. *Am J Physiol-Endocrinol Metab* 291: E1333–E1340, 2006. doi: 10.1152/ajpendo.00028.2006.

223. **Rozance PJ**, **Zastoupil L**, **Wesolowski SR**, **Goldstrohm DA**, **Strahan B**, **Cree-Green M**, **Sheffield-Moore M**, **Meschia G**, **William W. Hay J**, **Wilkening RB**, **Brown LD**. Skeletal muscle protein accretion rates and hindlimb growth are reduced in late gestation intrauterine growth-restricted fetal sheep. *J Physiol* 596: 67, 2018. doi: 10.1113/JP275230.

224. **Auchampach J**, **Han L**, **Huang GN**, **Kühn B**, **Lough JW**, **O'Meara CC**, **Payumo AY**, **Rosenthal NA**, **Sucov HM**, **Yutzey KE**, **Patterson M**. Measuring cardiomyocyte cell-cycle activity and proliferation in the age of heart regeneration. *Am J Physiol-Heart Circ Physiol* 322: H579–H596, 2022. doi: 10.1152/ajpheart.00666.2021.

225. **Botting KJ**, **McMillen IC**, **Forbes H**, **Nyengaard JR**, **Morrison JL**. Chronic Hypoxemia in Late Gestation Decreases Cardiomyocyte Number but Does Not Change Expression of Hypoxia-Responsive Genes. *J Am Heart Assoc* 3: e000531, 2014. doi: 10.1161/JAHA.113.000531.

226. **Greenwood PL**, **Slepetis RM**, **Bell AW**, **Hermanson JW**. Intrauterine growth retardation is associated with reduced cell cycle activity, but not myofibre number, in ovine fetal muscle. *Reprod Fertil Dev* 11: 281, 1999. doi: 10.1071/RD99054.

227. **Takahashi N**, **Nishida H**, **Arai T**, **Kaneda Y**. Abnormal cardiac histology in severe intrauterine growth retardation infants. *Pediatr Int* 37: 341–346, 1995. doi: 10.1111/j.1442-200X.1995.tb03326.x.

228. **Murotsuki J**, **Challis JR**, **Han VK**, **Fraher LJ**, **Gagnon R**. Chronic fetal placental embolization and hypoxemia cause hypertension and myocardial hypertrophy in fetal sheep. *Am J Physiol-Regul Integr Comp Physiol* 272: R201–R207, 1997. doi: 10.1152/ajpregu.1997.272.1.R201.

229. **Mayhew TM**, **Gregson C**, **Fagan DG**. Ventricular myocardium in control and growth-retarded human fetuses: growth in different tissue compartments and variation with fetal weight, gestational age, and ventricle size. *Hum Pathol* 30: 655–660, 1999. doi: 10.1016/s0046-8177(99)90090-4.

230. **Zebrowski DC**, **Engel FB**. The Cardiomyocyte Cell Cycle in Hypertrophy, Tissue Homeostasis, and Regeneration. In: *Reviews of Physiology, Biochemistry and Pharmacology, Vol. 165*, edited by Nilius B, Amara SG, Gudermann T, Jahn R, Lill R, Offermanns S, Petersen OH. Springer International Publishing, p. 67–96.

231. **Ahuja P**, **Sdek P**, **Maclellan WR**. Cardiac Myocyte Cell Cycle Control in Development, Disease and Regeneration. *Physiol Rev* 87: 521–544, 2007. doi: 10.1152/physrev.00032.2006.

232. **Normand G**, **King RW**. Understanding cytokinesis failure. *Adv Exp Med Biol* 676: 27–55, 2010. doi: 10.1007/978-1-4419-6199-0_3.

233. **Leone M**, **Magadum A**, **Engel FB**. Cardiomyocyte proliferation in cardiac development and regeneration: a guide to methodologies and interpretations. *Am J Physiol-Heart Circ Physiol* 309: H1237–H1250, 2015. doi: 10.1152/ajpheart.00559.2015.

234. **Soonpaa MH**, **Kim KK**, **Pajak L**, **Franklin M**, **Field LJ**. Cardiomyocyte DNA synthesis and binucleation during murine development. *Am J Physiol-Heart Circ Physiol* 271: H2183–H2189, 1996. doi: 10.1152/ajpheart.1996.271.5.H2183.

235. **Walsh S**, **Pontén A**, **Fleischmann BK**, **Jovinge S**. Cardiomyocyte cell cycle control and growth estimation in vivo—an analysis based on cardiomyocyte nuclei. *Cardiovasc Res* 86: 365–373, 2010. doi: 10.1093/cvr/cvq005.

236. **Alkass K**, **Panula J**, **Westman M**, **Wu T-D**, **Guerquin-Kern J-L**, **Bergmann O**. No Evidence for Cardiomyocyte Number Expansion in Preadolescent Mice. *Cell* 163: 1026–1036, 2015. doi: 10.1016/j.cell.2015.10.035.

237. **Patterson M**, **Barske L**, **Van Handel B**, **Rau CD**, **Gan P**, **Sharma A**, **Parikh S**, **Denholtz M**, **Huang Y**, **Yamaguchi Y**, **Shen H**, **Allayee H**, **Crump JG**, **Force TI**, **Lien C-L**, **Makita T**, **Lusis AJ**, **Kumar SR**, **Sucov HM**. Frequency of mononuclear diploid cardiomyocytes underlies natural variation in heart regeneration. *Nat Genet* 49: 1346–1353, 2017. doi: 10.1038/ng.3929.

238. **Ebelt H**, **Hufnagel N**, **Neuhaus P**, **Neuhaus H**, **Gajawada P**, **Simm A**, **Müller-Werdan U**, **Werdan K**, **Braun T**. Divergent Siblings. *Circ Res* 96: 509–517, 2005. doi: 10.1161/01.RES.0000159705.17322.57.

239. **Richardson GD**. Simultaneous Assessment of Cardiomyocyte DNA Synthesis and Ploidy: A Method to Assist Quantification of Cardiomyocyte Regeneration and Turnover. *J Vis Exp JoVE* : 53979, 2016. doi: 10.3791/53979.

240. **Bergmann O**, **Zdunek S**, **Alkass K**, **Druid H**, **Bernard S**, **Frisén J**. Identification of cardiomyocyte nuclei and assessment of ploidy for the analysis of cell turnover. *Exp Cell Res* 317: 188–194, 2011. doi: 10.1016/j.yexcr.2010.08.017.

241. **Paddock SJ**, **Swift SK**, **Alencar-Almeida V**, **Kenarsary A**, **Alvarez-Argote S**, **Flinn MA**, **Patterson M**, **O'Meara CC**. IL4Rα signaling promotes neonatal cardiac regeneration and cardiomyocyte cell cycle activity. *J Mol Cell Cardiol* 161: 62–74, 2021. doi: 10.1016/j.yjmcc.2021.07.012.

242. **Hirose K**, **Payumo AY**, **Cutie S**, **Hoang A**, **Zhang H**, **Guyot R**, **Lunn D**, **Bigley RB**, **Yu H**, **Wang J**, **Smith M**, **Gillett E**, **Muroy SE**, **Schmid T**, **Wilson E**, **Field KA**, **Reeder DM**, **Maden M**, **Yartsev MM**, **Wolfgang MJ**, **Grützner F**, **Scanlan TS**, **Szweda LI**, **Buffenstein R**, **Hu G**, **Flamant F**, **Olgin JE**, **Huang GN**. Evidence for hormonal control of heart regenerative capacity during endothermy acquisition. *Science* 364: 184–188, 2019. doi: 10.1126/science.aar2038.

243. **Tare M**, **Bensley JG**, **Moss TJM**, **Lingwood BE**, **Kim MY**, **Barton SK**, **Kluckow M**, **Gill AW**, **De Matteo R**, **Harding R**, **Black MJ**, **Parkington HC**, **Polglase GR**. Exposure to intrauterine inflammation leads to impaired function and altered structure in the preterm heart of fetal sheep. *Clin Sci Lond Engl 1979* 127: 559–569, 2014. doi: 10.1042/CS20140097.

244. **Slotkin TA**, **Seidler FJ**, **Kavlock RJ**, **Bartolome JV**. Fetal dexamethasone exposure impairs cellular development in neonatal rat heart and kidney: Effects on DNA and protein in whole tissues. *Teratology* 43: 301–306, 1991. doi: 10.1002/tera.1420430404.

245. **Matsuyama D**, **Kawahara K**. Oxidative stress-induced formation of a positive-feedback loop for the sustained activation of p38 MAPK leading to the loss of cell division in cardiomyocytes soon after birth. *Basic Res Cardiol* 106: 815–828, 2011. doi: 10.1007/s00395-011-0178-8.

246. **Liu Z**, **Yue S**, **Chen X**, **Kubin T**, **Braun T**. Regulation of Cardiomyocyte Polyploidy and Multinucleation by CyclinG1. *Circ Res* 106: 1498–1506, 2010. doi: 10.1161/CIRCRESAHA.109.211888.

247. **Anatskaya OV**, **Vinogradov AE**. Genome multiplication as adaptation to tissue survival: Evidence from gene expression in mammalian heart and liver. *Genomics* 89: 70–80, 2007. doi: 10.1016/j.ygeno.2006.08.014.

248. **Anatskaya OV**, **Runov AL**, **Ponomartsev SV**, **Vonsky MS**, **Elmuratov AU**, **Vinogradov AE**. Long-Term Transcriptomic Changes and Cardiomyocyte Hyperpolyploidy after Lactose Intolerance in Neonatal Rats. *Int J Mol Sci* 24: 7063, 2023. doi: 10.3390/ijms24087063.

249. **Aix E**, **Gutiérrez-Gutiérrez Ó**, **Sánchez-Ferrer C**, **Aguado T**, **Flores I**. Postnatal telomere dysfunction induces cardiomyocyte cell-cycle arrest through p21 activation. *J Cell Biol* 213: 571–583, 2016. doi: 10.1083/jcb.201510091.

250. **Beltrami CA**, **Di LC**, **Finato N**, **Yan SM**. DNA Content in End-Stage Heart Failure. *Adv Clin Path* 1: 59–73, 1997.

251. **Cao J**, **Wang J**, **Jackman CP**, **Cox AH**, **Trembley MA**, **Balowski JJ**, **Cox BD**, **De Simone A**, **Dickson AL**, **Di Talia S**, **Small EM**, **Kiehart DP**, **Bursac N**, **Poss KD**. Tension Creates an Endoreplication Wavefront that Leads Regeneration of Epicardial Tissue. *Dev Cell* 42: 600-615.e4, 2017. doi: 10.1016/j.devcel.2017.08.024.

252. **Herget GW**, **Neuburger M**, **Plagwitz R**, **Adler CP**. DNA content, ploidy level and number of nuclei in the human heart after myocardial infarction. *Cardiovasc Res* 36: 45–51, 1997. doi: 10.1016/S0008-6363(97)00140-5.

253. **Jiang Y-H**, **Wang H-L**, **Peng J**, **Zhu Y**, **Zhang H-G**, **Tang F-Q**, **Jian Z**, **Xiao Y-B**. Multinucleated polyploid cardiomyocytes undergo an enhanced adaptability to hypoxia via mitophagy. *J Mol Cell Cardiol* 138: 115–135, 2020. doi: 10.1016/j.yjmcc.2019.11.155.

254. **Meckert PC**, **Rivello HG**, **Vigliano C**, **González P**, **Favaloro R**, **Laguens R**. Endomitosis and polyploidization of myocardial cells in the periphery of human acute myocardial infarction. *Cardiovasc Res* 67: 116–123, 2005. doi: 10.1016/j.cardiores.2005.02.017.

255. **Swift SK**, **Purdy AL**, **Kolell ME**, **Andresen KG**, **Lahue C**, **Buddell T**, **Akins KA**, **Rau CD**, **O'Meara CC**, **Patterson M**. Cardiomyocyte ploidy is dynamic during postnatal development and varies across genetic backgrounds. *Dev Camb Engl* 150: dev201318, 2023. doi: 10.1242/dev.201318.

256. **Aye CYL**, **Lewandowski AJ**, **Lamata P**, **Upton R**, **Davis E**, **Ohuma EO**, **Kenworthy Y**, **Boardman H**, **Wopperer S**, **Packham A**, **Adwani S**, **McCormick K**, **Papageorghiou AT**, **Leeson P**. Disproportionate cardiac hypertrophy during early postnatal development in infants born preterm. *Pediatr Res* 82: 36–46, 2017. doi: 10.1038/pr.2017.96.

257. **Clubb FJ**, **Bishop SP**. Formation of binucleated myocardial cells in the neonatal rat. An index for growth hypertrophy. *Lab Investig J Tech Methods Pathol* 50: 571–577, 1984.

258. **Claycomb WC**. Cardiac-muscle hypertrophy. Differentiation and growth of the heart cell during development. *Biochem J* 168: 599–601, 1977.

259. **Kannan S**, **Kwon C**. Regulation of cardiomyocyte maturation during critical perinatal window. *J Physiol* 598: 2941–2956, 2020. doi: 10.1113/JP276754.

260. **Puente BN**, **Kimura W**, **Muralidhar SA**, **Moon J**, **Amatruda JF**, **Phelps KL**, **Grinsfelder D**, **Rothermel BA**, **Chen R**, **Garcia JA**, **Santos CX**, **Thet S**, **Mori E**, **Kinter MT**, **Rindler PM**, **Zacchigna S**, **Mukherjee S**, **Chen DJ**, **Mahmoud AI**, **Giacca M**, **Rabinovitch PS**, **Aroumougame A**, **Shah AM**, **Szweda LI**, **Sadek HA**. The Oxygen Rich Postnatal Environment Induces Cardiomyocyte Cell Cycle Arrest Through DNA Damage Response. *Cell* 157: 565–579, 2014. doi: 10.1016/j.cell.2014.03.032.

261. **Anatskaya OV**, **Vinogradov AE**. Heart and liver as developmental bottlenecks of mammal design: evidence from cell polyploidization: HEART AND LIVER AS BOTTLENECKS OF MAMMAL DESIGN. *Biol J Linn Soc* 83: 175–186, 2004. doi: 10.1111/j.1095-8312.2004.00377.x.

262. **Schipke J**, **Gonzalez-Tendero A**, **Cornejo L**, **Willführ A**, **Bijnens B**, **Crispi F**, **Mühlfeld C**, **Gratacós E**. Experimentally induced intrauterine growth restriction in rabbits leads to differential remodelling of left versus right ventricular myocardial microstructure. *Histochem Cell Biol* 148: 557–567, 2017. doi: 10.1007/s00418-017-1587-z.

263. **Botting KJ**, **Wang KCW**, **Padhee M**, **McMillen IC**, **Summers-Pearce B**, **Rattanatray L**, **Cutri N**, **Posterino GS**, **Brooks DA**, **Morrison JL**. Early origins of heart disease: low

birth weight and determinants of cardiomyocyte endowment. *Clin Exp Pharmacol Physiol* 39: 814–823, 2012. doi: 10.1111/j.1440-1681.2011.05649.x.

264. **Lewandowski AJ**, **Augustine D**, **Lamata P**, **Davis EF**, **Lazdam M**, **Francis J**, **McCormick K**, **Wilkinson AR**, **Singhal A**, **Lucas A**, **Smith NP**, **Neubauer S**, **Leeson P**. Preterm Heart in Adult Life: Cardiovascular Magnetic Resonance Reveals Distinct Differences in Left Ventricular Mass, Geometry, and Function. *Circulation* 127: 197–206, 2013. doi: 10.1161/CIRCULATIONAHA.112.126920.

265. **Elia A**, **Mohsin S**, **Khan M**. Cardiomyocyte Ploidy, Metabolic Reprogramming and Heart Repair. *Cells* 12: 1571, 2023. doi: 10.3390/cells12121571.

266. **Windmueller R**, **Leach JP**, **Babu A**, **Zhou S**, **Morley MP**, **Wakabayashi A**, **Petrenko NB**, **Viatour P**, **Morrisey EE**. Direct Comparison of Mononucleated and Binucleated Cardiomyocytes Reveals Molecular Mechanisms Underlying Distinct Proliferative Competencies. *Cell Rep* 30: 3105-3116.e4, 2020. doi: 10.1016/j.celrep.2020.02.034.

267. **Tchirikov M**, **Rybakowski C**, **Hüneke B**, **Schröder HJ**. Blood flow through the ductus venosus in singleton and multifetal pregnancies and in fetuses with intrauterine growth retardation. *Am J Obstet Gynecol* 178: 943–949, 1998. doi: 10.1016/s0002-9378(98)70528-9.

268. **Yajnik CS**. Obesity epidemic in India: intrauterine origins? *Proc Nutr Soc* 63: 387–396, 2004. doi: 10.1079/pns2004365.

269. **Yates DT**, **Macko AR**, **Nearing M**, **Chen X**, **Rhoads RP**, **Limesand SW**. Developmental programming in response to intrauterine growth restriction impairs myoblast function and skeletal muscle metabolism. *J Pregnancy* 2012: 631038, 2012. doi: 10.1155/2012/631038.

270. **Yates DT**, **Clarke DS**, **Macko AR**, **Anderson MJ**, **Shelton LA**, **Nearing M**, **Allen RE**, **Rhoads RP**, **Limesand SW**. Myoblasts from intrauterine growth-restricted sheep fetuses exhibit intrinsic deficiencies in proliferation that contribute to smaller semitendinosus myofibres. *J Physiol* 592: 3113–3125, 2014. doi: 10.1113/jphysiol.2014.272591.

271. **Yates DT**, **Cadaret CN**, **Beede KA**, **Riley HE**, **Macko AR**, **Anderson MJ**, **Camacho LE**, **Limesand SW**. Intrauterine growth-restricted sheep fetuses exhibit smaller hindlimb muscle fibers and lower proportions of insulin-sensitive Type I fibers near term. *Am J Physiol - Regul Integr Comp Physiol* 310: R1020–R1029, 2016. doi: 10.1152/ajpregu.00528.2015.

272. **Stremming J**, **Chang EI**, **Knaub LA**, **Armstrong ML**, **Baker PR**, **Wesolowski SR**, **Reisdorph N**, **Reusch JEB**, **Brown LD**. Lower citrate synthase activity, mitochondrial complex expression, and fewer oxidative myofibers characterize skeletal muscle from growth-restricted fetal sheep. *Am J Physiol-Regul Integr Comp Physiol* 322: R228–R240, 2022. doi: 10.1152/ajpregu.00222.2021.

273. **Posont RJ**, **Most MS**, **Cadaret CN**, **Marks-Nelson ES**, **Beede KA**, **Limesand SW**, **Schmidt TB**, **Petersen JL**, **Yates DT**. Primary myoblasts from intrauterine growth-restricted fetal sheep exhibit intrinsic dysfunction of proliferation and differentiation that coincides with enrichment of inflammatory cytokine signaling pathways. *J Anim Sci* 100: skac145, 2022. doi: 10.1093/jas/skac145.

274. **Cadaret CN**, **Posont RJ**, **Beede KA**, **Riley HE**, **Loy JD**, **Yates DT**. Maternal inflammation at midgestation impairs subsequent fetal myoblast function and skeletal muscle growth in rats, resulting in intrauterine growth restriction at term. *Transl Anim Sci* 3: 867–876, 2019. doi: 10.1093/tas/txz037.

275. **Allen RE**, **Boxhorn LK**. Regulation of skeletal muscle satellite cell proliferation and differentiation by transforming growth factor-beta, insulin-like growth factor I, and fibroblast growth factor. *J Cell Physiol* 138: 311–315, 1989. doi: 10.1002/jcp.1041380213.

276. **Johnson SE**, **Allen RE**. The effects of bFGF, IGF-I, and TGF-β on RMo skeletal muscle cell proliferation and differentiation. *Exp Cell Res* 187: 250–254, 1990. doi: 10.1016/0014-4827(90)90088-R.

277. **Liu JP**, **Baker J**, **Perkins AS**, **Robertson EJ**, **Efstratiadis A**. Mice carrying null mutations of the genes encoding insulin-like growth factor I (Igf-1) and type 1 IGF receptor (Igf1r). *Cell* 75: 59–72, 1993.

278. **Yu M**, **Wang H**, **Xu Y**, **Yu D**, **Li D**, **Liu X**, **Du W**. Insulin-like growth factor-1 (IGF-1) promotes myoblast proliferation and skeletal muscle growth of embryonic chickens via the PI3K/Akt signalling pathway. *Cell Biol Int* 39: 910–922, 2015. doi: 10.1002/cbin.10466.

279. **Limesand SW**, **Rozance PJ**, **Macko AR**, **Anderson MJ**, **Kelly AC**, **Hay WW**. Reductions in insulin concentrations and β-cell mass precede growth restriction in sheep fetuses with placental insufficiency. *Am J Physiol - Endocrinol Metab* 304: E516–E523, 2013. doi: 10.1152/ajpendo.00435.2012.

280. **Rosenthal SM**, **Cheng ZQ**. Opposing early and late effects of insulin-like growth factor I on differentiation and the cell cycle regulatory retinoblastoma protein in skeletal myoblasts. *Proc Natl Acad Sci U S A* 92: 10307–10311, 1995.

281. **Zanou N**, **Gailly P**. Skeletal muscle hypertrophy and regeneration: interplay between the myogenic regulatory factors (MRFs) and insulin-like growth factors (IGFs) pathways. *Cell Mol Life Sci CMLS* 70: 4117–4130, 2013. doi: 10.1007/s00018-013-1330-4.

282. **Chen B**, **You W**, **Wang Y**, **Shan T**. The regulatory role of Myomaker and Myomixer–Myomerger–Minion in muscle development and regeneration. *Cell Mol Life Sci CMLS* 77: 1551–1569, 2019. doi: 10.1007/s00018-019-03341-9.

283. **Olson EN**. Interplay between proliferation and differentiation within the myogenic lineage. *Dev Biol* 154: 261–272, 1992. doi: 10.1016/0012-1606(92)90066-P.

284. **Stremming J**, **White A**, **Donthi A**, **Batt D**, **Hetrick B**, **Chang E**, **Wesolowski S**, **Seefeldt M**, **McCurdy C**, **Rozance P**, **Brown L**. Sheep recombinant IGF-1 promotes organ-specific growth in fetal sheep. *Front Physiol* 13: 954948, 2022. doi: 10.3389/fphys.2022.954948.

285. **Stremming J**, **Chang EI**, **White A**, **Rozance PJ**, **Brown LD**. IGF-1 Infusion Increases Growth in Fetal Sheep When Euinsulinemia is Maintained. *J Endocrinol* 262: e240058, 2024. doi: 10.1530/JOE-24-0058.

286. **Yates DT**, **Macko AR**, **Nearing M**, **Chen X**, **Rhoads RP**, **Limesand SW**. Developmental programming in response to intrauterine growth restriction impairs myoblast function and skeletal muscle metabolism. *J Pregnancy* 2012: 631038, 2012. doi: 10.1155/2012/631038.

287. **Egner IM**, **Bruusgaard JC**, **Gundersen K**. Satellite cell depletion prevents fiber hypertrophy in skeletal muscle. *Dev Camb Engl* 143: 2898–2906, 2016. doi: 10.1242/dev.134411.

288. **Geiger AE**, **Daughtry MR**, **Yen C**, **Kirkpatrick LT**, **Shi H**, **Gerrard DE**. Dual effects of obesity on satellite cells and muscle regeneration. *Physiol Rep* 8: e14511, 2020. doi: 10.14814/phy2.14511.

289. **Boldrin L**, **Zammit PS**, **Morgan JE**. Satellite cells from dystrophic muscle retain regenerative capacity. *Stem Cell Res* 14: 20–29, 2015. doi: 10.1016/j.scr.2014.10.007.

290. **Moresi V**, **Marroncelli N**, **Adamo S**. New insights into the epigenetic control of satellite cells. *World J Stem Cells* 7: 945–955, 2015. doi: 10.4252/wjsc.v7.i6.945.

291. **Aiken CE**, **Ozanne SE**. Sex differences in developmental programming models. *Reprod Camb Engl* 145: R1-13, 2013. doi: 10.1530/REP-11-0489.

292. **Brown LD**, **Palmer C**, **Teynor L**, **Boehmer BH**, **Stremming J**, **Chang EI**, **White A**, **Jones AK**, **Cilvik SN**, **Wesolowski SR**, **Rozance PJ**. Fetal Sex Does Not Impact Placental Blood Flow or Placental Amino Acid Transfer in Late Gestation Pregnant Sheep With or Without Placental Insufficiency. *Reprod Sci Thousand Oaks Calif* 29: 1776–1789, 2022. doi: 10.1007/s43032-021-00750-9.

293. **Cortes-Araya Y**, **Cheung S**, **Ho W**, **Stenhouse C**, **Ashworth CJ**, **Esteves CL**, **Donadeu FX**. Effects of foetal size, sex and developmental stage on adaptive transcriptional responses of skeletal muscle to intrauterine growth restriction in pigs. *Sci Rep* 14: 8500, 2024. doi: 10.1038/s41598-024-57194-9.

294. **Kitzmann M**, **Carnac G**, **Vandromme M**, **Primig M**, **Lamb NJC**, **Fernandez A**. The Muscle Regulatory Factors MyoD and Myf-5 Undergo Distinct Cell Cycle–specific Expression in Muscle Cells. *J Cell Biol* 142: 1447–1459, 1998.

295. **Lassar AB**, **Skapek SX**, **Novitch B**. Regulatory mechanisms that coordinate skeletal muscle differentiation and cell cycle withdrawal. *Curr Opin Cell Biol* 6: 788–794, 1994. doi: 10.1016/0955-0674(94)90046-9.

296. **Sabourin LA**, **Rudnicki MA**. The molecular regulation of myogenesis. *Clin Genet* 57: 16–25, 2000. doi: 10.1034/j.1399-0004.2000.570103.x.

297. **Wei Q**, **Paterson BM**. Regulation of MyoD function in the dividing myoblast. *FEBS Lett* 490: 171–178, 2001. doi: 10.1016/S0014-5793(01)02120-2.